Review Article

The Alzheimer's Disease Neuroimaging Initiative: A review of papers published since its inception

Michael W. Weiner[a,b,c,d,e,*], Dallas P. Veitch[a], Paul S. Aisen[f], Laurel A. Beckett[g], Nigel J. Cairns[h,i], Robert C. Green[j], Danielle Harvey[g], Clifford R. Jack[k], William Jagust[l], Enchi Liu[m], John C. Morris[f], Ronald C. Petersen[n], Andrew J. Saykin[o,p], Mark E. Schmidt[q], Leslie Shaw[r], Judith A. Siuciak[s], Holly Soares[t], Arthur W. Toga[u], John Q. Trojanowski[v,w,x,y]; Alzheimer's Disease Neuroimaging Initiative

[a]Department of Veterans Affairs Medical Center, Center for Imaging of Neurodegenerative Diseases, San Francisco, CA, USA
[b]Department of Radiology, University of California, San Francisco, CA, USA
[c]Department of Medicine, University of California, San Francisco, CA, USA
[d]Department of Psychiatry, University of California, San Francisco, CA, USA
[e]Department of Neurology, University of California, San Francisco, CA, USA
[f]Department of Neurosciences, University of California San Diego, La Jolla, CA, USA
[g]Division of Biostatistics, Department of Public Health Sciences, University of California, Davis, CA, USA
[h]Knight Alzheimer's Disease Research Center, Washington University School of Medicine, Saint Louis, MO, USA
[i]Department of Neurology, Washington University School of Medicine, Saint Louis, MO, USA
[j]Division of Genetics, Department of Medicine, Brigham and Women's Hospital and Harvard Medical School, Boston, MA, USA
[k]Department of Radiology, Mayo Clinic, Rochester, MN, USA
[l]Helen Wills Neuroscience Institute, University of California Berkeley, Berkeley, CA, USA
[m]Janssen Alzheimer Immunotherapy, South San Francisco, CA, USA
[n]Department of Neurology, Mayo Clinic, Rochester, MN, USA
[o]Department of Radiology and Imaging Sciences, Indiana University School of Medicine, Indianapolis, IN, USA
[p]Department of Medical and Molecular Genetics, Indiana University School of Medicine, Indianapolis, IN, USA
[q]Neuroscience Therapeutic Area, Janssen Research and Development, Division of Janssen Pharmaceutica NV, Beerse, Belgium
[r]Department of Pathology and Laboratory Medicine, Perelman School of Medicine, University of Pennsylvania, Philadelphia, PA, USA
[s]The Biomarkers Consortium, Foundation for the National Institutes of Health, Bethesda, MD, USA
[t]Clinical Biomarkers, Bristol-Myers Squibb, Wallingford, CT, USA
[u]Laboratory of Neuroimaging, Department of Neurology, School of Medicine, University of California Los Angeles, Los Angeles, CA, USA
[v]Institute on Aging, Perelman School of Medicine, University of Pennsylvania, Philadelphia, PA, USA
[w]Alzheimer's Disease Core Center, Perelman School of Medicine, University of Pennsylvania, Philadelphia, PA, USA
[x]Udall Parkinson's Research Center, Perelman School of Medicine, University of Pennsylvania, Philadelphia, PA, USA
[y]Department of Pathology and Laboratory Medicine, Center for Neurodegenerative Research, Perelman School of Medicine, University of Pennsylvania, Philadelphia, PA, USA

Abstract

The Alzheimer's Disease Neuroimaging Initiative (ADNI) is an ongoing, longitudinal, multicenter study designed to develop clinical, imaging, genetic, and biochemical biomarkers for the early detection and tracking of Alzheimer's disease (AD). The study aimed to enroll 400 subjects with early mild cognitive impairment (MCI), 200 subjects with early AD, and 200 normal control subjects; $67 million funding was provided by both the public and private sectors, including the National Institute on Aging, 13 pharmaceutical companies, and 2 foundations that provided support through the Foundation for the National Institutes of Health. This article reviews all papers published since the inception of the initiative and summarizes the results as of February 2011. The major accomplishments of ADNI have been as follows: (1) the development of standardized methods for clinical tests, magnetic resonance imaging (MRI), positron emission tomography (PET), and cerebrospinal fluid (CSF)

biomarkers in a multicenter setting; (2) elucidation of the patterns and rates of change of imaging and CSF biomarker measurements in control subjects, MCI patients, and AD patients. CSF biomarkers are consistent with disease trajectories predicted by β-amyloid cascade (Hardy, J Alzheimers Dis 2006;9(Suppl 3):151–3) and tau-mediated neurodegeneration hypotheses for AD, whereas brain atrophy and hypometabolism levels show predicted patterns but exhibit differing rates of change depending on region and disease severity; (3) the assessment of alternative methods of diagnostic categorization. Currently, the best classifiers combine optimum features from multiple modalities, including MRI, [18F]-fluorodeoxyglucose-PET, CSF biomarkers, and clinical tests; (4) the development of methods for the early detection of AD. CSF biomarkers, β-amyloid 42 and tau, as well as amyloid PET may reflect the earliest steps in AD pathology in mildly symptomatic or even nonsymptomatic subjects, and are leading candidates for the detection of AD in its preclinical stages; (5) the improvement of clinical trial efficiency through the identification of subjects most likely to undergo imminent future clinical decline and the use of more sensitive outcome measures to reduce sample sizes. Baseline cognitive and/or MRI measures generally predicted future decline better than other modalities, whereas MRI measures of change were shown to be the most efficient outcome measures; (6) the confirmation of the AD risk loci *CLU*, *CR1*, and *PICALM* and the identification of novel candidate risk loci; (7) worldwide impact through the establishment of ADNI-like programs in Europe, Asia, and Australia; (8) understanding the biology and pathobiology of normal aging, MCI, and AD through integration of ADNI biomarker data with clinical data from ADNI to stimulate research that will resolve controversies about competing hypotheses on the etiopathogenesis of AD, thereby advancing efforts to find disease-modifying drugs for AD; and (9) the establishment of infrastructure to allow sharing of all raw and processed data without embargo to interested scientific investigators throughout the world. The ADNI study was extended by a 2-year Grand Opportunities grant in 2009 and a renewal of ADNI (ADNI-2) in October 2010 through to 2016, with enrollment of an additional 550 participants.

1. Introduction to Alzheimer's Disease Neuroimaging Initiative: Goals, history, and organization

1.1. Background

Alzheimer's disease (AD), the most common form of dementia, is a complex disease characterized by an accumulation of β-amyloid (Aβ) plaques and neurofibrillary tangles composed of tau amyloid fibrils [1] associated with synapse loss and neurodegeneration leading to memory impairment and other cognitive problems. There is currently no known treatment that slows the progression of this disorder. According to the 2010 World Alzheimer report, there are an estimated 35.6 million people worldwide living with dementia at a total cost of more than US$600 billion in 2010, and the incidence of AD throughout the world is expected to double in the next 20 years. There is a pressing need to find biomarkers to both predict future clinical decline and for use as outcome measures in clinical trials of disease-modifying agents to facilitate phase II-III studies and foster the development of innovative drugs [2]. To this end, Alzheimer's Disease Neuroimaging Initiative (ADNI) was conceived at the beginning of the millennium and began as a North American multicenter collaborative effort funded by public and private interests in October 2004. Although special issues focused on North American ADNI have been published in *Alzheimer's and Dementia* [3] and *Neurobiology of Aging* [4] in addition to a number of other review articles [5–12], the purpose of this review is to provide a detailed and comprehensive overview of the approximately 200 papers that have been published as a direct result of ADNI in the first 6 years of its funding.

1.2. Disease model and progression

One approach toward a greater understanding of the events that occur in AD is the formulation of a disease model [3,12–16]. According to the Aβ hypothesis, AD begins with the abnormal processing of the transmembrane Aβ precursor protein. Proteolysis of extracellular domains by sequential β and γ secretases result in a family of peptides that form predominantly β-sheets, the β-amyloids (Aβ) (Fig. 1). The more insoluble of these peptides, mostly Aβ42, have a propensity for self-aggregation into fibrils that form the senile plaques characteristic of AD pathology. Subsequently, it is thought that the microtubule-associated tau protein in neurons becomes abnormally hyperphosphorylated and forms neurofibrillary tangles that disrupt neurons. However, although ADNI and other biomarker data support this sequence of events, by direct examination of postmortem human brains, Braak and Del Tredici have shown that tau pathology in the medial temporal limbic isocortex precedes the development of Aβ deposits with advancing age in the human brain [17]. Downstream processes such as oxidative and inflammatory stress contribute to loss of synaptic and neuronal integrity, and eventually, neuron loss
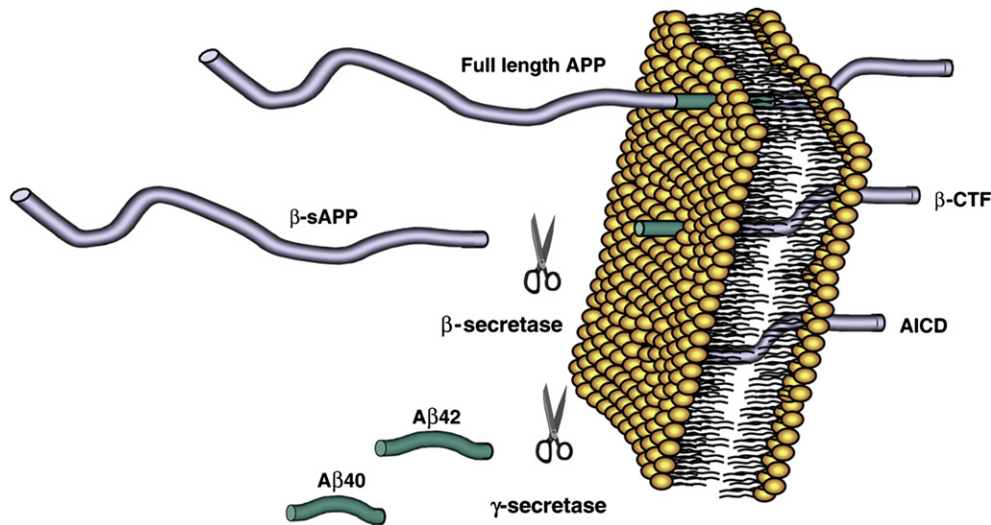
Fig. 1. Generation of soluble β-amyloid (Aβ) fragments from amyloid precursor protein. Reproduced with permission from Ref [7].

results in brain atrophy. Jack et al [14,16] presented a hypothetical model for biomarker dynamics in AD pathogenesis. The model begins with the abnormal deposition of Aβ fibrils, as evidenced by a corresponding drop in the levels of soluble Aβ42 in cerebrospinal fluid (CSF) and increased retention of the positron emission tomography (PET) radioactive tracer [^{11}C]-labeled Pittsburgh compound B (^{11}C-PiB) in the cortex. Sometime later, neuronal damage begins to occur, as evidenced by increased levels of CSF tau protein. Synaptic dysfunction follows, resulting in decreased [^{18}F]-fluorodeoxyglucose (FDG) uptake measured by PET. As neuronal degeneration progresses, atrophy in certain areas typical of AD becomes detectable by magnetic resonance imaging (MRI). The model provided by Jack et al [14] is highly relevant to many papers reviewed in section 4 (Studies of the ADNI cohort), which often provide empirical evidence to support it. An example of a model that proposes a series of pathological events leading to cognitive impairment and dementia is summarized in Fig. 2.

1.3. Mild cognitive impairment

Similar to many disease processes that originate in microscopic environments and are asymptomatic until the start of organ failure, the course of AD pathology is likely to be 20 to 30 years. It is now generally accepted that the initial AD pathology develops in situ while the patient is cognitively normal, sometimes termed the "preclinical stage" [18,19]. At some point in time, sufficient brain damage accumulates to result in cognitive symptoms and impairment. Originally defined in 1999, this has been classified in a number of ways, including as predementia AD or as mild cognitive impairment (MCI), a condition in which subjects are usually only mildly impaired in memory with relative preservation of other cognitive domains and functional activities and do not meet the criteria for dementia [5], or

as the prodromal state AD [18]. Epidemiological studies of participants aged 70 to 89 years who were nondemented found the prevalence of MCI in this population to be approximately 15%, with an approximate 2:1 ratio of two identified phenotypes, amnestic and nonamnestic [20,21]. Studies showed that MCI patients progressed to AD at a yearly rate of 10% to 15%, and that predictors of this conversion included whether the patient was a carrier of the ε4 allele of the apolipoprotein E (APOE) gene, clinical severity, brain atrophy, certain patterns of CSF biomarkers and of cerebral glucose metabolism, and Aβ deposition [5].

1.4. History of biomarker development

Although the etiology of AD was not known, there was sufficient knowledge of the mechanisms of AD pathology at the beginning of the past decade to allow the development of new drugs. Once transgenic mice expressing Aβ in their brains were available [22], development of treatments to slow the progression of AD began in earnest. Although considerable work had been done to develop quantitative measurements of cognitive function and activities of daily living for clinical trials of symptomatic treatments such as acetylcholinesterase inhibitors, it was recognized that changes in cognition did not necessarily signify "disease modification." Therefore, investigators from academia and the pharmaceutical industry became interested in how "disease modification" of AD could be detected using a variety of biomarkers, including brain MRI scanning, and blood and CSF analytes. This led to a decision by the National Institute on Aging (NIA) to fund the ADNI and to structure it as a public–private partnership.

The development of AD biomarkers for clinical trials, both for use in subject selection and as outcome measures, is paramount to the success of ADNI. During the genesis of the initiative, Frank et al [23] described the importance of biomarkers to ADNI and to clinical trials. In the first paper to come out of ADNI, Trojanowski [24] reviewed candidate
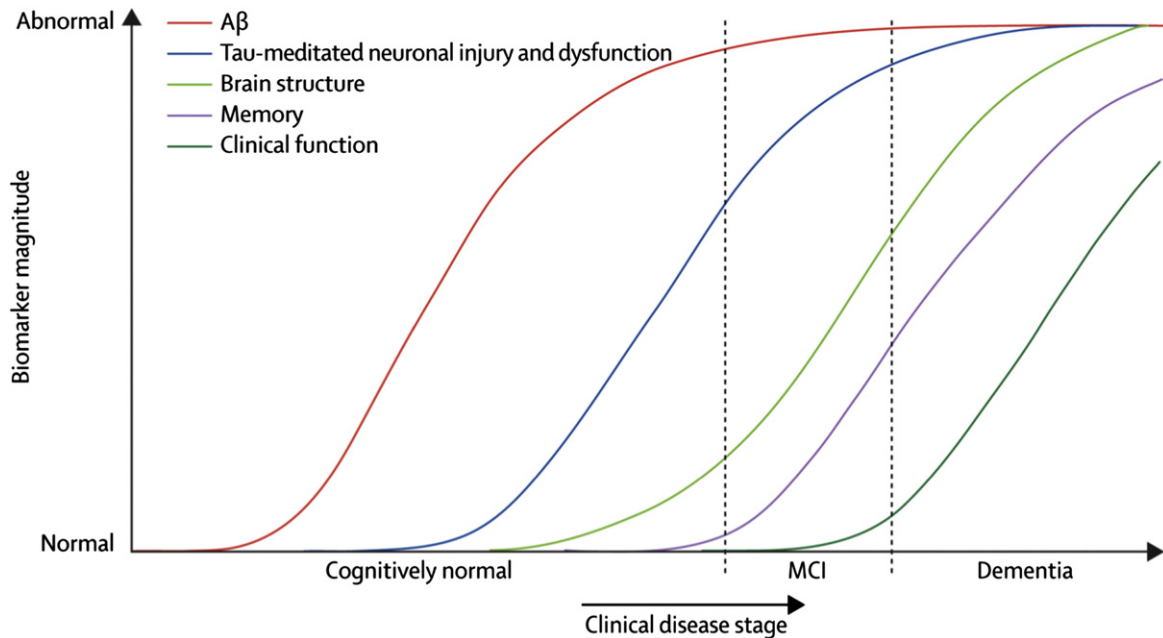
Fig. 2. Model for Alzheimer's disease (AD) progression. Reproduced with permission from Ref [14].

AD biofluid biomarkers thought to be most promising at the time, homocysteine, isoprostanes, sulfatide, tau, and Aβ, and described how ADNI was poised, as a large public–private collaboration, to identify and validate the best candidate AD biomarkers. Mueller et al [25] reported on the scientific background at the beginning of ADNI and the limitations of the clinical and neuropsychological tests available for monitoring disease progression at that time. Principally, a definitive diagnosis of AD required severe cognitive deficits and autopsy confirmation, whereas the clinical criteria for the detection of the MCI transitional phase were much less certain. Accordingly, outcome measures for assessing the efficacy of new drugs relied primarily on neurocognitive tests such as ADAS-cog (cognitive subscale of the Alzheimer's Disease Assessment Scale), the efficacy of which was limited by substantial ceiling effects and variability in subject performance over time. There was a clear need to develop biomarkers, biological tools that "mark" the presence of pathology, for the early diagnosis of AD and for measuring clinical drug trial outcomes [8].

Relatively early in the initiative, a major concern was developing an AD biomarker that distinguished AD from other dementias, such as Lewy body dementia, frontotemporal degeneration, and Parkinson disease with dementia [10]. Based on a model of AD pathogenesis fundamentally similar to that described in the paper by Jack et al [14], Shaw et al [10] reviewed a number of potential biomarkers, including some, such as isoprostanes and total plasma homocysteine, that did not subsequently prove to be of use. Others, such as levels of soluble Aβ42 or tau protein in CSF, reflected the increase in deposition of Aβ in fibrillar plaques or the later release of tau protein as a result of neuronal damage. Neuronal metabolism and neuronal degeneration could be mea-

sured using FDG-PET and by examining the concentrations of total tau protein (t-tau) and tau phosphorylated at serine 181 (p-tau$_{181p}$) in CSF, respectively. Volumetric changes to brain structure could be assessed by MRI of specific regions such as the hippocampus, entorhinal cortex, temporal and parietal lobes, and ventricles. Additional potential risk biomarkers included genetic susceptibility factors, such as the *APOE* genotype, plasma homocysteine levels, and isoprostanes as non-AD-specific indicators of oxidative stress. By the following year, the wide range of potential biomarkers had been substantially narrowed to include CSF Aβ42, t-tau and p-tau$_{181p}$ hippocampal volume, voxel-based volumetry, deformation-based morphometry (DBM), functional MRI, and FDG-PET [26]. In tandem with the development of these biomarkers, a new imaging technology using ^{11}C-PiB in PET scans was being developed [27,28], and the possibility of a diagnostic approach predicated on the concept of certain combinations of biomarkers providing complementary information was raised [8,26].

In 2008, twin reviews were published in *Neurosignals* [8,15] by members of the ADNI Biomarker Core at the University of Pennsylvania. The first paper reviewed potential biomarkers for the early detection of AD. In addition to the potential biomarkers described previously, these included MRI T$_1$ρ relaxation times to image neuritic plaques and single-photon emission computed tomography (SPECT) using a ^{125}I-labeled imidazole derivative (6-iodo-2-(4'-dimethylamino-)phenyl-imidazo[1,2]pyridine) as an alternative approach to amyloid PET imaging [29]. The second paper distinguished between diagnostic biomarkers and risk biomarkers, such as the *APOE* ε4 allele and plasma total homocysteine levels, suggesting that although they were not sufficiently sensitive for diagnostic purposes, they were

indicative of increased risk for AD and were predictive of disease progression. Finally, in 2010, Hampel et al [7] presented a review that updated our current understanding of tau and Aβ biomarkers, including levels of Aβ42 and activity of BACE1 (the major amyloid precursor protein-cleaving β-secretase in the brain) in CSF, blood plasma levels of Aβ40 and Aβ42, and human antibodies against Aβ-related proteins. Thus, the search for biomarkers to fulfill a variety of niches is an ongoing quest and is without doubt set to evolve even further as research progresses.

1.5. Goals of ADNI

A comprehensive description of the goals of ADNI is given in papers by Mueller et al [2] and Weiner et al [3]. At initiation, ADNI had the overall objective of characterizing clinical, genetic, imaging, and biochemical biomarkers of AD and identifying the relationships between them over the course of disease progression from normal cognition to MCI to dementia. Specific goals of ADNI included the development of optimized and standardized methods for use across multiple centers, the enrollment of a large cohort (>800) of healthy elderly subjects, MCI patients, and AD patients for baseline characterization and longitudinal studies, and the establishment of repositories of data and biological samples, both of which were to be accessible to the wider scientific community without embargo. A specific pre-specified goal was to identify those imaging (MRI and PET) and image analysis techniques and blood/CSF biomarkers that had the highest statistical power to measure change (defined as the sample size required to detect a 25% reduction of rate of change in 1 year) and thus, it was hoped, detect effects of treatments that would slow the progression of AD. With these goals, ADNI hoped to identify a combination of biomarkers that could act as a signature for a more accurate and earlier diagnosis of AD, and that could be used to monitor the effects of AD treatment [2,3].

When originally conceived, ADNI had not included aims around genetic or proteomic analysis. Additional add-on studies supported the evolution of the Genetics Core (see later in the text) and the study of protein changes in plasma and CSF. Plasma proteomic data from a 190-analyte multiplex panel have been posted to the ADNI Web site and are available for additional data mining.

1.6. The evolution of an idea: ADNI-1, ADNI Grand Opportunities, and ADNI-2

Drs. Neil Buckholz and William Potter had discussed the overall concept of a large biomarker project to study AD for many years. Dr. Buckholz convened an NIA meeting focused on AD biomarkers in 2000. In 2001, Drs. Michael Weiner and Leon Thal (since deceased) proposed a longitudinal MRI study of AD, MCI, and control subjects. Subsequently, Dr. Buckholz brought together a number of investigators from the field of AD as well as industry leaders, all of whom strongly supported the overall concept. The NIA published a Request for Applications, and ADNI was funded in 2004. The initial ADNI was projected to run for 5 years and to collect serial information, every 6 months, on cognitive performance; brain structural and metabolic changes; and biochemical changes in blood, CSF, and urine in a cohort of 200 elderly control subjects, 200 MCI patients, and 400 AD patients [2–4]. It was funded as a public–private partnership, with $40 million from the NIA and $27 million from 20 companies in the pharmaceutical industry and 2 foundations for a total of $67 million, with the funds from private partners provided through the Foundation for the National Institutes of Health. An interesting perspective of the process by which potential competitors in the race to develop new drugs for AD were brought together in a consortium under the auspices of the Foundation for the National Institutes of Health is given in the paper by Schmidt et al [30], who emphasize the importance of the cooperative, precompetitive nature of ADNI. When the ADNI grant was first submitted and funded, the significance and impact of ^{11}C-PiB [27,28] studies were not fully appreciated, and there was no infrastructure to conduct multisite clinical trials with ^{11}C-PiB. Therefore, Aβ imaging with ^{11}C-PiB was not included in the application. However, after the first year of funding, Chet Mathis proposed adding an ^{11}C-PiB substudy to ADNI, which was funded by the Alzheimer's Association and General Electric. In addition, further industry and foundation funding was secured to allow supplemental or "add-on" genomewide association studies (GWAS), and for additional lumbar punctures to obtain CSF, as new technologies emerged to make these studies feasible in a large-scale initiative such as ADNI.

In 2009, toward the end of the ADNI study, a Grand Opportunities grant, ADNI-GO, was secured to extend the original ADNI-1 studies with both longitudinal studies of the existing cohort and the enrollment of a new cohort of early MCI patients to investigate the relationship between biomarkers at an earlier stage of disease progression. Technical advances made it possible to add analyses of the new cohorts using AV45 (Florbetapir; Eli Lilly, Indianapolis, IN) amyloid imaging. Additional experimental MRI sequences included for evaluation of ADNI-GO and ADNI-2 are arterial spin labeling perfusion imaging and diffusion tensor imaging. The development of the [^{18}F]-labeled AV45 amyloid imaging agent with a substantially longer radioactive half-life than the ^{11}C form made it practicable to extend amyloid imaging studies to additional sites beyond those undertaken in ADNI-1 [7].

A competitive renewal of the ADNI-1 grant, ADNI-2, was awarded with total funding of $69 million on October 1, 2010, together with funding from the pharmaceutical industry in a cooperative agreement similar to the original initiative, to further extend these studies with additional cohorts [3,4,31]. It is anticipated that the study of very mild MCI patients in ADNI-GO and ADNI-2 will help identify subjects at risk who are candidates for preventative

therapy when they are mildly symptomatic or asymptomatic [30]. Table 1 summarizes details of the three initiatives.

1.7. Structure and organization of ADNI

A full description of ADNI structure is given in the paper by Weiner et al [3]. Briefly, ADNI is governed by a Steering Committee that includes representatives from all funding sources as well as principal investigators of the ADNI sites and is organized as eight cores, each with different responsibilities, under the direction of an Administrative Core, led by Dr. Weiner, as well as a Data and Publications Committee (DPC), led by Dr. Green (Fig. 3). The eight cores comprise (1) the Clinical Core, led by Drs. Aisen and Petersen, responsible for subject recruitment, collection and quality control of clinical and neuropsychological data, testing clinical hypotheses, and maintaining databases; (2) the MRI and (3) PET Cores, led by Drs. Jack and Jagust, respectively, responsible for developing imaging methods, ensuring qual-

ity control between neuroimaging centers, and testing imaging hypotheses; (4) the Biomarker Core, led by Drs. Shaw and Trojanowski, responsible for the receipt, storage, and analysis of biological samples; (5) the Genetics Core, led by Dr. Saykin, responsible for genetic characterization and analysis of participants as well as banking DNA, RNA, and immortalized cell lines at the National Cell Repository for Alzheimer's Disease; (6) the Neuropathology Core, led by Drs. Morris and Cairn, responsible for analyzing brain pathology obtained at autopsies of ADNI participants; (7) the Biostatistics Core, led by Dr. Beckett, responsible for statistical analyses of ADNI data; and (8) the Informatics Core, led by Dr. Toga, responsible for managing data sharing functions [2,3]. A schematic of ADNI structure is given in Fig. 3.

1.8. Data sharing and informatics

An objective of ADNI, in addition to its scientific goals outlined in section 1.5, was to make data available to the

Table 1
Comparison of ADNI-1, ADNI-GO, and ADNI-2

Study characteristics	ADNI-1	ADNI-GO	ADNI-2
Primary goal	Develop CSF/blood and imaging biomarkers as outcome measures	Act as bridging grant between ADNI-1 and ADNI-2, examine biomarkers in earlier stage of disease progression	Develop CSF/blood and imaging biomarkers as predictors of cognitive decline, and as outcome measures
Funding	$40 million federal (NIA), $20 million industry and foundation, $7 million industry for supplemental studies	$24 million American Recovery Act funds (stimulus finds)	$40 million federal (NIA), $27 million expected industry and foundation
Duration/start date	5 years/October 2004	2 years/September 2009	5 years/September 2011
Cohort	200 elderly control subjects 200 MCI 400 AD	Existing ADNI-1 cohort plus: 200 EMCI	Existing ADNI-1 and ADNI-GO cohort plus: 150 elderly control subjects 100 EMCI 150 MCI 150 AD
Study techniques			
MRI	X	X	X
fMRI		X	X
FLAIR (microhemorrhage detection)		X	X
T2* GRE (microhemorrhage detection)		X	X
Vendor-specific protocols (1) resting state (task-free) fMRI to Phillips systems, (2) perfusion imaging (ASL) to Siemens, and (3) DTI to General Electric		X	X
FDG-PET	X	X	X
AV45		X	X
Biosamples	X	X	X
"Add-on" studies	GWAS, PiB-PET, lumbar puncture		

Abbreviations: ADNI, Alzheimer's Disease Neuroimaging Initiative; ADNI-GO, Grand Opportunities grant; CSF, cerebrospinal fluid; NIA, National Institute on Aging; MCI, mild cognitive impairment; AD, Alzheimer's disease; EMCI, early mild cognitive impairment; MRI, magnetic resonance imaging; fMRI, functional magnetic resonance imaging; FLAIR, fluid attentuated inversion recovery; T2* GRE, T2* gradient echo; ASL, arterial spin labeling; DTI, diffusion tensor imaging; FDG-PET, [18F]-fluorodeoxyglucose-positron emission tomography; GWAS, genomewide association studies; PiB-PET, Pittsburgh compound B-positron emission tomography.
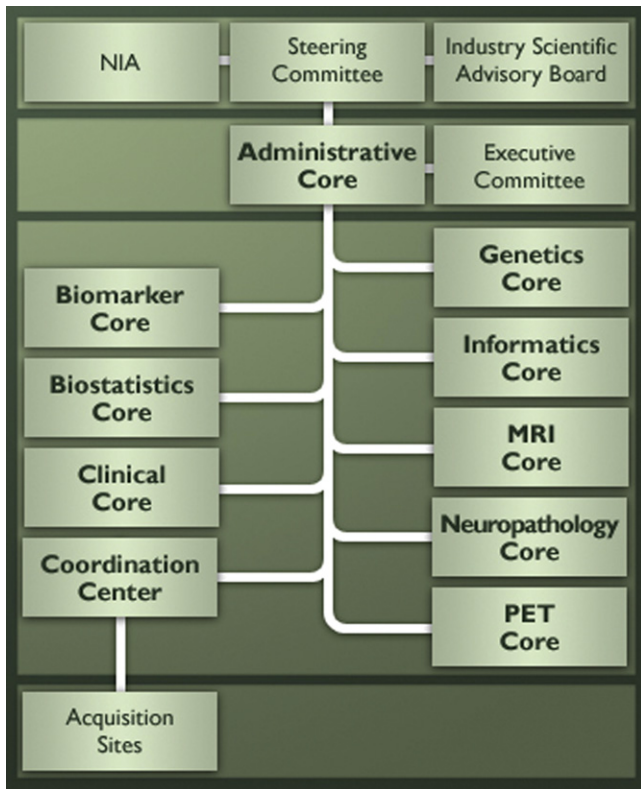
Fig. 3. Alzheimer's Disease Neuroimaging Initiative (ADNI) structure and organization.

scientific community, without embargo. To this end, DPC, in conjunction with the Bioinformatics Core of ADNI at the Laboratory of Neuroimaging (LONI) at UCLA, has developed policies and procedures for immediate, open-access data sharing on a previously unprecedented scale. The principles for this data sharing were developed in the initial months of the ADNI project by the DPC in consultation with the Executive Committee and presented to the Steering Committee for adoption in the first year. The infrastructure for implementing this policy is through the LONI data archive (LDA), enabling the widespread sharing of imaging, clinical, genetics, and proteomic ADNI results, while overcoming fundamental hurdles such as the question of ownership of the disseminated scientific data, and the collection of data from multiple sites in a form that supports data analysis [32]. Briefly, LONI has developed automated systems that deidentify and upload data from the 57 ADNI sites, ensure quality control of images before removing them from quarantine status and make them available for download, manage preprocessing and postprocessing of images and their linkage to associated metadata, support search functions, and manage user access and approval. Clinical data are collected by the Alzheimer's Disease Cooperative Study through their online data capture system and transferred to the ADNI repository at LONI through nightly data transfers. After these data are received at LONI, portions of the clinical data are used to update data in the ADNI repository to ensure consistency of demographic and examination data and to update the status of image data based on quality assessment results. Additional nightly processes integrate other clinical data elements, so they may be used in querying the data in the repository. Any researcher who has been granted access to ADNI data is able to analyze any part of the available data and can post results to LONI. In addition to ADNI data, LDA also contains data from the parallel Australian Imaging Biomarkers and Lifestyle (AIBL) Flagship Study of Ageing, which were collected using protocols comparable with those of ADNI. To date, from 35 countries worldwide, more than 1300 investigators from academic and governmental institutions, the pharmaceutical and biotechnology industries, and the scanner manufacturing sector have accessed ADNI data through the LDA [32]. The number of downloads of ADNI data has increased yearly since 2006, and in 2010, more than 400,000 images, 1416 sets of clinical data (including cognitive tests and levels of CSF biomarkers), 781 numeric summary results for all analyses, and 33,620 genetic single-nucleotide polymorphism (SNP) results were downloaded.

Although LONI acts as the ADNI data repository, the DPC is responsible for developing policy around data access and publication, granting access to the data to investigators around the world, and reviewing publications that result from this data use. Briefly, members of the scientific community can apply for access to ADNI data for either research or teaching purposes and must submit a data use agreement (available at: http://adni.loni.ucla.edu/wp-content/uploads/how_to_apply/ADNI_Data_Use_Agreement.pdf) for approval. As of April 2011, 1590 data applications from across the world had been approved, predominantly from academia, but also from the biotechnology, pharmaceutical, and other industries. Part of the data use agreement requires applicants to include certain language in manuscripts prepared from ADNI data, including citing "for the Alzheimer's Disease Neuroimaging Initiative" as an ADNI group acknowledgment, and the recognition of ADNI's role in data gathering in the Methods section and of ADNI's funding in the Acknowledgments. Manuscripts must be submitted for approval to the DPC before publication. The full publication policy can be found at: http://adni.loni.ucla.edu/wp-content/uploads/how_to_apply/ADNI_DSP_Policy.pdf. The role of the DPC in this step is primarily to check that manuscripts are compliant with ADNI publication policy, and not to provide a scientific peer review. Papers found to be noncompliant are returned to the authors for editing and can subsequently be resubmitted for approval. This process is primarily designed to track, tabulate, and standardize the publication of manuscripts using ADNI data.

1.9. The ADNI special issue of Alzheimer's and Dementia

Weiner et al [3] introduced the special ADNI issue of *Alzheimer's and Dementia* in 2010 with an overview of ADNI's background, rationale, goals, structure, methods, impact, and future directions. A set of papers followed highlighting the achievements of individual ADNI cores and perspectives of

the Industry Scientific Advisory Board (or ISAB), which is now referred to as the Private Partner Scientific Board (or PPSB). Jack et al [33] described the achievements of the MRI Core of ADNI in areas ranging from the development of MRI technology to the elucidation of AD biology, and concluded that this Core had succeeded in demonstrating the feasibility of multicenter MRI studies in ADNI and validity of this method as a biomarker in clinical trials. The progress of the PET Core of ADNI in developing FDG-PET and ^{11}C-PiB PET protocols, ensuring quality control, and acquiring and analyzing longitudinal data was reviewed by Jagust et al [34], who similarly concluded that the Core had successfully demonstrated both the feasibility of this technology in a multicenter setting and the potential of FDG-PET to reduce sample sizes in clinical trials. Trojanowski et al [12] reviewed progress by the Biomarker Core of ADNI in developing profiles of CSF or plasma biomarkers that would act as a "signature" of mild AD or predict future MCI to AD conversion. Moreover, the review described studies in support of a temporal sequence of changes in individual biomarkers that reflected proposed trajectories of Aβ deposition and the formation of neurofibrillary tangles in AD progression [14]. The accomplishments of the Clinical Core of ADNI were reviewed by Aisen et al [35], who reported that the Core had successfully recruited a cohort of >800 subjects, characterizing them both clinically and cognitively at baseline and following them longitudinally over the course of the study. As the Clinical Core provided data management support to ADNI, this review also reported on the contribution of ADNI biomarker and MRI findings to improving clinical trial design by determining the most powerful outcome measures and reducing sample size using subject selection strategies. The contribution of the Genetics Core of ADNI to untangling the apparently complex genetic contributions to AD was reviewed by Saykin et al [6], who reported considerable progress in the identification of novel AD susceptibility loci and of candidate loci worthy of further investigation, often using AD biomarkers as quantitative traits (QTs) in imaging genetics and GWAS. The role of the Neuropathology Core in developing procedures to improve the autopsy rate of ADNI patients and to standardize neuropathological assessment was reviewed by Cairns et al [36]. Finally, Schmidt et al [30] discussed the contributions of the Industry Scientific Advisory Board, including acting as a conduit of information to and from sponsoring companies and foundations, supporting add-on studies, and contributing to the scientific review of protocols and procedures.

2. Development and assessment of treatments for AD: Perspectives of academia and the pharmaceutical industry

Given that the ultimate goal of ADNI is to develop biomarkers to facilitate clinical trials of AD therapeutics, it is germane to consider the perspective of investigators from academia and the pharmaceutical industry on the development of these biomarkers. The aim of this section is to review those papers that focus on this issue.

Although ADNI is a natural history study, and it is not known whether its biomarkers can measure the effect of candidate treatments in drug trials, the primary focus of ADNI has been the development of diagnostic biomarkers for the early detection of AD and development of prognostic biomarkers that would be used to monitor disease progression [37]. Mueller et al [38] and Weiner et al [3] reaffirmed the definition of an ideal biomarker formulated at the first meeting of the NIA working group on AD biomarkers, which proposed that an ideal AD biomarker should detect a fundamental feature of AD pathology; be minimally invasive, simple to analyze, and inexpensive; and meet criteria with regard to specificity and sensitivity outlined in Table 2. Prognostic biomarkers should be representative of a stage of AD at which the treatment has maximal effect, and also be representative of the proposed mechanism of action of the treatment [3,38].

Both diagnostic and prognostic biomarkers are required for clinical trials. To date, such clinical trials have been frustratingly unsuccessful. It was thought that the failures of phase III clinical trials of high-profile putative antiamyloid therapies, flurizan and Alzhemed, were in part due to methodological difficulties, such as the initial subject selection, and the statistical comparison of results from multiple centers [7,9,39]. In the case of the first generation of clinical trials focusing on patients with MCI, there was a lack of consistency in numbers of patients progressing to AD over a certain period, likely due to the heterogeneous nature of MCI; it is possible that one-half of study participants did not have underlying AD pathology [7,11,40]. Correctly distinguishing patients with AD pathology is critical, especially considering the overlap that exists between various late-life neurodegenerative pathologies. For example, the Lewy bodies that characterize Parkinson's disease are found in >50% of patients with AD, in addition to neuritic plaques and tangles. Therefore, there is a real need for biomarkers that reliably distinguish between different types of dementias [8,10].

Diagnostic biomarkers that meet the criteria outlined previously are urgently needed for subject selection, thereby

Table 2
Characteristics of an ideal biomarker

Characteristic	Ideal
Sensitivity: % of patients correctly identified as having AD	>80%–85%
Specificity: % of patients correctly identified as not having AD.	>80%
Positive predictive value: % of patients who are positive for biomarker and have definite AD pathology at autopsy	>80%
Negative predictive value: % of patients who, at autopsy, prove not to have the disease	>80%

NOTE. Adapted from Refs [7] and [10].

allowing the stratification and enrichment of clinical trials. There is a need to select subjects at an early stage of the Alzheimer's continuum who are likely to progress through MCI to dementia, and also to eliminate subjects with other pathologies. In phase I, II, and III trials, biomarkers that detect the earliest indications of AD pathology, Aβ deposition, such as CSF Aβ42, and ^{11}C-PiB PET are most likely to be useful. FDG-PET as a measure of metabolism could also have potential [41].

The biomarkers used in a clinical trial will differ depending on the mechanism of action of the therapeutic, the goals of the trial, and questions at hand. In small, short phase I trials, CSF and plasma measures can be used to monitor Aβ turnover in healthy subjects. In phase II proof-of-principle or proof-of-concept trials, Aβ biomarkers in brain can be used to confirm the mechanism of action of a new treatment and "target engagement." For phase II and III trials, CSF tau and phosphorylated tau, MRI, and Aβ PET can be used to determine whether there is evidence of an effect of treatment on disease progression. Clinical MRI is used routinely for subject selection, to exclude confounding medical conditions, and for detection of vasogenic edema as a safety end point of "immune"-based treatments [41]. Finally, Aβ PET imaging, MRI, CSF and plasma biomarkers, and FDG-PET are candidates as prognostic biomarkers in phase II trials for selection of nondemented subjects at risk for developing AD to test whether treatments have the potential of preventing or delaying the onset of AD. The predictive power of these biomarkers in isolation or in combination varies and will need to be factored into consideration. None of the current generation of treatments proposed to modify the progression of AD is free of safety concerns. Estimation of the probability of developing AD will be required for assessing the risk versus possible benefit of participating in research trials [41]. Figure 4 shows ADNI biomarkers that could be used at different stages of the drug development process.

Looking at drug development as a whole, Cummings [37] saw a wide variety of roles for biomarkers, from identifying disease pathology and tracking disease progression, to demonstrating pharmacokinetic effects of the body on the drug, to facilitating proof-of-principle and determining doses for subsequent trials, to determining drug efficacy, and, finally, to contributing to corporate decision making, such as whether to proceed with riskier and more expensive later-phase trials (Fig. 5). Fleisher et al [9] reviewed progress in developing neuroimaging biomarkers, either alone or in conjunction with CSF biomarkers, for subject selection, and in developing biomarkers functioning at later stages in disease, such as MRI measures of brain atrophy or changes in cerebral glucose metabolism detected by FDG-PET as outcome measures. This review also highlighted the need for biomarkers in drug development and discussed the use of imaging biomarkers in replacing cognitive end points in clinical trials.

Both common sense and regulatory policies of the Food and Drug Administration (FDA) and regulators in other countries require that treatment trials need to demonstrate a significant effect on cognition and function. Although effects on biomarkers would provide additional evidence of treatment effect and evidence of disease modification, there are no validated surrogates for AD trials, and such surrogates will take many years to develop. Different biomarkers are likely to be effective over different phases of the disease [11,41]. To be used as surrogates for clinical measures, biomarkers would need to be validated as reflecting clinical and/or pathological disease processes with a high degree of specificity and sensitivity. To qualify for validation as an outcome measure, the biomarker must be shown to predict clinical outcome over several trials and several classes of relevant agents by following subjects through disease progression and even possibly to autopsy [3,9,37]. This validation process is likely to be aided by the contribution of ADNI to standardizing procedures, particularly for imaging techniques, to reduce measurement errors in clinical trials [42]. A review by Petersen and Jack [11] discussed neuroimaging and chemical biomarkers, either alone or in combination, for the prediction of the development of dementia in MCI patients. These authors provided an excellent and succinct summary of the issues facing clinical trials for AD-modifying drugs and the role of both U.S. and worldwide ADNI in developing biomarkers to facilitate these trials.
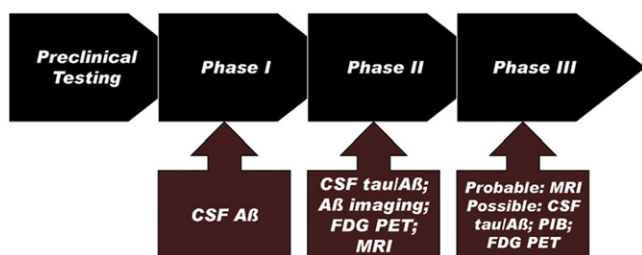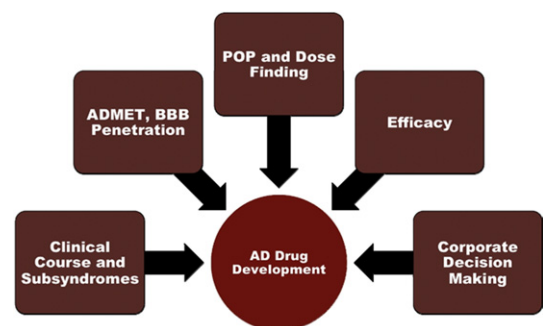

Fig. 4. AD drug development. Black arrows show the phases of drug development; the brick-colored arrows show the ADNI biomarkers that could be used in that stage. Reproduced with permission from Ref [37].

Fig. 5. Roles of biomarkers in AD drug development. Abbreviations: ADMET, absorption, distribution, metabolism, excretion, toxicity; BBB, blood–brain barrier; POP, proof of principle. Reproduced with permission from Ref [37].

A detailed discussion of the position of the FDA on biomarker validation is given by Carrillo et al [31], and it is likely that the process will require a wider population of well-characterized subjects than is available through ADNI. To this end, and for the further study of therapeutic interventions for AD, Petersen [40] proposed the establishment of a national registry of aging. In their editorial in the *Journal of the American Medical Association*, Petersen and Trojanowski [39] introduced a paper that reports on the evaluation of CSF biomarkers in a large multicenter study. Placing this in the context of other work in the same area, and in research undertaken as part of ADNI, they concluded that as biomarkers become more sophisticated, they will play even greater roles in AD clinical trials, and may one day be of use in clinical practice in a diagnostic capacity. Hill [41] concluded in his perspective on neuroimaging and its role in assessing safety and efficacy of disease-modifying therapies for AD: "….there is now sufficient experience of imaging for Alzheimer's disease in both natural history and therapeutic trials for a clear recipe for success to be emerging." Weiner [43] concluded that the use of biomarkers to select cognitively normal subjects who have AD-like pathology and as validated outcome measures in clinical trials "is the path to the prevention of AD."

ADNI has proven to be a rich data set for industry-sponsored research, including an assessment of disease progression in the AD population [44]. ADNI data have been combined with additional placebo data from clinical trials conducted in AD and are publicly available on the Coalition Against Major Disease Web site (http://www.c-path.org/CAMDcodr.cfm) for additional data mining. Modeling efforts have highlighted the importance of age, baseline cognitive status, and *APOE* status on disease progression rates; a model is currently under qualification review through newly developed European Medicines Agency (EMA) and FDA qualification procedures. These types of models will inform clinical trial design and streamline analysis for drug studies conducted in mild-to-moderate AD.

ADNI has also enabled clinical studies in predementia, and many have been posted to www.clinicaltrials.gov, highlighting the use of CSF and amyloid PET biomarkers in cognitively impaired subjects to enrich for predementia clinical trials. Application to registration-level, phase III studies remains a challenge, as the biomarkers in ADNI have not yet been qualified for use or received regulatory approval. To address some of the remaining challenges, precompetitive and industry-sponsored initiatives were recently conducted to qualify CSF Aβ-42 and t-tau as biomarkers for enrichment in predementia study with the EMA, and a positive qualification opinion was posted on the EMA site for these particular biomarkers. Additional efforts are ongoing with the FDA. For the most part, industry has been using the biomarkers as enrichment tools in predementia and mild-to-moderate AD studies, and as secondary or exploratory efficacy measures to assess impact of exploratory drugs on biomarker measures of disease progression.

3. Methods papers

A considerable proportion of papers published as a result of ADNI concerns the development and testing of methods for use in ADNI, in the cohorts of other studies, or in clinical trials. These run the gamut from papers examining the best way to reduce differences between scanners in multicenter studies to those describing a new way to discriminate between AD, MCI, and control subjects, to methods for enriching clinical trials to reduce required sample sizes and therefore the associated cost, to new methods for examining genotype–phenotype relationships in neuroimaging GWAS. This section presents an overview of these papers.

3.1. Standardization of ADNI procedures

3.1.1. Magnetic resonance imaging

3.1.1.1. Assessment of scanner reliability

A key feature of assessing the reliability of scanner hardware over longitudinal scans is the use of a high-resolution geometric "phantom" that can detect linear and nonlinear spatial distortion, signal-to-noise ratio, and image contrast, allowing these artifactual problems to be identified and subsequently eliminated. Although these are commonly used for periodic adjustments to quality control, they are scanned after every patient in the ADNI MRI protocol. Gunter et al [45] estimated that these artifactual problems would contribute to >25% imprecision in the metric used, and found that phantom analysis helped correct scanner scaling errors and/or miscalibration, thereby increasing the potential statistical power of structural MRI for measuring rates of change in brain structure in clinical trials of AD-modifying agents. The utility of a scanner phantom was once again underscored by Kruggel et al [46], who examined the influence of scanner hardware and imaging protocol on the variability of morphometric measures longitudinally and also across scanners in the absence of a phantom in a large data set from the ADNI cohort. Using different acquisition conditions on the same subject, the variance in volumetric measures was up to 10 times higher than under the sample acquisition conditions, which were found to be sufficient to track changes. Their results suggested that the use of a phantom could reduce between-scanner imaging artifacts in longitudinal studies. Kruggel et al [46] also investigated the effect of scanner strength and the type of coil used on image quality and found that a 3.0-T array coil system was optimal in terms of image quality and contrast between white matter (WM) and gray matter (GM). Ho et al [47] similarly tested the ability of 3.0-T and 1.5-T scanners to track longitudinal atrophy in AD and MCI patients using tensor-based morphometry (TBM). They saw no significant difference on the ability of either scanner type to detect neurodegenerative changes over a year, and found that TBM used at both field strengths gave excellent power to detect temporal lobe atrophy longitudinally.

While the scanning of a geometric phantom helps eliminate artifacts introduced by the machine, Mortamet et al [48] described an automated method for accounting for patient artifacts that can affect image quality, such as edge, flow, and aliasing artifacts. They developed two quality indices and tested their ability to differentiate between high- and low-quality scans, as assigned by an expert reader at the ADNI MRI center. Both indices accurately predicted the "gold standard" quality ratings (sensitivity and specificity >85%), and the authors proposed that this method could be integrated into a real-time or online MRI scanning protocol to eliminate the need to rescan at a later date due to a poor-quality scan, in keeping with the goal of placing as minimal burden on the patient as possible. Clarkson et al [49] examined within-scanner geometric scaling drift over serial MRI scans, as assessed by geometric phantoms, and developed a nine degrees-of-freedom registration algorithm to correct these scaling errors in longitudinal brain scans of patients. They found that the nine degrees-of-freedom registration was comparable with geometric phantom correction, allowing atrophy to be measured accurately, and the authors suggest that this registration-based scaling correction was the preferred method to correct for linear changes in gradient scaling over time on a given scanner. This in turn could obviate the need for scanning a phantom with every patient. Bauer et al [50] assessed the utility of collecting whole brain quantitative T2 MRI from multiple scanners using fast spin echo (FSE)/dual spin echo sequences, which have been shown to be useful in the early detection of AD pathology in MCI patients. Although FSE–T2 relaxation properties were related to the global dementia status, the authors concluded that the utility of the method was affected by the variability between scanners. Several papers were aimed at reducing between-scanner effects, including those by Gunter et al [45] and Clarkson et al [49]. Leung et al [51] presented a method aimed at overcoming variability in serial MRI scans for the detection of longitudinal atrophy by modifying the boundary shift integral (BSI) method of image analysis. Two improvements to the BSI method were made: (1) tissue-specific normalization was introduced to improve consistency over time, and (2) automated selection of BSI parameters was based on image-specific brain boundary contrast. The modified method, termed KN-BSI, had enhanced robustness and reproducibility and resulted in a reduction in the estimated sample sizes, required to see a 25% reduction in atrophy in clinical trials of AD-modifying drugs, from 120 to 81 AD patients (80% power, 5% significance).

3.1.1.2. Development of protocols

Jack et al [52] described the development of standardized MRI procedures for use in the multiple ADNI centers, a process guided by the principle of maximizing the scientific benefit of a scan while minimizing the burden on the patient. Using technology widely available in 2004 to 2005, and limiting scanner platforms to three vendors, they succeeded in developing a protocol that could be run

in <30 minutes and that included the use of a phantom scan to monitor scanner performance over time and across different centers, back-to-back T1-weighted magnetization-prepared rapid gradient echo scans to capture structural information while minimizing the need to rescan patients due to technical difficulties, and T2-weighted dual-contrast FSE sequences for the detection of pathologies. Postacquisition corrections were instituted to remove certain image artifacts. Serial MRI scans, such as those used in ADNI, often suffer from problems associated with the uniformity of signal intensity that introduce artifacts into the results. Boyes et al [53] tested the ability of nonparametric nonuniform intensity normalization (N3) to eliminate these artifacts on higher-field 3-T scanners, which had a newer generation of receiver coils, in serial 2-week scans of healthy elderly control subjects. They found that the robustness and reliability of the N3 correction were highly dependent on the selection of the correct mask to identify the region of the scan over which the N3 worked, and on the smoothing parameter used for head scans at different pulse sequences. Leow et al [54] also used serial scans, 2 weeks apart, of healthy elderly control subjects to investigate the stability of different pulse sequences. They used TBM to generate maps of computed changes that could be statistically analyzed and to give information on MRI reliability, reproducibility, and variability. This optimization of pulse sequences contributed to the design of the ADNI MRI protocol, and authors concluded that TBM is a useful tool for the study of longitudinal changes in brain structure.

3.1.2. Aβ- and FDG-PET

Variability across scanners is also a major factor in ADNI PET studies, which are spread over 50 different centers and involve 15 different scanner/software combinations. Joshi et al [55] tackled the problem of reducing between-scanner variability in PET images that has been observed despite the use of standardized protocols. Major sources of between-scanner variability are high-frequency differences, mostly related to image resolution, and low-frequency differences, mostly related to image uniformity and also to corrections for scatter and attenuation. Joshi et al [55] scanned a Hoffmann phantom at each participating center, and by comparing the scans to the Hoffman "gold standard" digital phantom, they developed corrections for both types of variability, which were tested on scans from the ADNI cohort. They found that the high-frequency correction, by smoothing all images to a common resolution, reduced interscanner variability by 20% to 50%, but that the low-frequency correction was ineffective, perhaps due to differences in geometry between the Hoffman phantom and the human brain. Jagust et al [34] reported the development of a standardized protocol for the acquisition of FDG-PET and ^{11}C-PiB PET data that first granted approval to participating sites based on the results from a pair of phantom scans on the three-dimensional (3-D) Hoffman brain phantom using defined acquisition and reconstruction parameters. These were

assessed for image resolution and uniformity using a quality control process that used the digital gold standard phantom for comparison. In this way, corrections were made for differences in PET images across sites.

3.1.3. Biomarkers

The measurement of CSF concentrations of Aβ-42, t-tau, and p-tau is recognized to reflect early AD pathology. Within ADNI, levels of these analytes are measured by flow cytometry using monoclonal antibodies provided in the INNO-BIA Alz Bio3 immunoassay kit (Innogenetics, Ghent, Belgium) with xMAP technology (Luminex, Austin, TX) [56,57]. The Biomarker Core of ADNI has worked to make this a standardized procedure across multiple ADNI sites, and Shaw et al [56] presented an analysis of within-site and intersite assay reliability across seven centers using aliquots of CSF from normal control subjects and AD patients. Five CSF pools were tested, each pool made up of either AD patients (n = 2) or controls (n = 3). Each center performed three analytical runs using separate fresh aliquots of each CSF sample and data were analyzed using mixed-effects modeling to determine assay precision. The coefficient of variation was 5.3% for Aβ-42, 6.7% for t-tau, and 10.8% for p-tau within center, and 17.9% for Aβ-42, 13.1% for t-tau, and 14.6% for p-tau between centers. The authors concluded that although they found good within-laboratory assay precision, the reason for the reduced interlaboratory precision is not fully understood and may be caused by many sources of variability.

3.2. Methods for MRI image preparation and processing

A large portion of ADNI research relies on the extraction of information from MRI images; therefore, the development of automated methods to reliably and robustly process thousands of scans from multiple centers is vital to the project. Processing steps include whole brain extraction, image registration, intensity normalization, tissue classification (segmentation), cortical thickness estimation, and brain atrophy estimation [58].

3.2.1. Whole brain extraction

The separation of brain from nonbrain voxels in neuroimaging data, known as whole brain extraction or "skull-stripping," is an important initial step in image analysis. Inaccuracies at this step can lead to the introduction of artifacts adversely affecting further analysis; therefore, a robust and accurate automated method for this step is highly desirable. To this end, Leung et al [58] compared the accuracy of a technique, multiatlas propagation and segmentation (MAPS), previously developed for hippocampal segmentation ([59]; see later section), with three other widely used automated brain extraction methods: brain extraction tool, hybrid watershed algorithm, and brain surface extractor. They found that compared with the semiautomated "gold standard" segmentation, MAPS was more accurate and reliable than the other methods and that its accuracy approached that of the gold standard, with a mean Jaccard index of 0.981 using 1.5-T scans and 0.980 using 3-T scans of control, MCI, and AD subjects.

3.2.2. Automated registration and segmentation

As manual registration and segmentation of images into WM, GM, and CSF is time-consuming, rater-dependent, and infeasible for a large study because of its often prohibitive cost, a number of studies have focused on developing automated registration and segmentation methods.

3.2.2.1. Atlas-based registration

Wolz et al [60] offered a solution in which atlases are automatically propagated to a large population of subjects using a manifold learned from a coordinate embedding system that selects similar images and reduces the potentially large deformation between dissimilar images, thereby reducing registration errors. This learning embeddings for atlas propagation method resulted in a more accurate segmentation of the hippocampus compared with other multiatlas methods [60].

The use of more than one atlas on which to register brain images has been recognized as a powerful way to increase accuracy of the automatic segmentation of T1-weighted MRI images, as it addresses the problem of brain variability. The steps of the process have been described by Lotjonen et al [61] and are presented in Fig. 6. Initially, multiple atlases are nonrigidly registered to the patient image, after which majority voting is applied to produce class labels for all voxels. Then, postprocessing by a variety of algorithms takes into account intensity distributions of different structures.

The addition of atlases has been found to increase segmentation accuracy in a logarithmic manner, that is, rapidly at first, but eventually slowing toward a maximum. This increased accuracy must be balanced by the increased computation time required for each additional atlas [61]. Lotjonen et al [61] obtained the best segmentation accuracy with relatively few [8–15] atlases, and, additionally, found that postprocessing using either the graph cuts or expectation maximization algorithms contributed to an optimized multiatlas segmentation method that balanced accuracy and computation times. They also found that the use of normalized intensity differences in the nonrigid registration step produced segmentation accuracy similar to that found using the more computationally intensive normalized mutual information method.

The selection of the atlases is a critical step. Heckeman et al [62] described the case in which the use of atlases based on the brains of young people resulted in occasional gross segmentation failures due to ventricular expansion in the older AD subjects. To overcome this problem, they modified a hierarchical registration approach by changing the first three levels to a tissue classification algorithm, instead of using native magnetic resonance (MR) intensity data. This
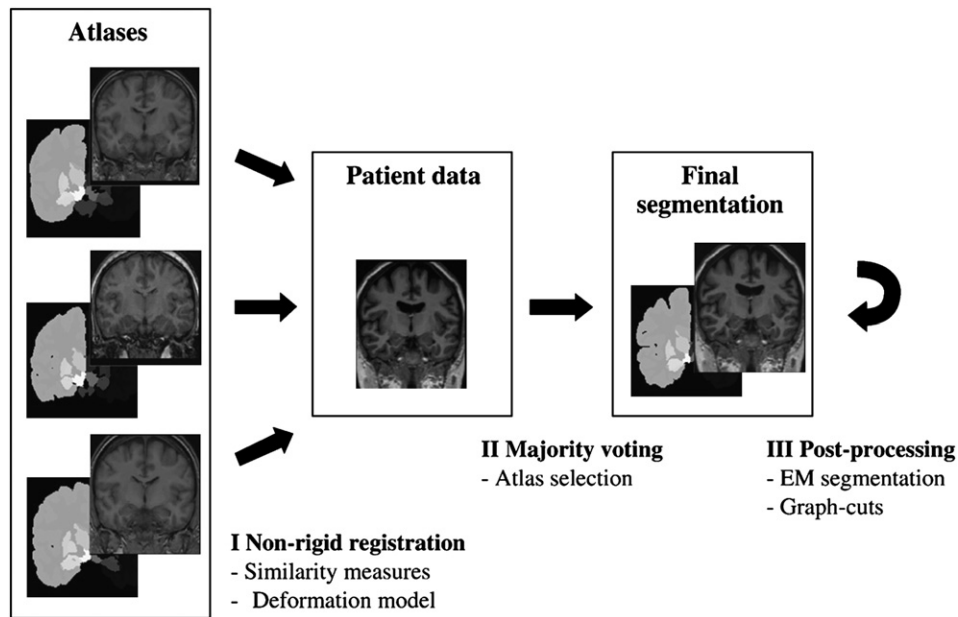
Fig. 6. Steps of multiatlas segmentation. (I) nonrigid registration used to register all atlases to patient data, (II) classifier fusion using majority voting for producing class labels for all voxels, and (III) postprocessing of multiatlas segmentation result by various algorithms, taking into account intensity distributions of different structures. Reproduced with permission from Ref [61].

multiatlas propagation with enhanced registration approach was found to create accurate atlas-based segmentations and was more robust in the presence of pathology than previous approaches.

Leung et al [58] generated multiple segmentations using nonlinear registration to best-matched manually segmented library templates and combined them using a simultaneous truth and performance level estimation algorithm. MAPS was then used to measure volume change over 12 months by applying the BSI. The accuracy of MAPS was found to compare favorably to manual segmentation, with a mean difference between automated and manual volumes of approximately 1% and a Dice score of 0.89 compared with other methods developed by ADNI (0.86: Morra et al [63]; 0.85: Wolz et al [64]; and 0.89: Lotjonen et al [61]).

3.2.2.2. Other registration methods

In addition to registration of images to one or more atlases, segmentation of images may use image statistics to assign labels for each tissue or use geometric information such as deformable models or active contours [65]. A method that combines elements of these two approaches was described by Huang et al [65], who used an edge-based geodesic active contour. They found that this method segmented a range of images more accurately and robustly than those using individual statistical or geometric features only.

Calvini et al [66] developed software for the automatic analysis of the hippocampus and surrounding medial temporal lobe (MTL) and the calculation of a novel statistical indicator, the Δ-box, computed on intensities of the automatically extracted regions Their method did not directly seg-ment the hippocampus, relying instead on the use of the Δ-box to assess intensities after a manual extraction step.

A computational processing application to measure subtle longitudinal changes using nonlinear registration to the baseline image was described by Holland and Dale [67]. This method, called quantitative anatomical regional change (QUARC), used nonrigid 12-parameter affine registration, image smoothing minimization, normalization of local intensity nonuniformity, direct calculation of the displacement field of the region of interest (ROI) rather than the Jacobian field, and bias correction. When QUARC was compared with four other common registration methods used on ADNI data, it produced significantly larger Cohen *d* effect sizes in several ROIs than FreeSurfer v4.3 (Athinoula A. Martinos Center for Biomedical Imaging, Massachusetts General Hospital, Boston, MA; http://surfer.nmr.mgh.harvard.edu/), voxel-based morphometry, and TBM, and a similar whole brain effect size to the standard KN-BSI method. Although, unlike the other methods, the signal-to-noise ratio of the raw images obtained using QUARC was enhanced by back-to-back repeat scans, the authors concluded that QUARC is a powerful method for detecting longitudinal brain morphometric changes in levels varying from the whole brain to cortical areas to subcortical ROIs.

3.2.3. Automated temporal lobe and hippocampal segmentation

In AD, atrophy in MTL and, in particular, the hippocampus is associated with declining cognitive function. It is not surprising, then, that a substantial body of work has been published on the subject of analyzing structural MRI

T1-weighted measurements of this region. Chupin et al [68] developed a fully automated method for hippocampal segmentation based on probabilistic information derived from an atlas built from the manually segmented hippocampi of 16 young subjects and anatomical information derived from stable anatomical patterns. Wolz et al [64] used a fully automated four-dimensional (4-D) graph-cut approach to hippocampal segmentation that segmented serial scans of the same patient. Power analysis of the method revealed that a clinical trial for an AD-modifying drug would require 67 AD or 206 MCI patients to detect a 25% change in volume loss (80% power and 5% significance). Morra et al [69] developed the auto context model (ACM), a fully automated method to segment the hippocampus, based on the machine learning approach, AdaBoost. After training the classifier on a training set, ACM was able to discriminate between AD, MCI, and control groups, suggesting that the automatic segmentation is sufficiently sensitive to detect changes in hippocampal volume over the course of disease progression. This method was compared with manual and other automated methods for hippocampal segmentation, and also with TBM, which was used to assess whole brain atrophy in an earlier paper by the same group [63]. These authors found that ACM compared well with hand-labeled segmentation and that the volume atrophy over clinical groups and correlation with clinical measures with ACM were comparable with that found with other automated methods and better than TBM, suggesting that the latter method may not be optimal for assessing hippocampal atrophy.

Automatic image segmentation is prone to systematic errors, which are introduced when these mostly knowledge-based protocols mistranslate manual segmentation protocols into the automatic format. Wang et al [70] presented a wrapper algorithm that can be used in conjunction with automatic segmentation methods to correct such consistent bias. The algorithm uses machine learning methods to first learn the pattern of consistent segmentation errors and then applies a bias correction to the mislabeled voxels detected in the initial step. When the algorithm was applied to four different segmentation methods, it decreased the number of mislabeled voxels by 14% (multiatlas hippocampal segmentation) to 72% (FreeSurfer hippocampal segmentation) and resulted in a higher Dice overlap than other hippocampal segmentation methods, including some of those by Leung et al, Chupin et al, and Morra et al, described in this review [59,68,69].

Beyond volumetric analysis of ROIs, recent research has focused on extracting more meaningful information from the shape of brain structures, but most studies have not considered the pose, or location and orientation of the structure. Bossa et al [71] presented a method for the statistical analysis of the relative pose of subcortical nuclei. The framework of the analysis was a variety of approaches based on similarity transformations with Reimannian metrics. Significant group differences were found between control subjects, MCI patients who did or did not subsequently convert to AD (MCI-c and MCI-nc, respectively), and AD patients, and

the authors suggested that the method may be particularly useful as an AD biomarker in conjunction with shape analysis, as both approaches leverage complementary information.

3.2.4. TBM and DBM

Bossa et al [72] used the method of TBM, which examines the deformation fields generated when an image is registered to a template. Previous work used large deformation algorithms for the nonrigid registration step, as they have the flexibility to characterize anatomical variability in cross-sectional studies. These algorithms are, however, computationally intensive, and the authors proposed a simplified version of the large deformation algorithms, stationary velocity field diffeomorphic registration. When the method was evaluated using ADNI subjects, it provided brain atrophy maps at high spatial resolution with lower computational requirements. Hua et al [73] examined two methods of image registration in TBM and found that the method in which each image is aligned to a single template was a more effective measure of brain deterioration. They also found TBM to be better suited to analyzing morphometric changes over larger areas, such as the entire temporal lobe, rather than specific ROIs, such as the hippocampus, and that atrophic changes detected by their method correlated well with clinical measures of brain deterioration (Mini-Mental State Examination [MMSE] and clinical dementia rating [CDR] scores).

Yushkevich et al [74] examined the use of DBM, a technique closely related to TBM in estimating longitudinal hippocampal atrophy in the ADNI cohort. They found that without a correction for asymmetry that arises during longitudinal image registration, substantial bias can result in the overestimation of the rate of change of hippocampal atrophy. Park and Seo [75] tackled the problem of accurate registration algorithms required in DBM to compute the displacement field. They proposed a method that uses multidimensional scaling to improve the robustness of the registration step, and found that this method improves the ability of DBM to detect shape differences between patients.

3.2.5. Quantification of brain morphometric changes

Several papers have focused on the development of methods for quantifying structural changes across the whole brain from structural MRI scans. Chen et al [76] developed a semiquantitative brain and lesion index based on T1- and T2-weighted imaging. They found that both the T1-based and T2-based scores correlated with age and cognitive performance and differentiated between control, MCI, and AD subjects. Acosta et al [77] presented a new accurate and computationally efficient voxel-based method for 3-D cortical measurement. The method, which uses an initial Lagrangian step to initialize boundaries using partial volume information and a subsequent Eulerian step to compute the final cortical thickness, offered higher statistical power to detect differences between clinical groups with a slight increase in computational time compared with methods using only the Eulerian step. The authors proposed that the increased

accuracy and precision are attributable to the Lagrangian step, which effectively achieves subvoxel accuracy.

3.2.6. Fractal analysis

A different approach for detecting atrophy in disease progression based on fractal analysis has been described by King et al [78]. Recognizing that the cerebral cortex has fractal properties, such as being statistically self-similar, this group investigated the effect of AD on gyrification using fractal analysis. They found that fractal analysis of cortical ribbons was able to discriminate between AD and control subjects in all of the seven regions tested, apart from the hippocampus, and suggested that this method may play a complementary role to ROI approaches, especially at earlier stages of disease progression. In a subsequent work, King et al [79] presented a new method for fractal dimension analysis of the cortical ribbon that also measured cortical thickness. When this method was compared with gray/white and pial surface cortical models, they found that it was the only measurement to have a significant correlation with cortical thickness and ADAS-cog scores, and that it best discriminated between control subjects and AD patients. The authors concluded that the fractal dimension of the cortical ribbon has strong potential as a quantitative marker of cerebral cortex atrophy in AD. Li et al [80] presented a method to reliably measure cortical thickness for longitudinal studies by incorporating 4-D information from successive scans directly into processing steps. In the absence of a gold standard against which to test their method, they used power analysis of the correlation between cortical thickness and the MMSE to show that this method improved longitudinal stability compared with 3-D methods that do not take the temporal factor into account.

3.2.7. Other MRI methods

Risser et al [81] presented a new method to compare imaged shapes, either longitudinally or against an atlas, on several different scales simultaneously, and to quantify the deformations on a single scale using large-scale deformation diffeomorphic mapping. When the method was applied to examine hippocampal atrophy in ADNI patients using baseline and 24-month scans, it was found to be able to extract information at the desired scale among all the scales.

A modification of the voxel-based analysis and statistical parametric mapping method for the detailed spatial analysis of image data without a priori defined ROIs was proposed by Zhang and Davatzikos [82]. Their method, optimally discriminative voxel-based analysis, uses non-negative discriminative projection applied to the spatial neighborhood around each voxel to find the optimally discriminative direction between two groups, determines a statistic for each group, and obtains a statistical parametric map of group differences. Optimally discriminative voxel-based analysis was found to perform well compared with traditional statistical parametric mapping using an ADNI data set.

3.3. Methods for AD classification from imaging data

The development of automatic methods for the accurate classification of patients into clinical groups from imaging data has been the aim of multiple ADNI studies. Many of these classification methods are based on support vector machines (SVMs), a set of algorithms that uses supervised learning of pattern recognition in a training set to build a classifier to predict the category to which a new example belongs. Some methods condense imaging data into one score that is reflective of brain abnormalities associated with AD to allow the direct comparison of patients, thereby facilitating their classification into patient group [83–85], whereas others examine which combination of imaging, CSF biomarkers, genetics, and other factors results in the most accurate classifiers [86,87], or formulate novel approaches for identifying AD-like patterns [87–90]. Other methods leverage the changes in spatial connectivity between different areas of the brain that most likely occur, as functional connectivity becomes affected during disease progression [65,83]. Finally, some methods [91,92] use an alternative approach to machine learning, a relevance vector machine (RVM), which, unlike the binary SVM, is a probabilistic machine learning algorithm. A brief description of these methods is given later in the text, and their results are presented and compared with existing methods of classification in section 5.4.1.

3.3.1. Magnetic resonance imaging

Fan et al [83] used an SVM to construct a classifier based on patterns of spatial distribution of brain tissue from T1-weighted MRI scans of control subjects and AD patients and applied this classifier to scans of MCI patients. The classifier, which acts as an indicator of how the structural profile of an individual fits that of AD or control subjects, also produced a structural phenotypic score (SPS) that allowed direct comparison of patients. This approach differs from ROI or voxel-based analyses, as it examines spatial patterns of atrophy rather than individual brain regions, and is also able to examine functional connectivity. Shen et al [89] also developed a method that integrated feature selection into the learning process, but used sparse Bayesian learning methods instead of an SVM. They reported that their automatic relevance determination and predictive automatic relevance determination, in general, outperformed the SVM used for comparison and classified patients more accurately than the method of Hinrichs et al [88]. Stonnington et al [91] used regression analysis based on an RVM to analyze T1-weighted MRI data and predict clinical scores, whereas Franke et al [92] used an RVM combined with an automatic preprocessing step and dimension reduction using principal component analysis to estimate the age of healthy subjects from T1-weighted MRI data, and found the method to be reliable, efficient, and scanner independent. In contrast to the supervised SVMs used in the aforementioned studies, Filipovych and Davatzikos [93] used a semisupervised SVM to classify MCI-c and MCI-nc patients. In the supervised approach, there is an

assumption that patterns in a heterogeneous construct like MCI are known, but in a semisupervised approach, only some of the data, in this instance, baseline MRIs from AD patients and control subjects, are labeled, whereas scans of MCI patients are left unlabeled. Using a leave-one-out approach, scans were then classified as having a degree of AD-like or normal-like anatomic features, as defined by Fan et al [83].

A more data-driven approach for patient classification that circumvents the need for a priori defined ROIs by using an initial independent component analysis (ICA) step was proposed by Yang et al [94]. Their preliminary study combined the ICA step to extract defining neuroimaging features with a subsequent SVM for classification of scans into AD, MCI, and control subjects, and the resulting method was tested on two cohorts, including ADNI. Pelaez-Coca et al [95] compared ability of anatomical versus statistically defined ROIs to discriminate between control and AD subjects. Using a variety of classifiers, they sought to restrict the number of features using principal component analysis and found that a higher number of features did not necessarily correspond with higher classification accuracy. When generalizability of the algorithm was tested by analyzing classification performance of 20 different experiments in which different subsets of the cohort were used as training and testing sets, they found that the resulting variability was larger than within the different classifiers used. Finally, they found that statistically defined ROIs representing voxels with the largest significance difference in a group comparison with an unbiased atlas (belonging to voxels in the hippocampi and amygdalae) resulted in better classification accuracy than anatomically predefined ROIs in the hippocampi, lateral ventricles, and amygdalae.

3.3.2. [^{18}F]-fluorodeoxyglucose-positron emission tomography

Haense et al [84] also used a discrimination procedure, developed by the European Network for Standardization of Dementia Diagnosis, which generates a measure reflective of scan abnormality from FDG-PET data. This measure, AD t-sum, is calculated from the sum of abnormal t-values in voxels known to be affected by AD, and was used for discrimination of clinical groups. A similar approach was used by Chen et al [85], who developed an automatically generated hypometabolic convergence index (HCI) reflective of the degree to which the patient's pattern and magnitude of cerebral hypometabolism corresponded to that of probable AD patients. Huang et al [65] identified changes in spatial connectivity patterns based on sparse inverse covariance estimation using FDG-PET data. Salas-Gonsalez et al [90] developed an automated procedure to classify AD patients from FDG-PET data using a *t* test to select voxels of interest and factor analysis to reduce feature dimension. The resulting factor loadings were tested on three different classifiers, two Gaussian mixture models with either linear or quadratic discriminant functions and an SVM. Lemoine et al [87] used a combination of feature selection and data fusion to construct SVMs from both FDG-PET and clinical data. To extract the most meaningful features from FDG-PET scans, they used an evolutionary algorithm in which each feature corresponded to one gene, the number of features was arbitrarily selected to be 30, and which was complete when an area under the curve (AUC) of 0.98 was achieved on the training data set. SVMs were also constructed for a range of clinical features, and the results of these and the FDG-PET classifiers were weighted and data finally fused to create a final classifier.

3.3.3. Cognitive methods

Llano et al [96] developed a cognitive test based on ADAS-cog as an alternative to imaging or CSF biomarkers for use as an outcome measure or for subject enrichment in clinical trials. The ADAS.Tree composite was derived by weighting test components of ADAS-cog based on their ability to discriminate between control, MCI, and AD subjects of the ADNI cohort using a Random Forests tree-based algorithm. ADAS.Tree discriminated between patient groups as well as, or better than, the best imaging or CSF biomarkers or cognitive tests. Optimal sets of markers for the prediction of 12-month decline were then determined using machine learning algorithms, and performance of the derived cognitive marker was found to be comparable with, or better than, other individual or composite baseline CSF or neuroimaging biomarkers. The authors suggest that the ADAS.Tree might prove more widely applicable than expensive and/or invasive imaging or CSF biomarkers.

3.3.4. Combined modalities

The new machine learning algorithm of Hinrichs et al [88], which uses data from both MR and FDG-PET images, integrates a spatial discrimination step to identify AD-related patterns in different brain regions, rather than assessing these relationships at the pre- or postprocessing steps.

3.4. Other imaging methods

Rousseau [97] presented a method for generating a high-resolution image from a low-resolution input, using jointly one low-resolution image and intermodality priors from another high-resolution image to create a super-resolution framework, for instance, a high-resolution T1-weighted image and a low-resolution T2-weighted image from the same patient. The method, when tested on clinical images from ADNI data, automatically generated high-resolution images from low-resolution input, and the authors suggest that this method may permit the investigation of multimodal imaging at high resolution.

The problem of representing a high dimensionality of brain images amassed in common neuroimaging applications was tackled by Gerber et al [98], who proposed that these images can be approximated by a low-dimensional, nonlinear manifold representative of variability in brain anatomy. They constructed a generative manifold model through kernel regression and tested this using ADNI data, and their finding was that important clinical trends were

captured by this manifold when learned manifold coordinates and clinical parameters were subjected to analysis by linear regression.

3.5. Statistical methods

Interpretation of imaging data is a key facet in the process of extracting meaningful information from these scans. As the volume of neuroimaging data generated by ADNI studies burgeons, there is an obvious need for more sophisticated analysis techniques. Habeck and Stern [99] reviewed advances in multivariate analysis techniques that are being developed to supersede the more commonly used univariate, voxel-by-voxel analysis of imaging data. By evaluating the correlation or covariance of activation across brain regions, these multivariate techniques produce results that can be interpreted as neural networks, thereby addressing brain functional connectivity. Habeck and Stern [99] directed this review specifically at neuroscientists to explain the "bewildering variety of (multivariate) approaches …presented…typically by people with mathematics backgrounds." In an effort to further spread the word to neuroscientists about this technique, a video article is also available [100].

Wu et al [101] presented a method to assess the reliability of hypometabolic voxels during the statistical inference stage of analysis. The aim of this method was to incorporate the differential involvement of each voxel into the multiple comparison correction, as opposed to current methods in which each location is treated equally. They used statistical parametric mapping and bootstrap resampling to create a bootstrap-based reliability index and compared this approach with the commonly used type I error approach, and found a strong, but nonlinear, association between the two methods. The authors suggest that this approach could have utility in both cross-sectional and longitudinal studies, in the early detection of AD, and in tracking disease progression in clinical trials.

Singh et al [102] presented a new method to relate complex anatomical changes observed in AD patients with changes in cognition based on a statistical analysis of large deformation diffeomorphic metric mapping. In this method, the diffeomorphic transformations were analyzed using a multivariate and partial least squares approach without segmentation or the use of a priori defined ROIs. They found that this approach associated ventricular expansion, cortical thinning, and hippocampal atrophy with worsening scores on neuropsychological variables such as ADAS-cog, Rey Auditory Verbal Learning Test (AVLT), and clinical dementia rating-sum of boxes (CDR-SB), confirming that this data-driven approach was able to reach similar conclusions as other studies based on predefined ROIs.

3.6. Genetics methods

Genetic contributions to AD are being revealed by GWAS that search for associations between QTs in the form of imaging or biomarker data and genetic loci. The standard approach (mass univariate linear modeling), which compares each phenotype–genetic loci pair individually and then ranks the association in terms of significance, is extremely computing-intensive and can miss information from areas surrounding a particular association. Vounou et al [103] proposed a new method, sparse reduced rank regression, which overcomes these problems by enforcing sparsity of regression. They found sparse reduced rank regression to be less computing-intensive and to have better power to detect deleterious genetic variants than mass univariate linear modeling. An alternative approach to reducing computational requirements, while retaining a high degree of significance to AD, has been presented by Chen et al [104], who used each of 142 preselected imaging ROIs as QTs in a GWAS. Heat maps and hierarchical mapping were then used to organize and visualize results and to select target SNPs, QTs, or associations for further analysis.

In addition to computational challenges, imaging genetics studies with multiple testing are also prone to false-positive results, and both familywise error and false discovery rate corrections are used to adjust significance thresholds across multiple voxels. Silver et al [105] measured false-positive rates using VBM to investigate the effect of 700 null SNPs on GM volume in the ADNI cohort. They found that although false-positive rates were generally found to be well controlled, under certain conditions, such as under low cluster-forming thresholds, the false-positive rates were substantially elevated. Consequently, they proposed the use of parametric random field theory cluster size inference and alternative non-parametric methods under different circumstances.

3.7. Methods papers: Summary and conclusions

Papers focused on method development have been instrumental in facilitating ADNI research thus far and promise to deliver improvements in reliability, efficiency, and effectiveness in ADNI-GO and ADNI-2. The establishment of standardized protocols that account for problems of variability, both across the multicenter setting of ADNI and longitudinally, has been a primary accomplishment. Likewise, the development of methods for automatic tissue registration and segmentation that avoid the necessity of time-consuming and costly manual segmentation is critical for the analysis of ADNI data. The majority of these approaches are atlas-based, although statistically based registration has also been proposed. Automatic segmentation of the hippocampus, a prominent AD biomarker, poses particular challenges because of its size and location, and several studies have made contributions to the analysis of its volume, shape, and pose. TBM and DBM methods and fractal approaches offer an alternative to volumetric ROI analysis. Methods to allow the classification of patients according to disease status have primarily been based on SVMs and the related RVMs, which are used to build classifiers that can include MRI, FDG-PET, biomarker, *APOE* ε4, and cognitive data.

Finally, statistical methods have been developed to deal with the complexities of the volume and diverse types of data generated by ADNI studies.

4. Studies of the ADNI cohort

4.1. Clinical characterization

Central to achieving the goals of ADNI was the recruitment of a study population that mirrors cohorts used in MCI and mild AD trials. Petersen et al [106] presented a baseline and 12-month longitudinal clinical characterization of the ADNI cohort, comprising 229 normal control subjects, 398 subjects with MCI, and 192 subjects with mild AD, and provided clear support for the success of ADNI in this regard. The demographic characteristics of the participant groups, given in Table 3, indicate that the cohort was mostly white and well educated, and that there were a high proportion of *APOE* ε4 carriers, consistent with populations recruited for clinical trials. At baseline, each study group differed significantly in a range of cognitive measures, with the MCI group intermediate between the control and AD groups in measures of memory impairment and in levels of CSF biomarkers (Table 4). In contrast to AD subjects who were impaired in virtually all cognitive measures, MCI subjects were only mildly impaired in nonmemory cognitive measures. After 12 months, 16.5% of MCI subjects had converted to AD, and a greater increase in the ADAS-cog was seen in the AD group compared with the MCI group. Little change was observed in control subjects. The study also found that baseline Aβ-42 levels were predictive of the progression of clinical measures over 12 months.

4.2. Medication use

Medication use among the ADNI cohort was investigated by Epstein et al [107]. They found a high rate of polypharmacy, with 85% of participants taking more than four medications, the average being eight (SD = 4). Moreover, 22% of participants reported taking one or more Beers list medications deemed to be potentially dangerous in the elderly population. The most common medications for symptomatic treatment of AD or MCI were the cholinesterase inhibitor donepezil and the *N*-methyl-D-aspartate partial receptor agonist memantine, which were frequently taken as a combination therapy. Despite the lack of FDA approval for use of these drugs to treat MCI, donepezil, memantine, and other cholinesterases were commonly used by MCI patients. Women, less educated, and more elderly participants were less likely to receive treatment. Schneider et al [108] focused on the use of cholinesterase inhibitors and memantine in the ADNI cohort. They found that 44% of MCI patients and 85% of mild AD patients were treated with cholinesterase inhibitors, and that 11% of MCI patients and 46% of mild AD patients were treated with memantine. In both patient groups, use of these medications was associated with increased cognitive impairment at baseline, a higher rate of clinical decline over 2 years, and a more rapid progression to dementia in MCI patients. Cholinesterase inhibitors and memantine appeared to be more frequently prescribed to patients diagnosed as having MCI due to AD, despite a lack of evidence from clinical trials and lack of FDA approval for this treatment. The authors suggested that use of these medications may affect the interpretation of clinical trial outcomes.

Table 3
Demographic characteristics of ADNI participant groups

Characteristic	Control subjects (n = 229)	MCI group (n = 398)	AD (CDR: 1.0) group (n = 192)	P value	P < .05*
Age, mean ± SD, years	75.8 ± 5.0	74.7 ± 7.4	75.3 ± 7.5	.137	
Education, mean ± SD, years	16.0 ± 2.9	15.7 ± 3.0	14.7 ± 3.1	<.001	b, c
Years from symptom onset	Not available	Not available	3.9 ± 2.5	NA	
% Female	48.0	35.4	47.4	.002	a, c
Marital status, %				.002	a
Married		80.2	81.2		
Widowed	17.5	12.1	10.4		
Divorced	7.4	6.3	4.7		
Never married	6.6	1.5	3.6		
Unknown	0.4	0	0		
APOE ε4, %				<.001	a, b, c
Carriers	26.6	53.3	66.1		
Noncarriers	73.4	46.7	33.9		
Ethnicity					
American Indian	0	0.3	0		
Asian American	1.3	2.3	1.0		
African American	7.0	3.5	4.2		
Hispanic	0.9	3.5	2.1		
White	90.8	90.5	92.2		
Other	0	0	0.5		

NOTE. Reproduced with permission from Ref [106].
*Multiple comparisons abbreviated as: (a) control subjects differ from subjects with AD, (b) subjects with MCI differ from subjects with AD, (c) control subjects differ from subjects with MCI.

Table 4
Baseline assessments of the ADNI cohort

Assortment variable	Control subjects Mean SD	MCI Mean SD	Z score MCI–control	AD Mean SD	Z score AD–MCI	P value	P < .05*
MMSE score	29.1 ± 1.0	27.0 ± 1.8	−18.8	23.3 ± 2.1	−21.3	<.001	a, b, c
CDR global score	0.0 ± 0.0	0.5 ± 0.0	397	0.7 ± 0.3	13.4	<.001	a, b, c
CDR-SB	0.0 ± 0.1	1.6 ± 0.9	34.9	4.3 ± 1.6	21.3	<.001	a, b, c
Memory	0.0 ± 0.0	0.6 ± 0.2	61.3	1.0 ± 0.3	16.5	<.001	a, b, c
Orientation	0.0 ± 0.0	0.2 ± 0.3	17.5	0.8 ± 0.4	17.7	<.001	a, b, c
Judgment	0.0 ± 0.1	0.4 ± 0.3	21.8	0.8 ± 0.4	14.6	<.001	a, b, c
Community affairs	0.0 ± 0.0	0.2 ± 0.2	13.1	0.7 ± 0.4	16.9	<.001	a, b, c
Hobbies	0.0 ± 0.0	0.2 ± 0.3	15.1	0.8 ± 0.5	15.9	<.001	a, b, c
Personal care	0.0 ± 0.0	0.1 ± 0.2	4.4	0.2 ± 0.4	4.3	<.001	a, b, c
Hachinski score	0.6 ± 0.7	0.6 ± 0.7	0.8	0.7 ± 0.7	0.7	.418	NA
GDS score	0.8 ± 1.1	1.6 ± 1.4	7.3	1.7 ± 1.4	0.6	<.001	a, b
FAQ	0.1 ± 0.6	3.9 ± 4.5	16.2	13.0 ± 6.9	16.8	<.001	a, b, c
ADAS-cog total	6.2 ± 2.9	11.5 ± 4.4	18.1	18.6 ± 6.3	14.0	<.001	a, b, c
ADAS word list immediate recall	2.9 ± 1.1	4.6 ± 1.4	16.8	6.1 ± 1.5	12.2	<.001	a, b, c
ADAS word list recognition	2.6 ± 2.3	4.6 ± 2.7	10.1	6.6 ± 2.8	8.2	<.001	a, b, c
ADAS-cog without word list	0.8 ± 0.9	2.3 ± 2.0	12.9	5.9 ± 4.1	11.4	<.001	a, b, c
ADAS word list delayed recall	2.9 ± 1.7	6.2 ± 2.3	20.8	8.6 ± 1.6	15.0	<.001	a, b, c
AVLT trials 1-5	43.3 ± 9.1	30.7 ± 9.0	−16.7	23.2 ± 7.7	−10.4	<.001	a, b, c
AVLT delayed recall	7.4 ± 3.7	2.87 ± 3.3	−15.6	0.7 ± 1.6	−10.3	<.001	a, b, c
AVLT DR/trial, 5%	65.8 ± 27.6	32.1 ± 33.1	−13.9	11.2 ± 22.0	−9.3	<.001	a, b, c
Trails A	36.5 ± 13.2	44.9 ± 22.8	5.9	68.0 ± 36.9	8.0	<.001	a, b, c
Trails B	89.2 ± 44.3	130.7 ± 73.5	8.8	198.9 ± 87.2	9.2	<.001	a, b, c
Category fluency (animal)	19.9 ± 5.6	15.9 ± 4.9	−9.1	12.4 ± 4.9	−8.1	<.001	a, b, c
Category fluency (vegetable)	14.7 ± 3.9	10.7 ± 3.5	−12.7	7.8 ± 3.3	−9.8	<.001	a, b, c
Number cancellation	0.4 ± 0.7	1.0 ± 0.9	8.0	1.8 ± 1.3	7.6	<.001	a, b, c
Boston Naming Test	27.9 ± 2.3	25.5 ± 4.1	−9.4	22.4 ± 6.2	−6.2	<.001	a, b, c
Digit backward	7.2 ± 2.2	6.2 ± 2.0	−6.0	5.0 ± 1.8	−7.2	<.001	a, b, c
Clock drawing	4.7 ± 0.7	4.2 ± 1.0	−7.6	3.4 ± 1.3	−7.5	<.001	a, b, c
CSF biomarkers (pg/mL)	(n = 114)	(n = 199)		(n = 102)			
Tau	69.7 ± 30.4	101.4 ± 62.2	6.0	119.1 ± 59.6	2.4	<.001	a, b
Aβ−42	205.6 ± 55.1	162.8 ±56.0	−6.6	143.0 ± 40.8	−3.5	<.001	a, b, c
p-tau$_{181P}$	24.9 ± 14.6	35.5 ± 18.0	5.7	41.6 ± 19.8	2.6	<.001	a, b, c

Abbreviations: GDS, Geriatric Depression Score; FAQ, Functional Activities Questionnaire; ADAS-cog, cognitive subscale of the Alzheimer's Disease Assessment Scale; AVLT, Rey Auditory Verbal Learning Test; CDR-SB, clinical dementia rating-sum of boxes.

NOTE. Reproduced with permission from Ref [106].

*Multiple comparisons abbreviated as: (a) control subjects differ from subjects with MCI, (b) control subjects differ from subjects with AD, (c) subjects with MCI differ from subjects with AD.

4.3. Baseline and longitudinal studies of brain morphometric changes during disease progression

ADNI has afforded a unique opportunity to examine brain morphometric changes that occur during disease progression in a large, well-defined cohort. Using MRI data, cross-sectional and longitudinal studies focused either on evaluating spatial pattern and regional rates of atrophy or on characterizing biomarkers for varying disease stages have together resulted in a more detailed and coherent picture of this complex process.

A cross-sectional study by Fennema-Notestine et al [109] examined the feasibility of high-throughput image analysis to detect subtle brain structural changes in the early stages of AD. They further divided the MCI group, based on neuropsychological performance, into single-domain and multidomain groups, which they proposed represented earlier and later stages in disease progression, respectively. Using comparisons of cortical thickness, they found a pattern of progressive atrophy from normal control subjects to single-domain MCI subjects, to multidomain MCI subjects, and finally to subjects with AD (Fig. 7). When ROIs were examined, they found that the regions that differed between the control group and the single-domain MCI group included not only the hippocampus and entorhinal cortex, which had the largest effect sizes, but also other temporal regions, the temporal horn of the lateral ventricle, rostral posterior cingulate, and several parietal and frontal regions. Relative to control subjects, multidomain MCI patients had greater differences in the same regions as well as in the lateral inferior, middle, and superior temporal gyri and fusiform cortices. Additional atrophy was seen in AD patients relative to control subjects in the inferior parietal, banks of the superior temporal sulcus, retrosplenial, and some frontal regions. Similar results were reported in a cross-sectional study by
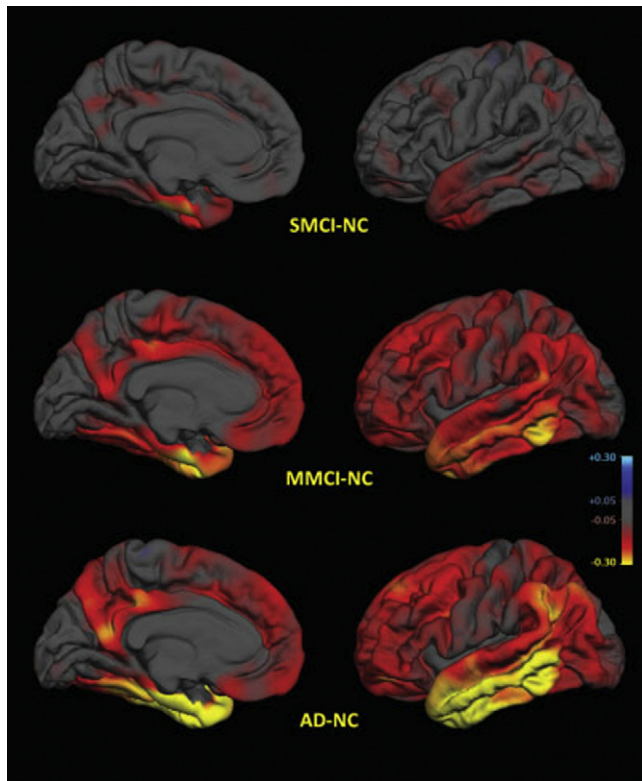
Fig. 7. Group differences in average thickness (mm) for left hemisphere. Top row: NC vs. SMCI; middle row: normal controls (NC) vs. MMCI; bottom row: NC vs. AD. Left mesial views, right lateral views. The scale ranges from < −0.3 (yellow) to > +0.3 (cyan) mm thickness. Areas on the red-yellow spectrum indicate regions of thinning with disease: approximate color scale in mm is −0.05 to −0.15 dark red, −0.20 bright red, −0.25 orange, and < −0.30 yellow. For thicker regions: +0.05 to +0.15 blue. Any differences smaller than ± 0.05 mm are gray. Reproduced with permission from Ref [109].

Karow et al [110], who found a pattern of atrophy spreading from the mesial temporal lobe in MCI patients to widespread areas in AD patients. Fennema-Notestine et al [109] also explored the trajectories of change of ROIs over the course of the disease and found that although some regions, such as mesial temporal regions, exhibited a linear rate of atrophy through both MCI stages to AD, other regions, such as the lateral temporal middle gyrus, retrosplenial cortex, inferior parietal cortex, and rostral middle frontal cortex, exhibited accelerated atrophy later in the disease.

The idea that rates of change of atrophy are not uniform but vary by disease stage is supported by several studies. When MCI groups were classified according to subsequent clinical outcome, Leung et al [59] found higher rates of hippocampal atrophy in MCI-c than MCI-nc patients. McDonald et al [111] examined regional rates of neocortical atrophy in the ADNI cohort, dividing MCI subjects into two groups by their CDR-SB scores. The less impaired MCI group had CDR-SB scores of between 0.5 and 1.0, whereas the more impaired group had CDR-SB scores of between 1.5 and 2.5 (AD subjects had CDR-SB scores of >2.5). They found that over the course of disease progression, atro-

phy changed from the medial and inferior lateral temporal, inferior parietal, and posterior cingulate cortices initially, to the superior parietal, prefrontal, and lateral occipital cortices, and finally to the anterior cingulate cortex (Fig. 8). Moreover, the rates of change differed among the three groups. The least impaired MCI patients showed the greatest rates of atrophy in the medial temporal cortex, whereas later in disease progression, rates of atrophy were higher in the prefrontal, parietal, and anterior regions. Similar patterns were found by several other groups using a range of MRI methods. Hua et al [112] and Leow et al [113] both used TBM to create 3-D maps of structural changes over 12 months. Risacher et al [114,115] examined a variety of structural MRI markers for their sensitivity to longitudinal change and clinical status using multiple methods, including VBM and ROIs, whereas Schuff et al [116] focused on changes in hippocampal volume, and McEvoy et al [117] calculated an atrophy score based on ROIs most associated with AD atrophy. Collectively, these studies showed atrophy spreading from the MTL to the parietal, occipital, and frontal lobes over the course of the disease, with MCI patients, in general, having a more anatomically restricted AD-like pattern of change. MCI subjects who converted to AD within the time frame of the study (MCI-c) had a more AD-like pattern of atrophy, and nonconverters (MCI-nc) had a pattern more intermediate between control and AD subjects (Fig. 9). Several studies [114,115,118,119] divided the MCI group into those patients who converted to AD within a year and those who remained stable. Each group had distinct profiles when assessed using a score derived from patterns of structural abnormality, the future converters having mostly positive scores that reflected a largely AD-like pattern of brain atrophy. Conversely, the distribution of abnormality scores in the MCI-nc group was bimodal, reflecting the heterogeneity of this group that appears to contain some members who, with abnormality scores close to those of AD patients, are likely to convert in the near future.

The highest rates of change occurred in AD subjects and MCI-c patients in measures of hippocampal volume and entorhinal cortex thickness [115,120]. Schuff et al [121] found that atrophy was detectable at 6 months and accelerated with time to 12 months in MCI and AD subjects, with the highest rates of atrophy seen in AD patients (Fig. 10). Hua et al [120] used TBM to examine the effects of age and sex on atrophic rates and found that the atrophic rates of women were 1% to 1.5% higher than for men. They also observed a 1% increase in atrophic rate and a 2% increase in ventricular expansion for every 10-year decrease in age, with correlations strongest in the temporal lobe.

A different data-driven approach to determining the time course of brain volume changes in healthy elderly, MCI, and AD subjects without using a priori models was taken by Schuff et al [116]. Using generalized additive models to analyze serial MRI scans over 30 months, they found that atrophy rates varied nonlinearly with age and cognitive status, most noticeably in temporal regions, and that atrophy tended
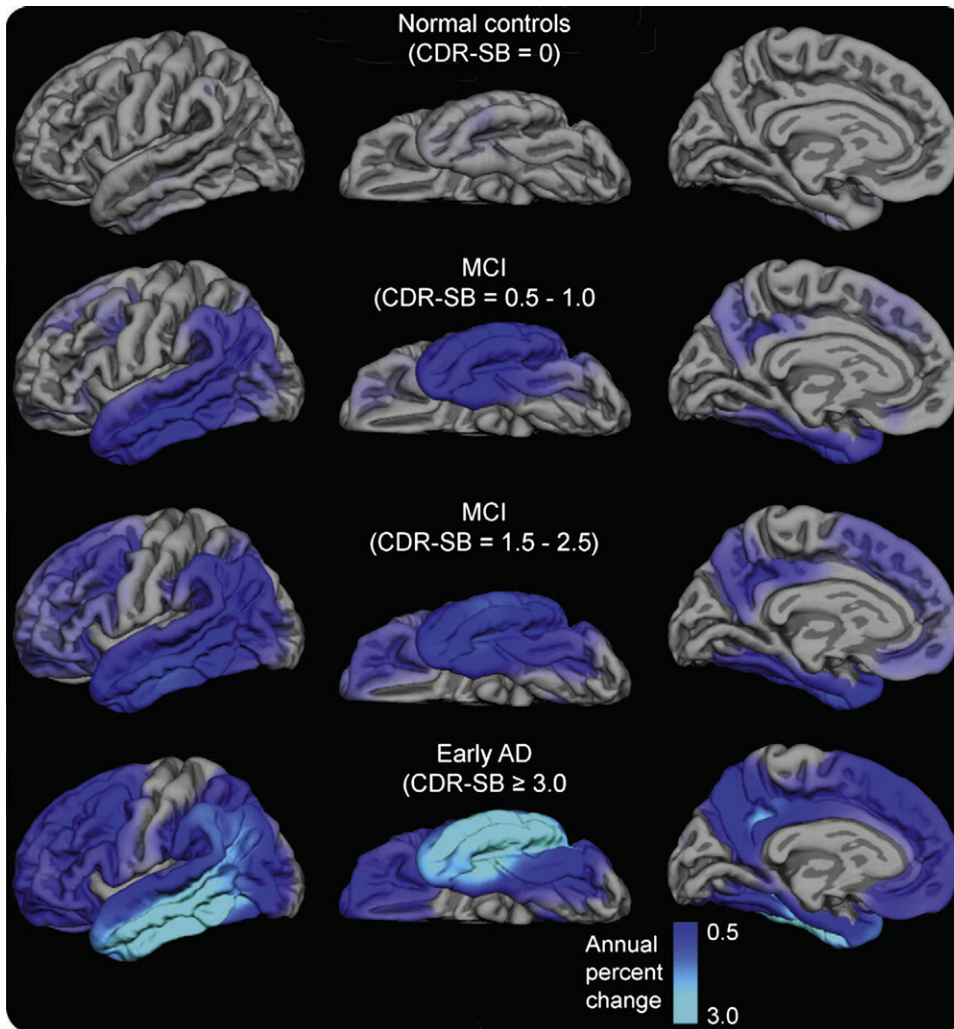
Fig. 8. Annual atrophy rates as a function of degree of clinical impairment. Clinical impairment measured using baseline clinical dementia rating-sum of boxes (CDR-SB) scores. Mean atrophy rates are represented as a percent change in neocortical volume and mapped onto the lateral (left), ventral (middle), and medial (right) pial surface of the left hemisphere. These data demonstrate that atrophy rates are most prominent in posterior brain regions early in the course of disease, spreading to anterior regions as the level of impairment increases, with relative sparing of sensorimotor regions. Reproduced with permission from Ref [111].

to level off in control and MCI-nc subjects, but decline further in MCI-c and AD patients. The authors suggest that these differences are a reflection of the different processes involved in healthy versus disease-related neurodegeneration. The regions with the greatest effect sizes between young control and AD subjects were the entorhinal cortex, the hippocampus, and the lateral ventricles, suggesting that rates of change in these regions have potential as biomarkers for the early detection of AD.

Beyond simple volumetric analysis, one approach to analyzing brain morphometric changes in greater detail has been to assess changes in shape of ROIs. Qiu et al [122] used large deformation diffeomorphic metric mapping to reveal that the anterior of the hippocampus and the basolateral complex of the amygdala had the most surface inward deformation in MCI and AD patients, whereas the most surface outward deformation was found in the lateral ventricles (Fig. 11). These results are in agreement with the volumetric

findings of Apostolova et al [123] and also with many findings documenting the enlargement of the lateral ventricles with disease progression.

4.4. Associations between characteristics of the ADNI cohort

A major area of focus in research using ADNI data has been the elucidation, both at baseline and longitudinally, of associations between various imaging, CSF, genetic, and clinical correlates in different clinical groups to gain a better understanding of the interplay of biomarkers throughout disease progression.

4.4.1. Magnetic resonance imaging

4.4.1.1. Temporal lobe

Structures within the temporal lobe have long been associated with AD decline because of their critical role in the
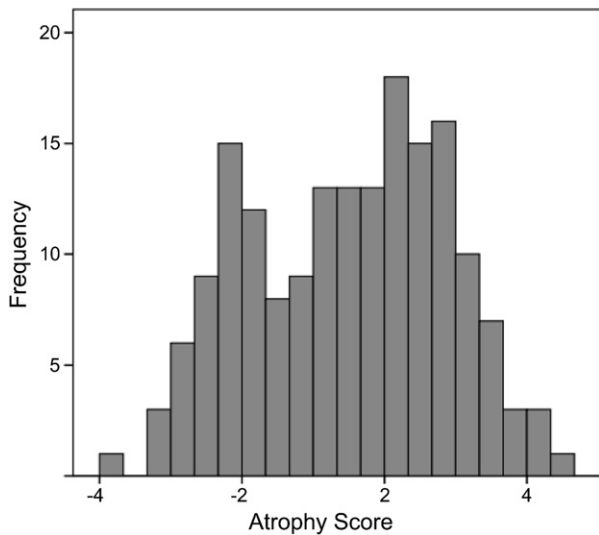
Fig. 9. Distribution of atrophy scores used to classify subjects with MCI. MCI atrophy score was derived from LONI data archive trained on data from all control subjects and subjects with AD. Discriminant model assumed equal prior group probabilities. Individuals were classified as having control phenotype if their scores were above –0.33. Cutoff score was chosen to maximize overall accuracy of classifying control subjects and subjects with AD on whom this model was trained. Average atrophy score for subjects with MCI was –0.50. Atrophy score is not normally distributed (Kolmogorov–Smirnov test = 0.73, $df = 175$, $P = .025$) but shows evidence of bimodal distribution. Reproduced with permission from Ref [117].

formation of long-term memory, one of the first functions to be affected in disease progression. Leow et al [113] found temporal lobe atrophy to be associated with increased cognitive impairment in MCI patients, as indicated by changes in CDR, MMSE scores, and the AVLT (Fig. 12). Among the structures of the temporal lobe, hippocampal atrophy is the best studied structural biomarker, as it is one of the earliest structures to degenerate in AD. In a small initial study, Morra et al [63] found that bilateral hippocampal atrophy at baseline was strongly correlated with both MMSE and CDR-SB (Table 5). A further larger study by the same group [124] examined rates of hippocampal atrophy over 12 months and found that these correlated with both baseline cognitive scores on MMSE and global and sum of boxes CDR and with longitudinal change in these measures (Table 5). Wolz et al [64] also revealed significant correlations between rates of hippocampal atrophy and both baseline MMSE and CDR, and changes in these measures over 12 months (Table 5). Additionally, a study by Schuff et al [121] found that rates of change of MMSE and ADAS-cog were associated with rates of hippocampal atrophy (Table 5). Using TBM, Hua et al [73] found that baseline temporal lobe atrophy was associated with both baseline and change in the CDR-SB in MCI and AD patients, but with change in the MMSE only in the AD group, providing further evidence for the acceleration of atrophic change with disease progression.

The relationships between hippocampal volume and memory retention were examined by Apostolova et al [123], who found that MCI patients had bilateral associa-

tions between hippocampal volume and radial distance and three tests of delayed recall (DR): ADAS-cog-DR, AVLT-DR, and the Wechsler Logical Memory Test II-DR, whereas associations between these tests in AD patients were stronger in the left hippocampus both at baseline and at the 12-month follow-up (Table 5). In addition, they found highly significant regional associations for memory performance, especially in the CA-1 subregion and the subiculum on the anterior hippocampal surface. Associations between temporal lobe degeneration and memory performance (Wechsler Memory Scale-Revised—Logical Memory, immediate recall and DR) were also found by Hua et al [73]. Along with hippocampal atrophy, ventricular expansion is a hallmark of brain morphometric changes that occur during AD progression and has great potential as a structural biomarker, as the lateral ventricles are comparatively easy to measure, because of their high contrast under MRI, and are highly sensitive to disease progression. Evans et al [125] found that ventricular expansion differentiated between patient groups was associated with ADAS-cog scores in AD patients, and that MCI-c patients had higher rates of ventricular expansion than MCI-nc patients. Chou et al [126] automatically mapped ventricular geometry and examined correlations between surface morphology, clinical decline, and CSF biomarkers. They found that ventricular enlargement at baseline correlated with diagnostic group, depression severity, both baseline and rates of change of cognitive function (MMSE and CDR-SB), and lower CSF Aβ-42. In a subsequent study by the same group [127] using automated radial mapping to generate statistical maps, ventricular enlargement was found to correlate with a large number of measures of clinical decline as well as with lower levels of CSF Aβ-42 and the *APOE* ε4 allele (Fig. 13). Chou et al [126] also noted expansion of the posterior regions of the ventricles in MCI patients and in the frontal regions of the superior horns in AD patients compared with control subjects, suggesting a topographic sequence of morphometric change throughout disease progression.

The studies of Morra et al [124], Wolz et al [64], Hua et al [112], and Risacher et al [115] all found that carriers of the *APOE* ε4 allele had higher rates of hippocampal atrophy than noncarriers. In contrast, Schuff et al [121] found that increased rates of hippocampal atrophy were associated with *APOE* ε4 in the AD, but not MCI or control, group. Using Structural Abnormality Index (STAND) scores to reflect the overall level of AD-like anatomic features, Vemuri et al [128] also found that the *APOE* ε4 allele contributed to MRI atrophy. Hua et al [112] found that the *APOE* ε4 allele had a dose-dependent detrimental risk with greater atrophy in the hippocampus and temporal lobe in homozygotes than heterozygotes in MCI and AD groups (Fig. 13). The recently identified AD risk allele *GRIN2b* was associated with higher rates of temporal lobe atrophy in the pooled group, but more weakly than *APOE* ε4 [120]. Other thus far unidentified genetic risk factors likely contribute to AD, with epidemiological studies suggesting maternal history of the disease
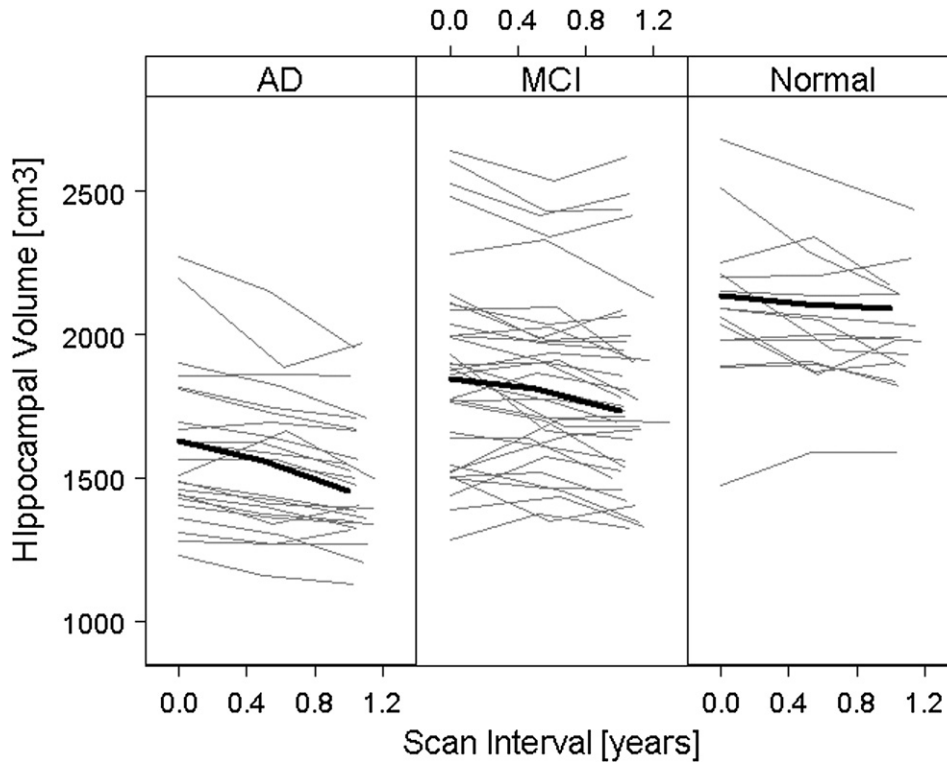
Fig. 10. Individual trajectories of hippocampal volume change. Thick black lines indicate the mean trajectory change of each group. Reproduced with permission from Ref [121].

increases the risk of developing AD. Andrawis et al [129] examined the influence of maternal history of dementia on hippocampal atrophy and found smaller baseline and 12-month follow-up hippocampal volumes in MCI patients with maternal, but not paternal, history. *APOE* ε4-positive patients also had decreased hippocampal volumes, regardless of parental history. These results suggest the involvement of maternally inherited genetic material, encoded on either the X chromosome or mitochondrial genome. The latter may be more likely, given that decline in mitochondrial function has been found to lead to increased generation of reactive oxygen species, enhanced apoptosis, cell loss, and brain atrophy [129].

4.4.1.2. Other ROIs

Although the caudate has not been the subject of intensive AD research, it plays a crucial role in the formation of new associations required for the acquisition of explicit memories. Madsen et al [130] found that baseline caudate atrophy was associated with a number of clinical and biochemical measures, including, most strongly, body mass index (BMI), in the AD group alone and in the pooled sample, and CDR-SB and MMSE scores at baseline (Table 5). There appeared to be preferential right caudate atrophy in AD patients, and the authors proposed that caudate atrophy might function as a complementary biomarker to other structural measures. The inferior parietal lobe (IPL) is involved in
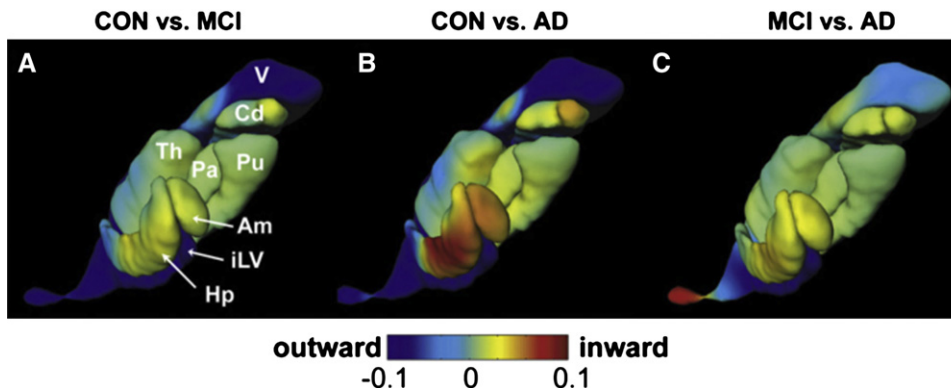

Fig. 11. Group differences in regional shape deformations. Abbreviations: Am, amygdala; Hp, hippocampus; V, ventricles; iLV, inferior lateral ventricles; Cd, caudate; Pu, putamen; Pa, globus pallidus; Th, thalamus. Reproduced with permission from Ref [122].
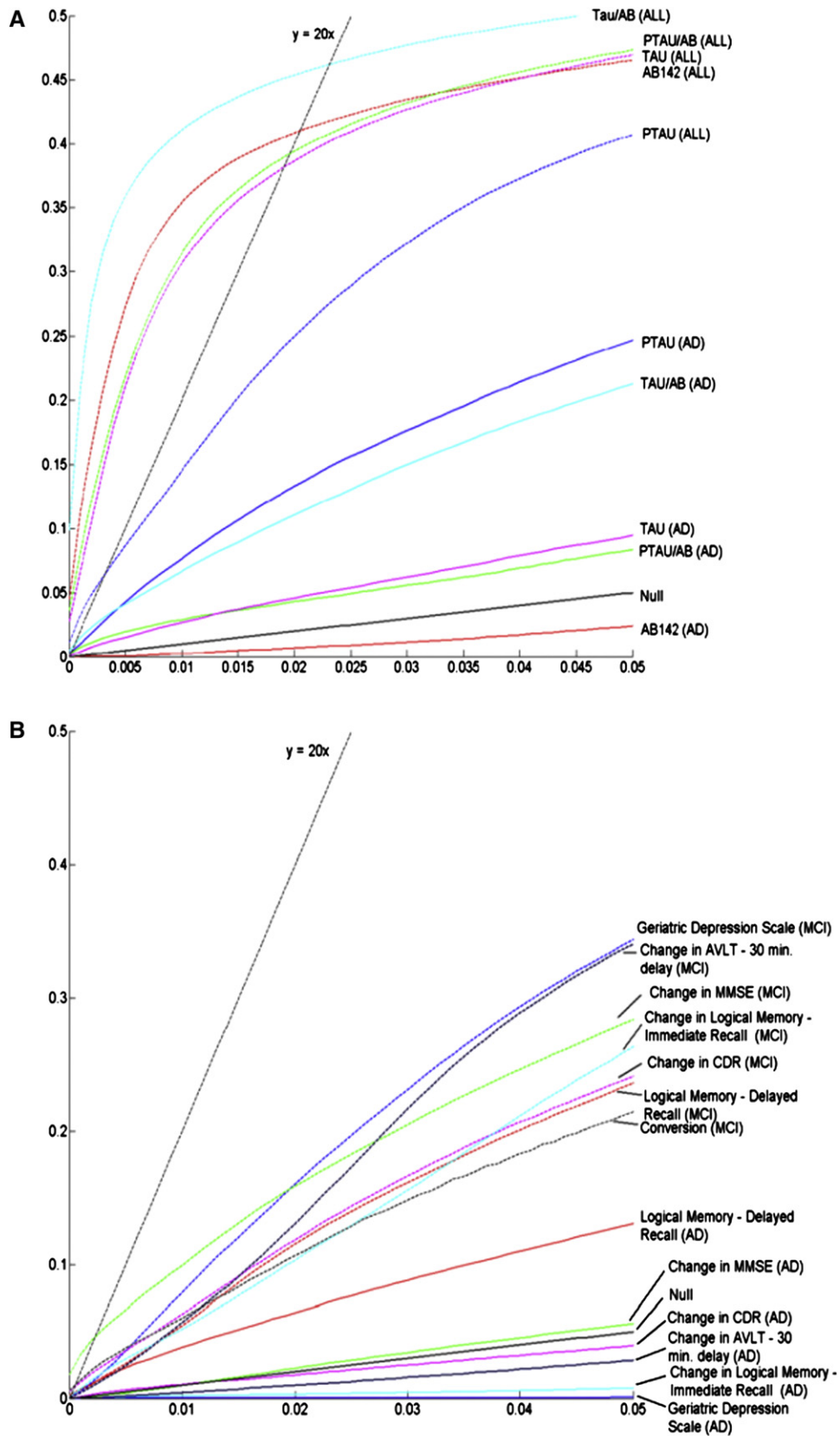
Fig. 12. Cumulative distribution function (CDF) plots for voxelwise correlation of progressive temporal lobe tissue loss in MCI, AD, and pooled groups. (A) Correlations with various biomarker indices, including Aβ-42 (AB142), tau protein (TAU), phosphorylated-tau 181 (PTAU), tau/Aβ-42 ratio (TAUAB), and p-tau/Aβ-42 ratio (PTAUAB), and (B) correlations with various clinical measures. Reproduced with permission from Ref [113].

Table 5
Associations between biomarker and clinical measures in ADNI cohort (correlation coefficients)

Biomarker	N	Clinical group	MMSE	ΔMMSE	CDR-SB	ΔCDR-SB	ADAS-cog	ΔADAS-cog	LM-II-DR	AVLT	TMT A and B	Reference
Hippocampal volume (L/R)	21	Pooled sample	0.423*/0.529†		−0.369*/−0.705†							[63]
12-month hippocampal atrophy rate (L/R)	490	Pooled sample	−0.191†/−0.168†	0.117†/0.136†	0.173†/0.181†	−0.174†/−0.171†						[124]
12-month hippocampal atrophy rate (L/R)	555	Pooled sample	−0.52‡/−0.43‡	0.36‡/0.30‡	0.47‡/0.38‡	−0.27‡/−0.21‡						[64]
Hippocampal radial distance (L/R)	245	MCI					−0.20†/−0.17†		0.24§/0.31§	0.27§/0.25§		[123]
	98	AD					−0.21*/NS		NS/NS	0.21*/NS		
Hippocampal atrophy rate	498	Pooled sample						0.18*				[121]
	607	MCI								Learning 0.36‡ Retention 0.37‡		[140]
Cortical thickness												
Entorhinal										0.33‡ / 0.33‡		
Parahippocampal										0.22‡ / 0.23‡		
Frontal caudal middle										0.16‡ / NS		
Rostral middle										0.23‡ / 0.16c		
Lateral orbitofrontal										0.16‡ / NS		
Inferior parietal										0.24‡ / 0.17‡		
Precuneus										0.25‡ / 0.16‡		
Cortical thickness (L/R)	536	Pooled sample										
Posterior cingulate										0.14‡/0.13†	0.22†/0.19†	[138]
Caudal middle										NS/NS	0.17†/0.15†	High EF: TM A + B Low EF: AVLT
Rostral middle										0.30†/0.13‡	0.18†/0.21†	
Superior frontal										NS/0.13†	0.16†/0.17†	
Operculum										NS/NS	0.14†/0.16†	
Lateral bifrontal										NS/NS	0.15†/NS	
Frontal polar										NS/NS	0.17†/NS	
STAND score	399	Pooled sample	−0.50‡		0.59‡							[132]
	192	MCI	−0.19†		0.26‡							
	98	AD	−0.29†		0.34‡							
Aβ−42	399	Pooled sample	0.31‡		−0.37‡							
	192	MCI	NS		NS							
	98	AD	NS		NS							
Caudate volume	400	Pooled sample	0.175*		−0.209*							[130]
Hippocampal volume [130]			0.349*		−0.365*							
Ventricular volume			−0.205*		0.225*							

(Continued)

Table 5
Associations between biomarker and clinical measures in ADNI cohort (correlation coefficients) (*Continued*)

| Biomarker | N | Clinical group | Clinical correlates | | | | | | ΔADAS-cog | LM-II-DR | AVLT | TMT A and B | Reference |
			MMSE	ΔMMSE	CDR-SB		ΔCDR-SB	ADAS-cog					
Predicted scores from whole brain gray matter volumes	586	Pooled sample											[91]
MMSE			$0.47^{\ddagger}$										
ADAS-cog									$0.49^{\ddagger}$				
AVLT											NS		

| Biomarker | N | Clinical group | Clinical correlates | | | | | | | LM-II-DR | AVLT | TMT A and B | Reference |
			MMSE	ΔMMSE	CDR-SB	ΔCDR-SB	FAQ	ADAS-cog					
FDG 12 months ROI decline in CMRgl	154	MCI		$0.22^{\dagger}$		-0.19^{*}				NS			[104]
	69	AD		NS		-0.25^{*}				NS			
FDG-PET regional-to-whole brain CMRgl (L/R)													[134]
Posterior cingulate	298	Pooled sample	NS		$-0.47^{\S}$/NS								
Precuneus			$0.36^{\S}/0.37^{\S}$		$-0.46^{\S}/-0.49^{\S}$								
Parietal			$0.26^{\S}/0.36^{\S}$		$-0.42^{\S}/-0.47^{\S}$								
Temporal			$0.43^{\S}/0.32^{\S}$		$-0.41^{\S}/-0.41^{\S}$								
Frontal			$0.23^{\S}/0.22^{\S}$		$-0.24^{\S}/-0.26^{\S}$								
Medial temporal			NS		$-0.36^{\S}/-0.41^{\S}$								
Occipital			$0.31^{\S}/0.22^{\S}$		$-0.37^{\S}/-0.26^{\S}$								
ΔPiB uptake	$61^{\P}$	Pooled sample		-0.22 ($P = .09$)		NS							[16]
Ventricular expansion				$-0.52^{\dagger}$		$-0.42^{\dagger}$							
	161	Pooled sample									Learning	Recognition	[136]
Hippocampal volume											$0.35^{\S,**}$	$0.34^{\S,**}$	
Parahippocampal complex volume											NS	$0.17^{*,**}$	
Precuneus cortical thickness											$0.22^{\dagger,**}$	NS	
Inferior parietal lobe metabolism											$0.23^{\dagger,**}$	NS	
Hippocampal metabolism											$0.15^{*,**}$	$0.25^{\S,**}$	
APOE genotype											NS	$0.14^{*,**}$	
FDG-ROIs baseline	95	AD					NS	$-1.95^{\dagger,**}$					[135]
ΔFDG-ROIs							$-1.21^{\dagger,**}$	$-3.25^{\ddagger,**}$					

							Δ LM-II	Boston Naming	Category fluency	TMT B	
FDG-ROIs baseline	208	MCI				$-0.88^{\ddagger,**}$	$-0.66^{\dagger,**}$				
ΔFDG-ROIs						NS	$-1.08^{\ddagger,**}$				
Hypometabolic convergence index	188	Pooled sample	−0.48	0.54		0.53		−0.43	0.45		[85]
	50	MCI									[155]
Hippocampal volume			NS	NS		0.41*					
Retrosplenial volume			−0.42*	−0.43*		NS					
Retrosplenial metabolism			0.47*	NS		NS					
Entorhinal metabolism			0.38*	NS		NS					
							Δ LM-II	Boston Naming	Category fluency	TMT B	[142]
Right medial lobe atrophy rate				$-0.41^{\ddagger,\dagger\dagger}$							
Left entorhinal cortex							$0.47^{\ddagger,\dagger\dagger}$				
Left lateral lobe thinning								$0.31^{\ddagger,\dagger\dagger}$			
Left temporal lobe atrophy rate									$0.38^{\ddagger,\dagger\dagger}$		
Left frontal lobe — pars orbitalis										$0.33^{\ddagger,\dagger\dagger}$	
							Learning	Delayed recall			[110]
Hippocampal volume	156	MCI				−0.388	0.279	0.459			
Entorhinal metabolism						−0.406	0.175	0.318			

Abbreviations: ROI, region of interest; CMR-gl, cerebral metabolic rate for glucose; TMT, Trail Making Test; NS, not significant.

*$P < .05$.

†$P < .01$.

‡$P < .001$.

§$P < .0001$.

¶Includes 23 subjects from the Mayo Clinic Study of Aging.

**β values from regression model.

††Figures from a mixed effect model that examined baseline level and longitudinal change as independent variables as predictors of change.

Fig. 13. Apolipoprotein E (*APOE*) gene effects on regional brain volumes. Maps show the mean percent differences in regional brain volumes for four different group comparisons. Percent differences are displayed on models of the regions implicated: (A) ventricular cerebrospinal fluid (CSF), (B) sulcal CSF, (C) hippocampi, and (D) temporal lobes; dotted lines show the boundary of the hippocampus. Reproduced with permission from Ref [112].

sensory and motor association and possibly comprises part of the memory circuitry. Greene and Killiany [131] examined the associations between subregions of the IPL (gyrus, banks, and fundus) and cognitive measures in control, MCI, and AD subjects. They found that compared with control subjects, MCI patients differed only in the thickness of the banks of the left IPL, a change that correlated with decreased scores in the AVLT-DR, whereas AD patients had significant morphometric changes in all subregions of the right IPL. These results suggest a temporal sequence of changes during disease progression, with atrophy beginning in the left IPL and spreading to the right.

4.4.1.3. Multiple ROIs and whole brain studies

Other MRI studies have used approaches based on the whole brain or multiple ROIs, rather than specific ROIs. Evans et al [125] examined brain atrophy rates using the brain BSI technique and found atrophy to be associated with MMSE and ADAS-cog scores in MCI and AD patients. Within the MCI group, they found greater rates of change, in a range similar to that observed in the AD group, in subjects who converted to AD within the time frame of the study.

Stonnington et al [91] found that whole brain GM at baseline predicted baseline scores on the ADAS-cog and, MMSE, but not on the AVLT (Table 5). The latter is a more specific test of memory, and the authors suggest that whole brain methods may be preferentially more highly sensitive to tests, unlike the AVLT, that involve diverse brain regions. Vemuri et al [132] used STAND scores as a measure of the degree of AD-like anatomic features to assess correlations between brain morphometric changes and cognitive scores, and found that STAND scores were highly correlated with CDR-SB and MMSE scores in individual groups and the pooled sample (Table 5). These studies lend support for atrophy of the whole brain or multiple ROIs as biomarkers, based on their ability to differentiate between patient groups and healthy control subjects, and to track disease progression and clinical decline.

A measure derived from a multidimensional scaling method for quantifying shape differences using DBM [75] had a strong inverse correlation with the MMSE ($r = -0.53$), although the findings were limited by small sample size. Using the related method of TBM, Ho et al [133] created regional maps of changes in brain tissue and used the

resulting Jacobian values to represent brain tissue excess or deficit relative to a template. They found that lower brain volume in the frontal, parietal, occipital, and temporal lobes was associated with higher BMI in MCI and AD patients, and that ventricular expansion correlated with higher BMI in AD, but not MCI, patients (Fig. 14). Every unit increase in BMI was associated with a 0.5% to 1.5% decrease in brain volume in patients of the ADNI cohort.

4.4.2. [^{18}F]-fluorodeoxyglucose-positron emission tomography

FDG-PET has been used by several groups to investigate relationships between cerebral glucose hypometabolism and other factors, including cognitive measures and CSF biomarkers. Several papers confirmed that there is a characteristic regional pattern of hypometabolism in MCI and AD patients. Wu et al [101] found that hypometabolic voxels were associated with the posterior cingulate/precuneus and parietotemporal regions. Lower bilateral cerebral metabolic rate for glucose (CMRgl) at baseline in these regions and in the frontal cortex was associated with higher CDR-SB and lower MMSE scores in MCI and AD groups [134] (Table 5). Although the pattern of hypometabolism was similar in the two groups, the magnitude and spatial extent were greater with increasing disease severity. In the AD group alone, however, lower MMSE correlated with lower left frontal and temporal CMRgl, suggesting that the characteristic pattern of baseline reductions in glucose metabolism shifts to the frontal cortex after the onset of dementia. Chen et al [104] investigated declines in CMRgl in statistically predefined ROIs associated with AD over 12 months in the ADNI cohort and found significant changes in MCI and AD groups compared with control subjects bilaterally in the posterior cingulate, medial and lateral parietal, medial and lateral temporal, frontal, and occipital cortices. These changes correlated with CDR-SB, but not ADAS-cog, scores in both groups, and with MMSE scores in the MCI group (Table 5). Landau et al [135] found a greater decline in CMRgl in all a priori defined ROIs in AD patients and in a composite score of ROIs in MCI patients compared with control subjects. Longitudinal

glucose decline was associated with concurrent ADAS-cog scores and decline on the Functional Activities Questionnaire (FAQ), validating the relevance of longitudinal measures of glucose metabolism to both cognitive and functional decline. The annual decline in the ADAS-cog and FAQ was greatest in AD patients, followed by the MCI and control groups, in accordance with an acceleration of the disease process over time (Table 5). The hypometabolism index reported by Chen et al [85] correlated with cognitive measures of disease severity, hippocampal volume, and CSF biomarkers (Table 5). These papers support the use of glucose metabolism as a sensitive measure of cognition in AD.

4.4.3. Cognitive

A number of studies have focused on the relationship between cognitive function and imaging or CSF biomarkers. Atrophic changes in the episodic memory network (Fig. 15), which is composed of MTL structures, medial and lateral parietal cortical areas, and prefrontal cortical areas and is involved in the formation of new episodic memories, are presumed to underlie ongoing memory loss in AD. Walhovd et al [136] studied how baseline brain morphometry and metabolism within the episodic memory network and *APOE* genotype predicted memory, as assessed by the AVLT. They found that in the total sample of the ADNI cohort, hippocampal volume and metabolism, parahippocampal thickness, and *APOE* genotype predicted recognition, whereas hippocampal volume and metabolism, cortical thickness of the precuneus, and inferior parietal metabolism predicted learning, suggesting that MTL structures are related to learning, recall, and recognition, whereas parietal structures are involved solely in learning (Table 5). The authors concluded that MRI and FDG-PET imaging have differential sensitivity to memory in AD and thus provide complementary information. Episodic memory likely involves a number of different cognitive processes, such as initial encoding, learning on repeated exposure, and DR, which may be subserved by disparate components of the episodic memory network. Wolk and Dickerson [137]
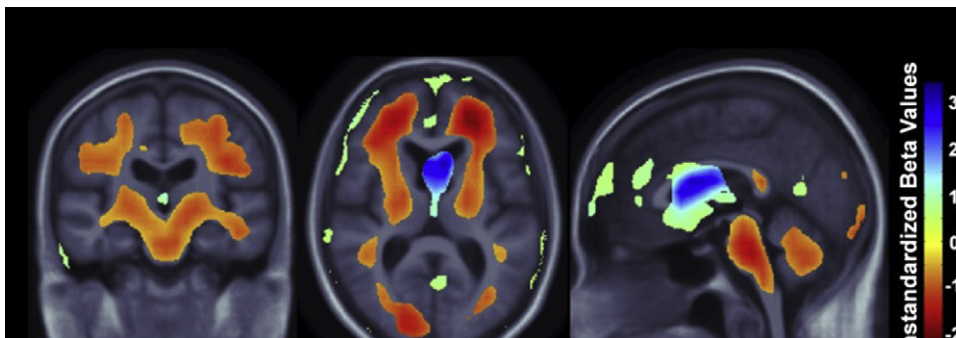

Fig. 14. Association of regional brain tissue volumes with body mass index. These represent the estimated degree of tissue excess or deficit at each voxel, as a percentage, for every unit increase in body mass index, after statistically controlling for the effects of age, sex, and education on brain structure. Images are in radiological convention (left side of the brain shown on the right) and are displayed on a specially constructed average brain template created from the subjects within each cohort (mean deformation template). Reproduced with permission from Ref [133].
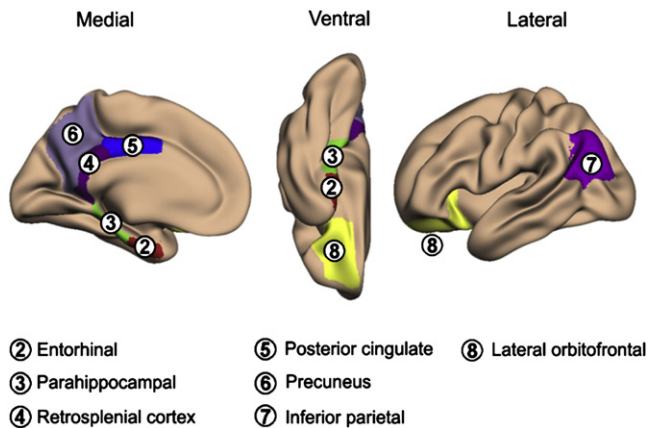
Fig. 15. The episodic memory network. Along with the hippocampal formation, the cortical areas shown here are part of the episodic memory network. Shown here are pial cortical representations of selected parcellations in the left hemisphere. From left to right: medial, ventral, and lateral views. Reproduced with permission from Ref [136].

investigated whether verbal episodic memory could be fractionated into dissociable anatomic regions in mild AD patients, using cortical thickness of predefined "AD signature" ROIs and hippocampal volume as structural measures and different stages of the AVLT as a verbal memory measure. They found that initial immediate recall trials were most significantly associated with the temporal pole region, but that regions in the MTL became more significantly associated in later trials. In tests of DR, only the hippocampus correlated with performance, whereas the perirhinal/entorhinal cortex was most strongly associated with delayed recognition discrimination. The authors concluded that their results lend support to models hypothesizing that dissociable brain regions are involved in differential episodic memory processes. Associations between memory learning and brain morphometry in the MTL were found in a study by Chang et al [138]. MCI patients were differentiated into learning-deficit and retention-deficit subgroups using the AVLT. Low memory retention was associated with changes in the medial temporal regions, particularly the hippocampus and entorhinal cortex, whereas low memory learning correlated with a more widespread pattern of morphometric changes beyond the temporal lobe, including areas of the frontal and parietal lobes (Table 5). While memory loss is a hallmark of AD, a subset of MCI patients is impaired primarily in their executive function. Dickerson and Wolk [139] identified dysexecutive and amnestic phenotypes in patients with MCI or very mild AD based on performance on the Trail Making Test and ADAS-cog subscale: Word recognition. They found that the memory-impaired group had a more frequent occurrence of the *APOE* ε4 allele status than the dysexecutive group, and that patients with low executive function had thinner frontoparietal cortical regions and were more impaired in daily life than those with predominantly memory impairment. A further study by Chang et al [140] found that MCI patients with high executive function

performed better on tests of verbal memory than those with low executive function, and that morphometric measures of the two groups differed primarily in the dorsolateral prefrontal and posterior cingulate cortices, where more thinning was evident in low executive function patients (Table 5). Results from both studies suggest that the dysexecutive phenotype may reflect differences in underlying pathology in brain regions beyond the MTL.

The ideas that different brains regions subserve different cognitive functions and that MCI is a heterogeneous construct led Wolk et al [141] to examine the influence of *APOE* genotype on memory and executive function in AD. When cortical thickness in predefined ROIs was examined in carriers and noncarriers of the *APOE* ε4 allele who had a CSF biomarker profile consistent with AD, carriers were more impaired in measures of memory retention and had greater atrophy in medial temporal regions, whereas noncarriers were more impaired in tests of executive function, working memory, and lexical access and had greater frontoparietal atrophy. The finding that neuroanatomic regions thought to subserve different cognitive processes are differentially affected by *APOE* ε4 allele status supports the hypothesis that this allele exerts its effect on AD by influencing different large-scale brain networks.

The question of whether domain-specific cognitive deficits in MCI are caused by global atrophy or progressive atrophy within specific regions was studied by McDonald et al [142], who examined 2-year regional atrophy rates in MCI patients. Stepwise regression models revealed that left entorhinal atrophy, left lateral lobe thinning, left temporal lobe atrophy, left frontal lobe atrophy rate, and the right MTL atrophy rate were associated with memory decline (Logical Memory II), naming decline (Boston Naming Test), semantic fluency decline (Category Fluency Test), executive function (Trail Making Test B; TMT-B), and clinical decline (CDR-SB), respectively (Table 5). This study affords a glimpse into the specific structure–function relationships that occur early in disease progression and enhances our understanding of the neural basis of cognitive impairments.

Although studies, such as those described previously, have focused on the relationship between brain atrophy, *APOE* ε4 status, and cognitive decline, relatively little is known about the biomarkers of functional decline, a hallmark of AD. Accordingly, the rate of decline in the FAQ, a measure of the ability of patients to maintain daily function, and how it is affected by cerebral atrophy and *APOE* ε4 allele status, was studied by Okonkwo et al [143]. They found that AD patients had a higher rate of functional decline than control subjects, with the rate of MCI patients intermediate between the two. Moreover, MCI patients who subsequently progressed to dementia had higher rates of decline on the FAQ than stable MCI patients. Increasing ventricle-to-brain ratio, the measure of neurodegeneration chosen for the study, correlated with increased functional impairment in MCI patients. Those patients who were both *APOE* ε4-positive and had elevated ventricle-to-brain ratio were the most functionally impaired.

These results parallel studies that have shown neurodegeneration and *APOE* ε4 status to be associated with cognitive decline. In a further study by the same group, Okonkwo et al [144] investigated the relationships between CSF biomarkers and everyday function, as assessed by the FAQ. They found that biomarkers were more sensitive to functional decline in control subjects and MCI patients than in AD patients, and that in the latter group, scores on the ADAS-cog were more highly correlated with functional activity. Combinations of tau and Aβ-42 abnormalities had the steepest rates of functional decline across clinical groups. The authors suggested that the effect of CSF abnormalities on functional decline is partially mediated by their effect on cognitive status.

In elderly populations, in addition to brain atrophy or genetic studies, BMI has been associated with cognitive decline. Cronk et al [145] examined the relationship between BMI and cognition in MCI patients and found that lower BMI at baseline was associated with a decline in the MMSE, ADAS-cog, and a global composite of the ADNI neuropsychological battery, but not with CDR-SB scores or conversion to AD. The causal relationships between BMI and cognitive decline in MCI remain to be elucidated, but the authors suggest either that low BMI is a result of factors associated with MCI or that MCI patients with low BMI are predisposed to more rapid disease progression.

4.4.4. CSF biomarkers

The relationship between CSF biomarkers and neuronal degeneration has been investigated by a number of groups within and outside ADNI following the seminal publication by Shaw et al [57], which defined cut points for CSF tau and Aβ-42 based on an ADNI-independent cohort of autopsy-confirmed AD patients as well as normal control subjects and then applied these cut points successfully to the ADNI cohort. Follow-up studies went on to test the hypothesis that changes in levels of biomarkers occur early in disease and thus are likely predictive of future brain atrophy, if not directly associated with all parts of the degenerative process. For example, Tosun et al [146] examined how rates of regional brain trophy were related to levels of CSF biomarkers in MCI patients and healthy elderly control subjects. They found that lower CSF Aβ-42 levels and higher tau levels were associated with increased atrophy in numerous brain regions, beginning primarily in the temporal and parietal cortices in MCI patients and extending to regions not normally associated with amyloid pathology, such as the caudate and accumbens areas, in AD patients. Schuff et al [121] also found that increased rates of hippocampal atrophy were associated with lower levels of Aβ-42 in the MCI, but not AD or control, group. Leow et al [113] used TBM to examine rates of atrophy and found that lower CSF Aβ-42 levels, higher tau levels, and a higher p-tau/Aβ-42 ratio were significantly associated with temporal lobe atrophy in the pooled group, and, additionally, that within the AD group, levels of CSF p-tau and the p-tau/Aβ-42 ratio were also significantly associated. Fjell et al [147] investigated

whether baseline levels of CSF biomarkers were associated with baseline brain morphometric differences between control, MCI, and AD subjects, as measured by cortical thickness in a number of ROIs. They found that although CSF biomarkers levels could not account for baseline differences, they were moderately associated with longitudinal change in multiple areas, including medial temporal regions and beyond.

A second focus of research into CSF biomarkers has been how they are modulated by *APOE* genotype and their association with cognitive measures. Shaw et al [57] reported that Aβ-42 concentrations were dose dependent on the number of *APOE* ε4 alleles, with the highest concentrations found in homozygotes. Vemuri et al [128] found that Aβ-42 is more closely associated with *APOE* genotype than cognitive function (MMSE, CDR-SB), but that *APOE* genotype had no significant effect on levels of t-tau (Fig. 16). An earlier study by the same group [132] investigated the relationship between CSF biomarkers and cognitive function (MMSE and CDR-SB), and found that the CSF biomarkers Aβ-42, t-tau, and p-tau$_{181p}$ were only significantly correlated with cognitive function in the pooled sample (Table 5). Ott et al [148] studied the relationship between CSF biomarkers and ventricular expansion with the hypothesis that ventricular dilation may reflect faulty CSF clearance mechanisms resulting in reduced levels of Aβ. They found that ventricular expansion was associated with reduced CSF Aβ levels in normal elderly carriers of *APOE* ε4, but that in *APOE* ε4-positive AD patients, ventricular expansion was associated with increased levels of tau and not Aβ. The authors suggested that the *APOE* ε4 allele may exert its effect through modulation of CSF–blood–brain barrier function.

The results from these studies support a model in which changes in the levels of CSF biomarkers are an early step in the course of the disease that reflects the degree of AD pathology, and in which Aβ-42 is modulated by the *APOE* ε4 allele, which functions in the early stages of pathology by reducing the efficiency of Aβ-42 clearance. As described in the Genetics section 5.3, Kim et al [149] performed a genomewide search for markers associated with CSF analyte levels in the ADNI cohort. Overall, CSF Aβ-42 and tau, in conjunction with imaging measures of atrophy, are promising biomarkers for early detection of AD.

4.4.5. ^{11}C-PiB PET imaging

A complementary method for assessing amyloid deposition is ^{11}C-PiB PET imaging. Jack et al [16] investigated the relationship between amyloid deposition and ventricular expansion in the ADNI cohort by examining serial ^{11}C-PiB PET and MRI scans. They found no difference in the rate of global PiB retention between clinical groups, and changes in global PiB retention only weakly correlated with concurrent decline on MMSE and CDR-SB. In contrast, ventricular expansion increased from control subjects to MCI to AD groups and correlated strongly with concurrent cognitive decline (Table 5). The relationship between
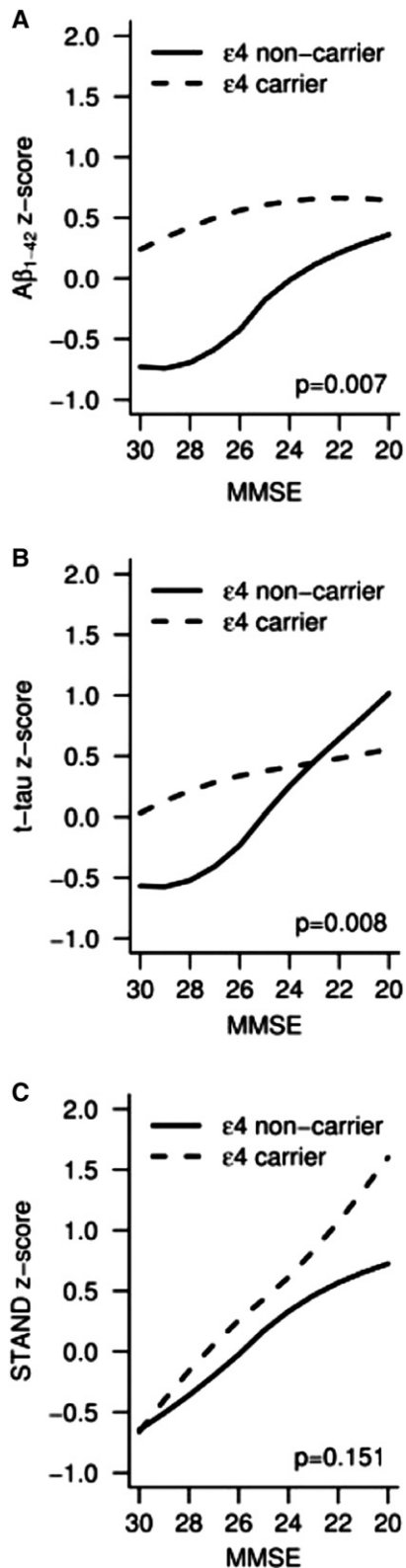
Fig. 16. Correlations between biomarker levels, structural abnormalities, and cognitive performance in *APOE* ε4 carriers and noncarriers. Smoothed biomarker (A and B) or STAND (C) *z* score curves plotted as a function of cognitive performance (Mini-Mental State Examination, MMSE). Abbreviation: STAND, Structural Abnormality Index. Reproduced with permission from Ref [128].

PET and CSF biomarkers and cognitive measures in the ADNI cohort at baseline was investigated by Jagust et al [150]. CSF Aβ-42 and ^{11}C-PiB PET were found to be in substantial agreement as measures of amyloid deposition, and neither measure correlated with MMSE scores. In contrast, FDG-PET, as a measure of cerebral glucose metabolism, was strongly correlated with MMSE scores, but much less so with CSF biomarkers (Table 6). Apostolova et al [151] also examined associations between hippocampal atrophy, CSF biomarkers, and average cortical, precuneal, and parietal uptake of ^{11}C-PiB. They found that although all CSF biomarkers were associated with hippocampal atrophy, the strongest correlations were with p-tau$_{181p}$ and the weakest with Aβ-42. Precuneal ^{11}C-PiB uptake was most strongly associated with hippocampal atrophy. Jack et al [152] examined the relationship between log relative hazard of progressing from MCI to AD and both hippocampal atrophy and amyloid load, measured as a composite of ^{11}C-PiB PET and CSF Aβ-42 data. They found that although the risk profile was linear throughout the range of hippocampal atrophy, amyloid load reached a ceiling at a certain concentration earlier in disease progression. These papers support a disease model in which initial amyloid deposition occurs in the early stages and does not correlate with cognitive decline, but stabilizes later in disease, and in which neurodegeneration accelerates with disease progression with concomitant cognitive decline.

4.4.6. Combined modalities

The dynamics of CSF, MRI, and FDG-PET biomarkers in the ADNI cohort were studied by Caroli and Frisoni [153] in an effort to understand how they change over the course of the disease. Each biomarker differed between clinical groups after post hoc analysis, and the authors found that these measures of disease progression fit better in sigmoidal, rather than linear, models, suggesting that individual biomarkers vary in their rate of change during disease progression. Aβ-42 imaging signals increased early in disease progression and then plateaued, whereas CSF Aβ-42 declined early and then plateaued, and hippocampal volume followed a similar trajectory, with volumes increasing later in disease progression. In contrast, FDG-PET measures of glucose metabolism and CSF tau began to increase early in disease progression and only stabilized at later stages of disease, suggesting that there is an ongoing reduction in glucose metabolism and tau-mediated neurodegeneration throughout the early stages of AD (blue line in Figs. 2 and 17). Carriers of the *APOE* ε4 allele had earlier hippocampal atrophy. A similar study by Beckett et al [154] also found that measures associated with early disease, such as Aβ-42, had greater changes in MCI patients than in AD patients, and that those associated with later changes, such as those in FDG-PET ROIs, were more evident in AD patients (Table 7). The authors hypothesized that changes in biomarkers may not be linear and that for each biomarker, there may be steeper rates of change in some stages of

Table 6
Associations between imaging, clinical, and CSF biomarkers (correlation coefficients)

Imaging or clinical biomarker	N	Clinical group	CSF biomarker correlates				FDG-PET composite ROI	Mean cortical PiB SUVR	Reference
			Aβ−42	t-tau	p-tau$_{181p}$	t-tau/Aβ−42			
Hippocampal volume (L/R)	388	Pooled sample	0.11*/0.17[†]	−0.17[†]/0.21[‡]	−0.17[†]/−0.23[‡]	−0.17[†]/−0.21[‡]		−0.24*/−0.23*	[151]
Mean cortical PiB SUVR	55	Pooled sample	−0.73[‡]	−0.42[§]	0.49[‡]		0.28*		[34]
FDG-PET composite ROI			0.33[†]	0.24 (P = .08)	0.34[†]				
MMSE			NS	0.26 (P = .055)	0.28*		0.63[‡]	NS	
Aβ−42				0.38[†]					
APOE ε4	77	CN	−0.50[‡]	NS	NS				[146]
	119	MCI	−0.49[‡]	0.39[‡]	0.34[†]				
	54	AD	−0.53[‡]	NS	NS				

Abbreviations: NS, not significant; SUVR, standard uptake value ratio.
*P < .05.
[†]P < .01.
[‡]P < .001.
[§]P < .0001.

disease progression than others. In seeking an optimum combination of imaging and CSF biomarkers to predict normal control/AD classification, Walhovd et al [155] examined the relationships between the best predictive biomarkers and changes in cognitive scores in the MCI group. They found that changes in MMSE scores correlated with retrosplenial volume and metabolism as well as entorhinal volume, but that only hippocampal volume was associated with the Logical Memory II-DR, and only retrosplenial volume was associated with changes in CDR-SB. No CSF biomarkers were significantly associated with cognitive scores in this clinical group (Table 5). Once again, these results are consistent with the disease progression model in that earlier changes that are reflected in CSF biomarkers do not correlate with clinical measures, whereas changes in brain metabolism and morphometry occur at later stages of the disease and therefore correlate better with cognitive measures. Further support for this model comes from the study of the annual change in MRI and CSF biomarkers and how these are influenced by *APOE* genotype in control, MCI, and AD subjects [156]. Levels of neither Aβ-42 nor t-tau changed significantly over 12 months in any clinical group, but annual changes in ventricular volume increased with disease severity and were correlated with worsening cognitive and functional indices. *APOE* ε4 carriers had higher rates of change in ventricular volume, but not in levels of CSF biomarkers, consistent with the model in which levels of Aβ and tau plateau as neurodegeneration becomes detectable by MR measures.

The question of whether structural or metabolic measures are the most sensitive biomarkers of changes associated with early stages of AD was investigated by Karow et al [110]. Directly comparing the ability of MR and FDG-PET measures in prespecified ROIs to detect such changes by quantifying and comparing their effect sizes (Cohen *d*), they found

that largest morphometric effect size (hippocampal volume: 1.92) was significantly greater than the largest metabolic effect size (entorhinal metabolism: 1.43). Both measures were significantly associated with ADAS-cog and AVLT scores in AD patients, but in MCI patients, the relationship was only maintained with hippocampal volume (Table 5). The authors concluded that for the detection of early AD, MRI may be preferable to FDG-PET, as it is more sensitive, more widely available, less invasive, and less costly.

4.4.7. Summary and conclusions of papers concerning associations of the ADNI cohort

ADNI has succeeded in recruiting a cohort of MCI and mild AD patients that mirrors populations used for clinical trials of AD therapies. A number of cross-sectional and longitudinal studies have lent support to a model of disease progression in which the earliest indications of neurodegeneration occur within the MTL, particularly the hippocampus, and atrophy becomes more widespread in later stages, ultimately encompassing areas of the parietal, occipital, and frontal lobes. Rates of atrophy are initially fastest in the temporal lobe, but accelerate in other regions as the disease progresses. Cortical atrophy and that of specific regions identified in the model of disease progression as well as ventricular enlargement have been correlated with measures of clinical severity. Structure–function relationships within the brain are being elucidated with findings that atrophy in dissociable anatomic regions, especially within the episodic memory network, is associated with different cognitive functions. Patterns of glucose hypometabolism associated with AD have been identified, with the precuneus and posterior cingulate typically displaying the most reduced CMRgl and with reduced metabolism in these key areas being associated with lower scores on cognitive tests. The differential effects of an SNP in brain-derived neurotrophic factor suggest that genetics may modulate
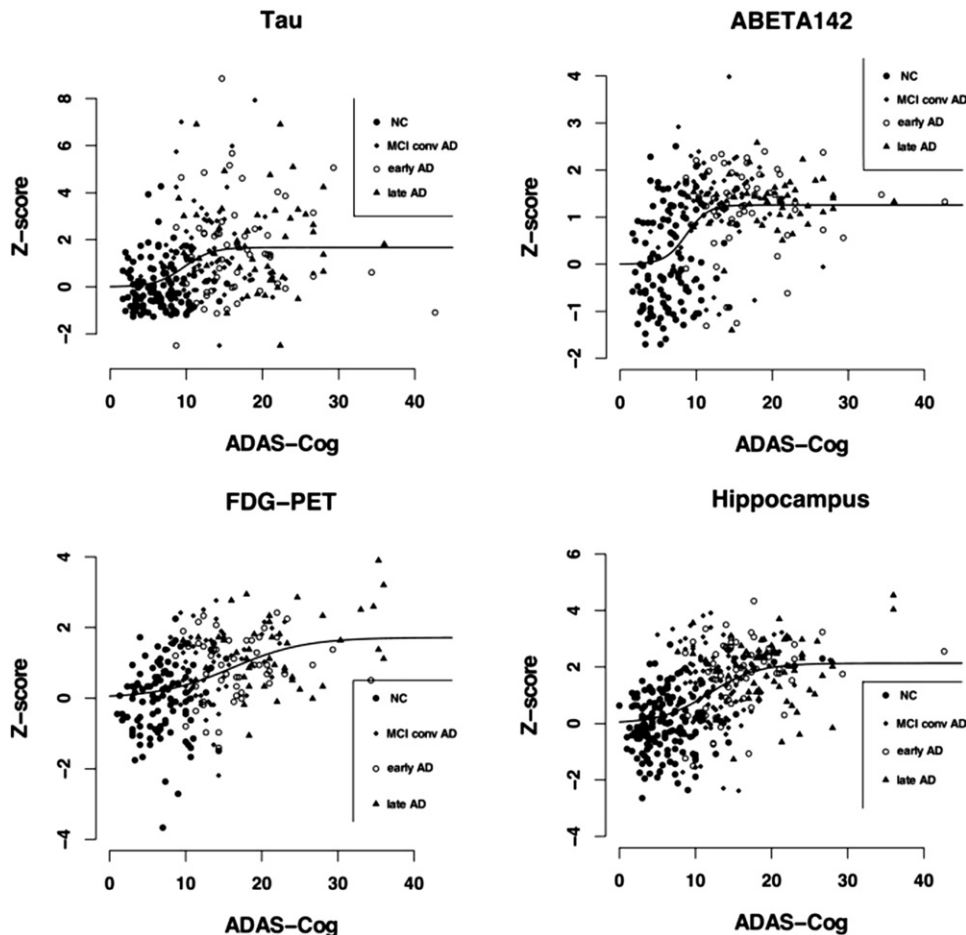
Fig. 17. Biomarker trajectories through disease progression. For each biomarker, individual *z* scores are plotted against ADAS-cog (cognitive subscale of the Alzheimer's Disease Assessment Scale) scores, and the fitted sigmoid curve is displayed. Full circles denote healthy control subjects, full squares MCI patients converted to AD, empty circles early AD, and full triangles late AD patients. Sigmoid fitting was better than linear fitting for tau, Aβ-42, and hippocampus (for the latter: sigmoid nonsignificantly better than linear); linear fitting was better for [^{18}F]-fluorodeoxyglucose-positron emission tomography (FDG-PET). Reproduced with permission from Ref [153].

glucose metabolism. Levels of CSF biomarkers, particularly Aβ and tau, have been associated with earlier stages of neurodegeneration. ^{11}C-PiB PET Aβ imaging has largely confirmed that decreased levels of CSF Aβ and increasing ^{11}C-PiB PET

Table 7
Mean (standard deviation) of annualized change for selected ADNI variables

Variable name	Annualized mean change by diagnosis		
	Normal control	MCI	AD
CSF Aβ−42	−0.94 (18)	−1.4 (17)	−0.1 (14)
CSF tau	3.45 (13)	2.34 (21)	1.24 (24)
PiB	0.098 (0.18)	−0.008 (0.18)	−0.004 (0.25)
FDG-PET: ROI-avg	−0.006 (0.06)	−0.015 (0.064)	−0.081 (0.047)
Hippocampus	−40 (84)	−80 (91)	−116 (93)
Ventricles	848 (973)	1551 (1520)	2540 (1861)
ADAS-cog total	−0.54 (3.05)	1.05 (4.40)	4.37 (6.60)
MMSE	0.0095 (1.14)	−0.64 (2.5)	−2.4 (4.1)
CDR-SB	0.07 (0.33)	0.63 (1.16)	1.62 (2.20)
AVLT 5-trial total	0.29 (7.8)	21.37 (6.6)	23.62 (5.6)

NOTE. Reproduced with permission from Ref [154].

represent an early event in disease progression, and neither amyloid imaging nor studies of CSF biomarkers have found that levels of these biochemicals are strongly associated with cognitive decline. Levels of CSF biomarkers have been found to be abnormal (i.e., decreased CSF Aβ and increased CSF tau) early in disease and then plateau with little detectable change, whereas glucose metabolism remains relatively stable until the latest stages of disease progression. Presence of the *APOE* ε4 allele has been shown to enhance neurodegeneration and to modulate levels of CSF biomarkers, but the exact mechanism by which it exerts its effect remains unclear. Likewise, the role of BMI has been the subject of contradictory reports, and it is unknown whether changes in BMI influence disease development or occur as a result of the disease.

4.5. Diagnostic classification of study participants

The ability to accurately diagnose to which clinical group a subject belongs is a crucial one in the clinical trial design. To this end, some researchers have investigated the ability of individual MRI, FDG-PET, and CSF biomarkers to discriminate

between ADNI AD participants and ADNI control subjects, and between MCI-c and MCI-nc subjects. Others have tried to determine the optimum combination of these biomarkers for ADNI participant classification, with many studies leveraging knowledge of associations between various structural and fluid biomarkers and the sequence of brain morphometric change over the course of disease to guide development of marker combinations. Discrimination between the clinically distinct ADNI participant groups offers an important first step in identifying biomarker diagnostic tools that can be validated in representative population-based studies before clinical use.

4.5.1. Magnetic resonance imaging

4.5.1.1. Temporal lobe structures

Atrophy of the hippocampus, the best studied structure affected by AD, has been used in patient classification by a number of groups. Chupin et al [68] correctly distinguished AD patients from control subjects 76% of the time, and MCI patients who would convert within 18 months from control subjects 71% of the time (Table 8). Karow et al [110] found that hippocampal volume discriminated between control subjects and AD patients with an AUC of 0.90, and between control subjects and MCI patients with an AUC of 0.75 (Table 8). The discriminative ability of the rate of hippocampal atrophy was investigated by Wolz et al [64], who found that their method correctly classified 75% to 82% of AD patients and 70% of MCI patients who converted to AD over 12 months. Their method was also able to discriminate between MCI-c and MCI-nc patients at a rate of 64% (Table 8). Calvini et al [66] derived a statistical indicator from the hippocampus and other MTL structures and were able to discriminate between AD and control groups, and between MCI and control groups, with AUCs of 0.863 and 0.746, respectively (Table 8).

4.5.1.2. Multiple ROIs and whole brain

Other methods have focused on many ROIs across the brain, using the degree of association with AD to construct a score reflective of the anatomic profile of AD. These include temporal, cingulate, and orbitofrontal regions. The classifier developed by Fan et al [83] produced an SPS that allowed direct comparison of patients and was able to discriminate between AD and control subjects, between MCI and control subjects, and between AD and MCI subjects with AUCs of 0.965, 0.846, and 0.750, respectively (Table 8). Similarly, Misra et al [118] extracted an abnormality score that discriminated MCI-c patients from MCI-nc patients with a classification accuracy of 81.5 and an AUC of 0.77 (Table 8). Using a semisupervised SVM, Filipovych and Davatzikos [93] discriminated between MCI-c and MCI-nc patients with an AUC of 0.69, comparing favorably with fully supervised SVM methods (Table 8). They also found that 79.4% of all converters were classified as AD-like (the remainder being classified as normal-like). In addition, 51.7% of nonconverters were classified as normal-like and the remainder as AD-like, perhaps representing a proportion of MCI patients who would convert to AD further in the

future. The authors also found that semisupervised SVM performed better than a fully supervised SVM in instances when there were a small number of labeled images. The classifier developed by Yang et al [94], which relied on image features defined by ICA, discriminated between control and AD subjects with an accuracy of 80.7%, a sensitivity of 81.9%, and a specificity of 79.5%, and between control and MCI subjects with an accuracy of 71.1%, a sensitivity of 73.2%, and a specificity of 68.6%, based on GM images and a training set-to-test set ratio of 90%:10% (Table 8).

McEvoy et al [117] presented data from their fully cross-validated linear discriminant model compared with partially cross-validated models, and found that the fully cross-validated model discriminated between AD and control subjects with an accuracy of 89%, a sensitivity of 83%, a specificity of 93%, and an AUC of 0.915 (Table 8). They noted that these numbers were lower than those obtained using the partially cross-validated model, suggesting that numbers presented by other studies using partially cross-validated models may be artificially high. Hinrichs et al [88] used a classifier based on GM probability maps and found that it discriminated between AD and control subjects with a sensitivity of 85% and a specificity of 80%. Park and Seo [75] tested their method of multidimensional scaling (MDS) of DBM and compared it with the ability of hippocampal volume to discriminate between AD and control subjects. They found that their MDS method outperformed hippocampal volume, yielding accuracies of 86.3% and 75.0%, respectively (Table 8). Further details of classifier construction using SVMs are given in the Methods section 3.3.

Longitudinal measurements of cortical thickness were the focus of a classifier constructed by Li et al [157]. They found that although the pattern of cortical thinning was similar in all patient groups, the rate of thinning and ratio of follow-up to baseline measures provided a better tool for distinguishing between MCI-c and MCI-nc patients. An additional complementary component in the form of a brain network feature computed from the correlations of cortical thickness changes with ROIs further improved classification accuracy. The final classifier, comprising static, dynamic, and network measures, discriminated between normal control subjects and AD patients with an accuracy of 96.1%, and between MCI-c and MCI-nc patients with an accuracy of 81.7% (Table 8).

4.5.1.3. Comparison of MRI methods

Cuingnet et al [158] directly compared 10 methods for the automatic classification of AD patients from anatomical MR data using the ADNI database. Five voxel-based approaches, three cortical approaches, and two methods based on hippocampal shape and volume were tested for their ability to discriminate between control, MCI-c, MCI-nc, and AD subjects. They found that voxel- or cortical thickness-based whole brain methods yielded highest sensitivities for AD versus control subjects (maximum of 81%), but that sensitivities were substantially lower for discriminating between MCI-c and MCI-nc subjects (maximum of 70%).

Table 8
Methods for the classification of MCI and AD patients

Method	Control vs AD				Control vs MCI				Control vs MCI-c				MCI-c vs MCI-nc				Cross-validated?	Reference
	SEN	SPE	ACC	AUC	SEN	SPE	ACC	AUC	SEN	SPE	ACC	AUC	SEN	SPE	ACC	AUC		
Hippocampal volume	75	77	76		61	71	72		72	67			66	60				[68]
Hippocampal volume	82	89							49	89			62	67				[68]**
12-month hippocampal atrophy rates	81	83	82	0.88	59	71	63	0.71	73	78	76		62	68	66			[60]
MTL structural atrophy	74	85		0.86	45	85		0.75	85	83		0.88						[66]
SPS score			82	0.97			76	0.85									Yes	[83]
SPS score	71	77							70	73			62	69				[83]**
ROI atrophy score	83	93	89	0.92													Yes	[117]
DBM-multidimensional scaling			86.3															[75]
ROI atrophy score															81.5	0.70	Yes	[118]
Semisupervised SVM, SPS score	79.6	85.7	82.9													0.69	Yes	[93]
ICA and SVM–gray matter	81.9	79.5	80.7		73.2	68.6	71.1											[94]
FDG-PET abnormality index	83	78		0.90														[84]
FDG-PET functional connectivity	88	88															Yes	[65]
FDG-PET factor analysis feature selection	98.1	92.5	95.2		91.2	80.8	88.0										Yes	[90]
AD-like brain regions																	Yes	[88]
MRI	85	80	82	0.88														
FDG-PET	84	82	84	0.87														
Hippocampal volume																		[110]
MRI					0.90				0.75									
Entorhinal metabolism																		
FDG-PET					0.71				0.63									
AD-like brain regions–Bayesian approach			87.6															[89]
Hippocampal volume, ventricular expansion, APOE, age			82	0.95													Yes	[86]
Hippocampal volume, ventricular expansion, age							71	0.86										
T-tau	69.3	92.3	80.6	0.83														[57]
Aβ−42	96.4	76.9	87.0	0.91														
p-tau$_{181p}$	67.9	73.1	70.4	0.75														
t-tau/Aβ−42	85.7	84.6	85.2	0.92														
p-tau$_{181p}$/Aβ−42	91.1	71.2	81.5	0.86														
LR$_{TAA}$ model	98.2	79.5	89.9	0.94														
Cortical normalized thickness index (NTI)																0.76	Yes	[165]
AVLT																0.67		
ADAS-cog–DR																0.67		
MMSE																0.64		
Longitudinal cortical thickness: static, dynamic, and network features			96.1												81.7	0.88		[225]

MRI: Hippocampal volume, entorhinal thickness, retrosplenial thickness			85.0		[155]
FDG-PET: Entorhinal, retrosplenial, lateral orbitofrontal metabolism			82.5		
CSF: t-tau/Aβ−42			81.2		
Combination: Hippocampal volume, retrosplenial thickness; entorhinal, retrosplenial, orbitofrontal metabolism, t-tau/Aβ−42			88.8		
t-tau/Aβ–42, left entorhinal cortex, hippocampal volume	82.5	90.1	86.7	Yes	[161]
t-tau/ Aβ−42, RAVLT immediate and delayed recall, TMT−B*	93.8	95.6	94.8		
LT_{RAA}, left entorhinal cortex, hippocampal volume	90.1	92.1	91.1		
LT_{RAA}, left entorhinal cortex, hippocampal volume, RAVLT immediate and delayed recall, TMT-B	92.2	97.5	95.2		
ADAS-cog			0.93	Yes	[87]
FDG-PET–30 best features			0.94		
Combined classifier			0.97		

Abbreviations: t-tau, total tau; SEN, sensitivity; SPE, specificity; ACC, accuracy; AUC, area under the curve; SPS, structural phenotypic score; MTL, medial temporal lobe; DBM, deformation-based morphometry; SVM, support vector machine; ICA, independent component analysis.

*MRI measures no longer significant in this model ** in [158].

4.5.2. *[¹⁸F]-fluorodeoxyglucose-positron emission tomography*

As AD affects not only morphology but also metabolism in the brain, Haense et al [84] used the AD t-sum measure of scan abnormality from FDG-PET data to discriminate between AD and control subjects with a sensitivity of 83% and a specificity of 78% (Table 8). The HCI of Chen et al [85], which also capitalized on hypometabolism data across the entire brain, was significantly different in control, MCI-nc, MCI-c, and AD subject groups. The method of Hinrichs et al [88], described in the MRI section, was also used with FDG-PET data and was able to discriminate between AD and control subjects with a sensitivity of 78% and a specificity of 78% (Table 8). Huang et al [65] used FDG-PET data to examine functional connectivity between brain regions and then leveraged the patterns they found to be typical of AD for classification purposes. They found that compared with control subjects, AD patients had decreased temporal lobe inter-regional connectivity, especially in the hippocampus, and weaker between-lobe and between-hemisphere connectivity. In contrast, MCI patients had increased connectivity between occipital and frontal lobes compared with control subjects, illustrating the uniqueness of this condition. This method discriminated between AD and control subjects with a specificity of 88% and a sensitivity of 88% (Table 8). Using their method based on feature selection using factor analysis and an SVM, Salas-Gonzalez et al [90] discriminated between AD and control subjects with sensitivity, specificity, and accuracy of 98.1%, 92.5%, and 95.2%, respectively, and between MCI and control subjects with sensitivity, specificity, and accuracy of 92.1%, 80.8%, and 88.0%, respectively (Table 8). Having identified entorhinal metabolism as the FDG-PET measure with the largest effect size for the detection of early AD, Karow et al [110] found that this measure discriminated between control and AD subjects with an AUC of 0.71, and between control and MCI subjects with an AUC of 0.63 (Table 8). Mormino et al used ¹¹C-PiB PET imaging to deduce a cutoff point to optimally separate PiB-positive from PiB-negative MCI patients, and found that PiB-positive MCI patients had lower hippocampal volumes and greater episodic memory loss compared with MCI patients with ¹¹C-PiB levels below the cutoff point of 1.465.

4.5.3. *CSF biomarkers*

Shaw et al [57] examined CSF biomarkers in the ADNI cohort as well as in a cohort of non-ADNI autopsy-confirmed AD patients, with the goal of developing a "biomarker signature" best able to predict AD and to classify patients correctly. Like many smaller studies, they found that t-tau and p-tau$_{181p}$, as well as the t-tau/Aβ-42 and p-tau$_{181p}$/Aβ-42 ratios, all increased in MCI patients compared with control subjects, whereas CSF Aβ-42 decreased. The best single measure for discriminating between AD and control subjects was CSF Aβ-42, which had an AUC of 0.913, a sensitivity of 96.4%, a specificity of 76.0%, and an accuracy of 87% (Table 8). Linear regression analyses determined which variables, including *APOE* genotype, contributed most to the discrimination, and a final linear regression model, which included Aβ-42, *APOE* ε4 carriers, and t-tau (LR$_{TAA}$ model), resulted in enhanced discrimination over individual factors (Table 8). De Meyer et al [159] used an unsupervised learning method that did not presuppose clinical diagnosis to identify biomarkers of AD. A mixture modeling approach derived a signature, consisting of both Aβ-42 and t-tau concentrations, which had a sensitivity of 94% in autopsy-confirmed AD patients from an independent cohort and was present in 90%, 72%, and 36% of patients with AD, MCI, and no cognitive impairment, respectively (Fig. 18). *APOE* ε4 carriers were over-represented in those patients with the AD biomarker signature by a factor of 6.88:1. Interestingly, when modeling single biomarkers, the cutoff concentration of Aβ-42 that optimally delineated AD patients from healthy elderly subjects was found to be 188 pg/mL, close to that found by Shaw et al [57] and Schott et al [160]. Moreover, the proportion of healthy elderly subjects with an identifying AD CSF biomarker signature was similar to that found by Schott et al [160], and likely reflects a proportion of cognitively normal elderly subjects who will progress to MCI and AD in the future. Further, De Meyer et al [159] examined another data set with MCI patients (n = 57) followed up for 5 years, and they showed that their model had a sensitivity of 100% in patients progressing to AD. The finding that AD pathology is detectable in significant numbers of healthy elderly control subjects has important implications for future clinical trials and suggests the possibility of presymptomatic treatment studies of potential AD-preventive compounds.

4.5.4. *Clinical*

Llano et al [96] compared the ADAS-cog and MMSE tests with a new form of ADAS-cog in which the subscores were given weights using a Random Forests tree algorithm, thereby resulting in a new metric, the composite ADAS.Tree. Therefore, ADAS.Tree represents a multivariate model in which subscales have been weighted according to their importance in discriminating between AD and control subjects. When the ability of ADAS.Tree to classify control, MCI, and AD subjects was compared with that of ADAS-cog and MMSE, the composite model generated a numerically highest test statistic. The authors suggest that this derivative of an internationally recognized and easily administered test may offer a more widely useful and less expensive approach to other imaging and CSF biomarkers that can be invasive and/or expensive.

4.5.5. *Combined modalities*

The approach of Kohannim et al [86] combined multiple factors, including MRI and FDG-PET measures, CSF biomarkers, *APOE* genotype, age, sex, and BMI, to enhance machine learning methods for AD diagnosis. They found that the optimum combination of factors to discriminate between AD and control subjects—hippocampal volume, ventricular expansion, *APOE* genotype, and age—yielded an
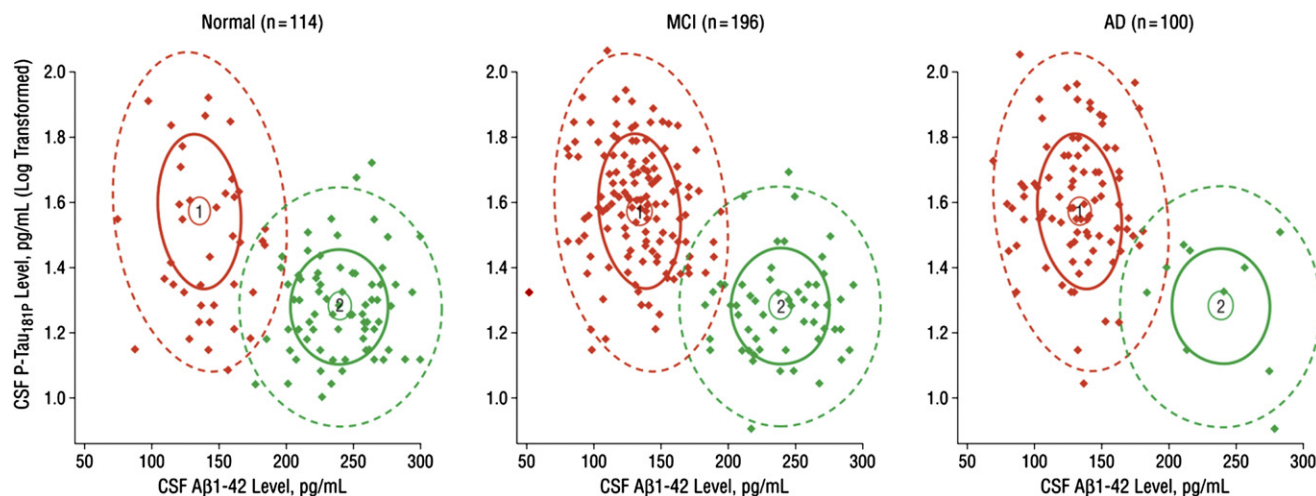
Fig. 18. Separation of control, MCI, and AD subjects using a CSF Aβ-42/t-tau mixed model signature. A combined CSF Aβ-42/t-tau mixed model was applied to the subject groups. Densities of each signature are represented with confidence ellipses, and signature membership of the subject based on the mixture is indicated with the corresponding color (signature 1 is the AD signature [red]; signature 2 is the healthy signature [green]). Reproduced with permission from Ref [159].

AUC of 0.945 with an accuracy of 82%, whereas to detect MCI patients, the optimum combination of hippocampal volume, ventricular expansion, and age yielded an AUC of 0.860 and an accuracy of 71% (Table 8). Walhovd et al [155] likewise sought the optimum discriminatory combination of biomarkers. They found that the best MRI combination to discriminate between AD and control subjects consisted of hippocampal volume, entorhinal thickness, and retrosplenial thickness (85% accuracy); the best FDG-PET combination was entorhinal, retrosplenial, and orbito-frontal metabolism (82.5% accuracy); and the best CSF combination was t-tau/Aβ-42 (81.2% accuracy). Using step-wise linear regression, they developed a final model that included retrosplenial thickness and the t-tau/Aβ-42 ratio as predictors and which achieved 88.8% accuracy in the classi-fication of AD versus control subjects. For the discrimina-tion of MCI from control subjects, the optimum combination of factors was found to be hippocampal volume and the t-tau/Aβ-42 ratio, with an accuracy of 79.1 % (Table 8). Ewers et al [161] tested a variety of cross-validated models of single or multiple predictors for their ability to discriminate between control and AD subjects. They found that the addition of neuropsychological tests, specifically the AVLT immediate free recall and DR and the TMT-B, to models that included only CSF and/or genetic biomarkers and imaging measures resulted in increased overall classification accuracy. The best model, which in-cluded CSF t-tau/Aβ-42, the number of *APOE* ε4 alleles (the previously described LR_{TAA} model [57]), left entorhinal volume, and hippocampal volume, in addition to the afore-mentioned neuropsychological tests, resulted in an accuracy of 95.2%, a sensitivity of 92.2%, and a specificity of 97.5% (Table 8). Van Gils et al [162] also demonstrated that cogni-tive tests such as the CDR, MMSE, and the neuropsycholog-ical battery comprised the most important feature category

of all classifiers designed to discriminate between different patient groups. The classifier constructed by Lemoine et al [87] from data fusion of both FDG-PET and clinical data dis-criminated between control and AD subjects with an AUC of 0.97, an improvement over the best single FDG-PET classi-fier (AUC = 0.94) or the best clinical classifier (derived from ADAS-cog data: AUC = 0.93) (Table 8). Vemuri et al [132] compared STAND score measures from MRI with CSF and concluded that CSF and MRI biomarkers independently contribute to intergroup diagnostic discrimination, and the combination of CSF and MRI provides better prediction than either source of data alone.

4.5.6. Summary and conclusions of diagnostic classification papers

A variety of approaches have been used to diagnose MCI and AD, some based on single measures, others on compos-ite scores of a single modality, and still others on a combina-tion of factors from different modalities. It should be emphasized that ADNI was not designed as a diagnostic classification study; none of the imaging methods used in ADNI is as accurate as a clinical diagnosis, and the enrolled cohort represents typical cases rather than the types of diffi-cult diagnostic problems that clinicians often confront. How-ever, a number of conclusions can be drawn from the results of these studies. Single features, such as hippocampal vol-ume, are not as accurate as multiple features, such as whole brain or cortical thickness measurements. The best classi-fiers combine optimum features from different modalities, including CSF biomarkers, MRI, FDG-PET, and cognitive measures, as well as factors such as age and *APOE* ε4 allele status. The most discriminative measures include hippocam-pal volume, entorhinal cortical thickness, entorhinal metab-olism, the t-tau/Aβ-42 ratio, and ADAS-cog scores. In some of these models, FDG-PET measures appear to lose

significance to cognitive and MRI measures; however, glucose hypometabolism alone has been shown to have high classification accuracy. ADAS-cog scores, either used directly or in a model using weighted components, appear to be an excellent diagnostic tool, although the highest accuracies were found with the addition of MRI measures. Although most classifiers used baseline measurements, there is some evidence to suggest that longitudinal data may provide even more accurate diagnoses, but it remains to be seen whether this approach is more generally applicable to other modalities. Currently, the best classifiers are able to discriminate between control and AD subjects with accuracies in the mid-90% range, but have considerably lower accuracies when discriminating between control and MCI subjects or between MCI-nc and MCI-c subjects, although data for the latter diagnoses, arguably the more important distinction to make, are far less reported. It is as yet unknown whether the application of some of the promising classifiers to these problems will result in increased diagnostic accuracy. Another key question is how methods that perform well in ADNI, with its sharply delineated diagnostic groups and exclusion of mixed dementias and borderline cases, will translate to the community or general clinic setting for wider diagnostic use. Validation studies in population-based samples will be required to address this issue.

4.6. Improvement of clinical trial efficiency

One of the primary goals of ADNI is to improve the efficiency of clinical trials of AD-modifying treatments. Selection of the study population and development of more sensitive outcome measures are two approaches to increasing the power of clinical trials and therefore reducing the number of participants required, the length of time required before a disease-modifying effect is observed, and therefore the overall cost. This section details the results of studies examining the use of structural, fluid, and genetic biomarkers in the improvement of clinical trial efficiency.

4.6.1. Prediction of cognitive decline

Beyond the simple classification of clinical trial participants, an important strategy for increasing clinical trial efficiency is the enrichment of clinical trial populations, normally MCI patients, with participants who are likely to progress to AD within a short time frame. In particular, the early and reliable detection of MCI subjects who convert early to AD could support clinical decisions for or against therapy with disease-modifying drugs. Many studies have therefore focused on identifying baseline predictors of future decline, with "future decline" meaning both decline in clinical measures such as the MMSE, ADAS-cog, and CDR-SB, and conversion of MCI to AD status. However it is measured, it is desirable for appreciable decline to occur over a relatively short time frame, typically 12 months. Imaging measures, CSF biomarkers, and *APOE* ε4 allele status, in combination or alone, have been identified as baseline future

predictors, and several studies have focused on determining the optimum combination of all modalities that results in the most power for clinical trials.

4.6.1.1. Magnetic resonance imaging

4.6.1.1.1. Temporal lobe

Hua et al [112] used TBM to create Jacobian maps of temporal lobe atrophy at baseline and examined the relationship between the maps and cognitive decline over the following year, as assessed by both the CDR-SB and the MMSE. They found that baseline temporal lobe atrophy predicted decline in the MMSE in AD patients and also predicted the conversion of MCI to AD over 12 months (Fig. 19; Table 9). Baseline atrophy of MTL structures was also found to best predict the progression of MCI patients to AD in a study by Desikan et al [163]. These measures, including the volumes of the hippocampus and amygdala and the thickness of the entorhinal cortex, temporal lobe, and parahippocampal gyrus, were found to be better predictors of clinical decline than levels of CSF Aβ-42 or FDG-PET ROIs. The combination of CSF biomarkers and FDG-PET ROIs predicted time to progression of MCI to AD with an AUC of 0.70, a sensitivity of 93%, and a specificity of 48% compared with MRI temporal lobe factors, which had an AUC of 0.83, a sensitivity of 87%, and a specificity of 66%. The addition of CSF or FDG-PET measures to the combined Cox proportional hazards model did not significantly increase prediction accuracy, with the combined model predicting conversion with an AUC of 0.83,
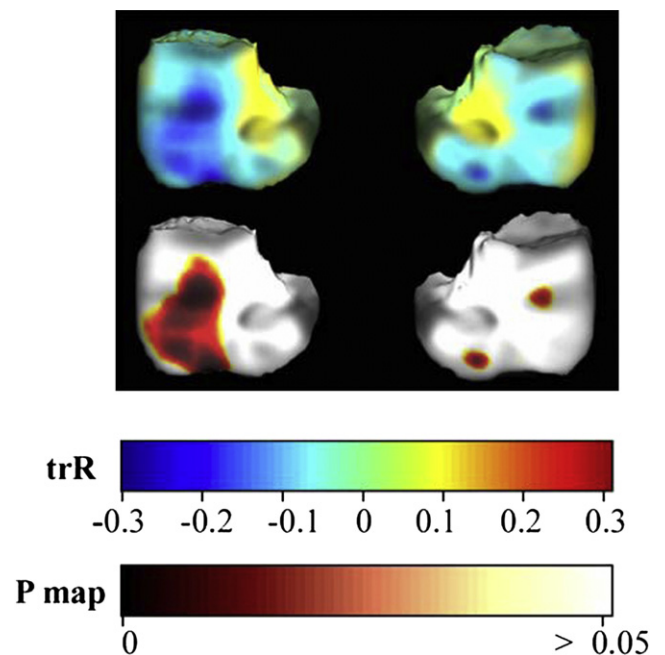
Fig. 19. Association between temporal lobe atrophy and conversion to AD. Subjects who converted from MCI to AD over a period of 1 year after their first scan were coded as "1"; nonconverters were coded as "0." A negative correlation suggests that temporal lobe degeneration predicts future conversion to AD. Reproduced with permission from Ref [112].

Table 9
Predictors of future decline

Predictor	Measurement of decline	Statistical measurement	Patient group	Cross-validated?	Reference
Baseline temporal lobe measures	MMSE	$P < .05$	MCI		[112]
	MCI to AD conversion	$P < .05$	MCI		
	CDR-SB	$P < .05$	CN, MCI, AD		
Baseline temporal lobe measures	CDR-SB	AUC = 0.83, SEN = 87%, SPE = 66%	MCI	Yes	[163]
CSF biomarkers + FDG-PET ROIs		AUC = 0.70, SEN = 93%, SPE = 48%			
TL measures + CSF + FDG-PET ROIs		AUC = 0.83, SEN = 90%, SPE = 69%			
Baseline hippocampal, amygdala, temporal horn volume	MMSE	β (P) = 0.14 (.04), 0.18 (.004), −0.2 (.003)	Pooled sample		[164]
	CDR-SB	β (P) = −0.19 (.005), −0.12 (.06), 0.2 (.005)			
Baseline hippocampal volume	MCI to AD conversion	Cohen d = 0.603	MCI-nc vs MCI-c		[114]
Baseline inferior temporal gyrus volume		Cohen d = 0.535			
Baseline middle temporal gyrus volume		Cohen d = 0.529			
Baseline entorhinal cortical volume		Cohen d = 0.493			
Baseline ventricular expansion	MMSE, global CDR, CDR-SB	$P < .05$	Pooled sample		[126]
Baseline ventricular expansion	MMSE, global CDR, CDR-SB	$P < .05$	Pooled sample		[127]
Baseline right caudate volume	MMSE	$P < .05$	Pooled sample		[130]
	MCI to AD conversion	$P < .05$			
Baseline cortical thickness in ROIs	MCI to AD conversion	Accuracy = 76%	MCI	Yes	[165]
Baseline cortical thickness in ROIs					[147]
Longitudinal cortical thickness	MCI to AD conversion	Accuracy = 81.7%	MCI	Yes	[157]
Baseline white matter hyperintensity volume	ADAS-cog	β (P) = 0.34 (.05)	Pooled sample		[166]
	MMSE	β (P) = −0.096 (<.001)			
Multiple ROI atrophy score	MMSE	r (P) = 0.39 (<.001)	MCI		[117]
Structural phenotypic score	MCI to AD conversion	AUC = 0.77	MCI	Yes	[118]
STAND score	CDR-SB		MCI, AD		[167]
	MCI to AD conversion	Cox proportional hazards ratio = 2.6	MCI		
Log (t-tau/Aβ−42)	MCI to AD conversion	Cox proportional hazards ratio = 2.0			
SPARE-AD score	MCI to AD conversion	AUC = 0.734, SEN = 94.7%, SPE = 37.8%	MCI	Yes	[119]
	MMSE	$P < .05$			
FDG-PET hypermetabolic convergence index	MCI to AD conversion	Cox proportional hazards ratio = 7.38	MCI		[85]
FDG-PET HCI + hippocampal volume		Cox proportional hazards ratio = 36.72			
Aβ load	MCI to AD conversion	75th vs 25th percentile Cox HR = 2.6 ($P < .001$)	MCI		[152]
Baseline hippocampal volume		25th vs 75th percentile Cox HR = 2.6 ($P < .001$)			
Baseline ADAS-cog (from meta-analysis)	ADAS-cog	Slope of disease progression = 5.49 points/yr, baseline five point increase in ADAS-cog effect on slope = 0.669/yr	MCI, AD		[171]

(*Continued*)

Table 9
Predictors of future decline (*Continued*)

Predictor	Measurement of decline	Statistical measurement	Patient group	Cross-validated?	Reference
Baseline ADAS.Tree	MCI to AD conversion	P = 6.23E-10, AUC = 0.746	MCI	Yes	[96]
Baseline MMSE		P = .0188, AUC = 0.589			
Baseline hippocampal volume	CDR-SB, MMSE, LM delayed change	r = −0.29, 0.29, 0.41	MCI		[155]
Baseline entorhinal volume		r = −0.17, 0.23, 0.34			
Baseline retrosplenial volume		r = −0.43, 0.42, 0.35			
Baseline entorhinal metabolism		r = −0.30, 0.38, 0.28			
Baseline retrosplenial volume		r = −0.22, 0.47, 0.11			
t-tau/Aβ−42		r = 0.02, 0.08, −0.23			
APOE ε4+	Hippocampal volume change (P< .05). Multivariate model	Coefficient of effect on annual change = −0.36	MCI		[154]
FDG-PET ROI-avg		Coefficient of effect on annual change = 9.3			
CSF tau		Coefficient of effect on annual change = −8.7	AD		
FDG-PET ROIs	MCI to AD conversion	β (SE) = 1.00 (0.51), Cox HR = 2.72	MCI		[173]
AVLT		β (SE) = 1.46 (0.64), Cox HR = 4.30			
FDG-PET ROIs	ADAS-cog	β (SE) = 1.26 (0.43)			
p-tau$_{181}$/Aβ−42		β (SE) = 1.10 (0.53)			
Right entorhinal cortical volume	MCI to AD conversion	Prediction accuracy (95% CI) = 68.5% (59.5, 77.4)	MCI	Yes	[161]
TMT-B test		Prediction accuracy = 64.6% (55.5, 73.4)			
p-tau$_{181}$/Aβ−42, hippocampalvolume, TMT−B, age		Prediction accuracy = 76.3 (68.4, 84.2)			

a sensitivity of 90%, and a specificity of 69% (Table 9). Similar structures were found to predict future decline in cognitive status by Kovacevic et al [164], who used high-throughput volumetry to segment ROIs in control, MCI, and AD subjects. They found that after adjusting for age, education, and *APOE* genotype, smaller baseline volumes of the hippocampus and the amygdala and larger temporal horn volume predicted 6-month decline in both the MMSE (β [P] = 0.14 [.04], 0.18 [.004], and −0.2 [.003], respectively) and CDR-SB (β [P] = −0.19 [.005], −0.12 [.06], and 0.2 [.005], respectively) in all groups (Table 9). Risacher et al [114] also found atrophy of structures within the MTL to be the best antecedent of imminent conversion of MCI to AD. The largest effect sizes were for hippocampal and amygdalar volume and cortical thickness of the entorhinal cortex and inferior, middle, and superior gyri (Fig. 20; Table 9).

4.6.1.2. Ventricles

Baseline ventricular morphology has been shown to predict future clinical decline in studies of the ADNI cohort. Chou et al [126] found that this measure predicted decline in MMSE, global CDR, and CDR-SB over 12 months (Fig. 21; Table 9). These findings were confirmed in a subsequent larger study by the same group [127], and further extended by examining additional cognitive criteria. Only right

ventricular baseline anatomy was correlated with future decline in DR memory scores, but there was no correlation between ventricular anatomy and changes in depression scores, despite a baseline association between these measures (Table 9).

4.6.1.3. Other regions

Targeting the caudate, a region not traditionally associated with AD, Madsen et al [130] found that baseline atrophy in the right caudate predicted both the conversion of MCI patients to AD and cognitive decline of this group, as assessed by the MMSE (Fig. 22; Table 9). Querbes et al [165] created a normalized thickness index, which was derived from the cortical thicknesses of regions most likely to show atrophy in AD and to distinguish between MCI-c and MCI-nc patients, primarily the left lateral temporal, right medial temporal, and right posterior cingulate. They found that the normalized thickness index predicted conversion of MCI patients to AD with 76% accuracy compared with accuracies ranging from 63% to 72% by cognitive scores (Table 9). The additional dimension of time increased the ability of cortical thickness measurements to predict the conversion of MCI to AD in a study by Li et al [157]. By incorporating both static baseline and follow-up measures, dynamic measures of thinning speed, the ratio of follow-up to baseline thicknesses in ROIs, and a network feature that examined
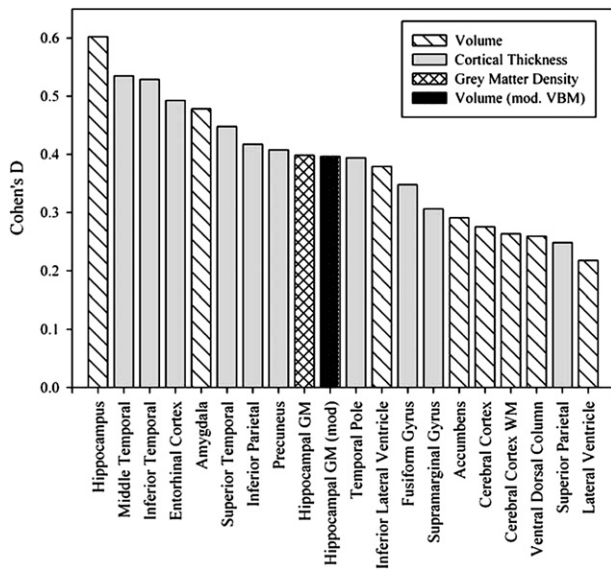
Fig. 20. Effect size of imaging biomarkers for MCI converters versus MCI nonconverters. Effect sizes (Cohen *d*) of the comparison between MCI stable (MCI nonconverter) and MCI converter groups evaluated for selected imaging biomarkers. Reproduced with permission from Ref [114].

correlations between longitudinal thickness change in different ROIs, Li et al constructed a classifier that correctly identified 81.7% of MCI-c patients 6 months ahead of their conversion (Table 9).

White matter hyperintensities (WMH) may represent an accrual of nonspecific neuronal injury over a lifetime. Carmichael et al [166] investigated the relationship between WM disease and cognition over a year, and found that both baseline and longitudinal change in WMH were associated with worsening of ADAS-cog and MMSE scores over 12 months (Table 5), raising the possibility of the use of WMH as a biomarker and highlighting its ability to predict future clinical decline (Table 9).

A number of studies have leveraged information on atrophy from multiple brain regions to distill a number or a score that is more predictive of future clinical decline than single regions alone. McEvoy et al [117] found that an atrophy score derived from mesial and lateral temporal, isthmus cingulate, and orbitofrontal areas was predictive of 1-year decline in MMSE scores and progression of MCI patients to AD. They found that the atrophy score was a better predictor than right or left hippocampal volume or the thickness of the left or right entorhinal cortex (Table 9). Similarly, a structural abnormality score extracted from baseline MRI data by Misra et al [118] was higher in MCI patients who converted to AD over the following year than stable MCI patients, and an SPS derived by Fan et al [83] from a complex pattern of spatial atrophy predicted decline in MMSE scores within a year from baseline (Table 9). Vemuri et al [167] found that STAND scores that reflected greater baseline atrophy in regions associated with AD predicted greater subsequent decline on the CDR-SB and also a shorter time to conversion for MCI patients than CSF analytes (Table 9). Davatzikos et al [119] focused on structural changes occurring at the early stages of AD and derived SPARE-AD scores (Spatial Pattern of Abnormalities for Recognition of Early AD) largely from changes in the temporal regions, posterior cingulate cortex, precuneus, and orbitofrontal cortex. They found that higher SPARE-AD scores predicted conversion of MCI to AD (Table 9).

McEvoy et al [168] also investigated enrichment strategies for constraining recruitment into clinical trials by selecting MCI patients most likely to progress. Their first strategy, which selected MCI patients with an *APOE* ε4 allele, reduced sample sizes by an estimated 10% to 40%, but this was discounted because of the possibility that restricting patient genotype may invalidate trial findings. Their second strategy, based on baseline MRI atrophy in regions previously shown to be predictive of disease progression,
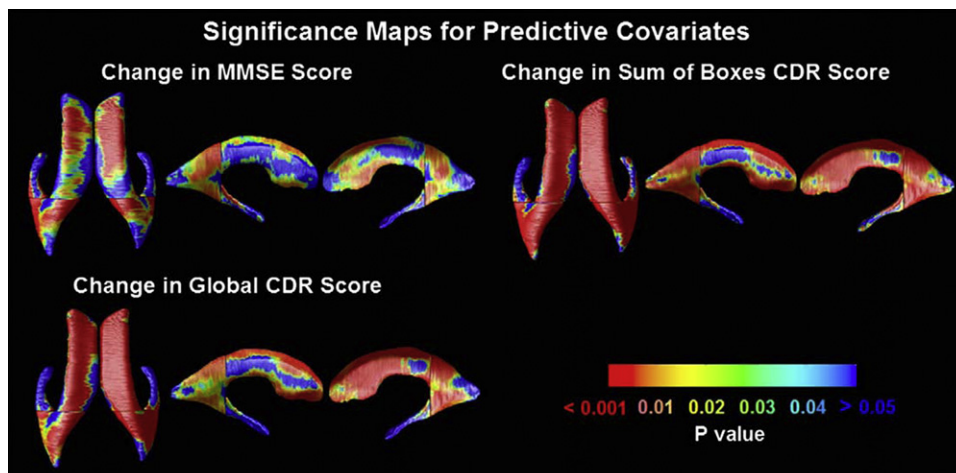
Fig. 21. Significance maps of correlation between ventricular shape and cognitive decline. Significance maps correlate baseline ventricular shape with subsequent decline, over the following year, in three commonly used clinical scores. Reproduced with permission from Ref [126].
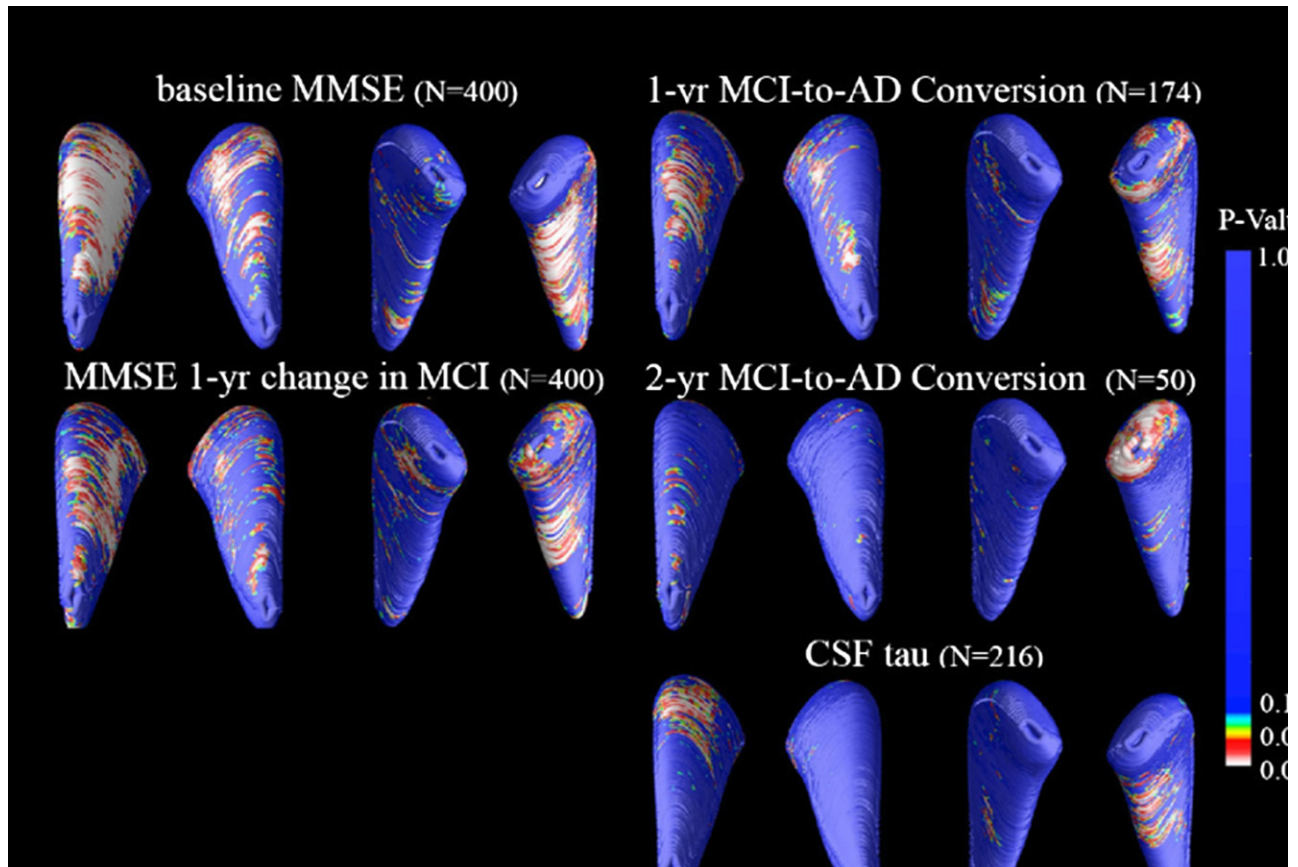
Fig. 22. Maps of associations with MMSE scores at baseline and 1 year later, MCI-to-AD conversion, and CSF concentrations of tau. Three-dimensional maps show areas of significant associations between local volumetric atrophy in the caudate and MMSE scores at baseline and after a 1-year follow-up interval, with *P* values color-coded at each surface voxel. Reproduced with permission from Ref [130].

resulted in an estimated sample size reduction of 43% to 60% (Table 11).

4.6.1.2. [^{18}F]-fluorodeoxyglucose-positron emission tomography

Chen et al [85] reported that their HCI outperformed other measures such as hippocampal volume, cognitive scores, *APOE* genotype, and CSF biomarkers in the prediction of conversion of MCI patients to AD. In a univariate model, patients with an HCI above a predefined cutoff had an average Cox proportional hazards ratio for the estimated risk of conversion to probable AD within 18 months of 7.38 compared with 6.34 for hippocampal volume, 4.94 for p-tau$_{181p}$, and 3.91 for ADAS-cog, the most significant of the other measures tested. Moreover, patients with a combination of both high HCI score and hippocampal volume below a similarly defined threshold value had a Cox proportional hazards ratio of 36.72 (Table 9). This study suggests that data from FDG-PET analyses represent a powerful tool for the prediction of future decline in AD that is complementary to MRI data.

4.6.1.3. CSF biomarkers

Vemuri et al [167] examined the ability of CSF biomarkers to predict decline in CDR-SB and MMSE scores over 2 years and the time to conversion from MCI to AD. Although all CSF biomarkers were predictive of future decline, the best predictor was log (t-tau/Aβ-42), which was comparable with the MRI-derived STAND scores. In contrast, Aβ-42 alone was only weakly predictive of conversion to AD, reflecting its status as a marker of early AD pathology. Used in combination with STAND scores, only log (t-tau/Aβ-42) improved the predictive ability of the MRI measure (Table 9). Jack et al [152] compared the ability of amyloid load, measured either by levels of CSF Aβ-42 or by ^{11}C-PiB PET imaging, and hippocampal volume to predict MCI to AD progression. Using a new method to pool CSF and ^{11}C-PiB PET data [169] and to extract a score representative of Aβ load from the pooled information, they found that the group of MCI patients classified as being Aβ positive had higher frequencies of the *APOE* ε4 allele and smaller baseline hippocampal volumes and a threefold higher chance of progressing to AD within 3 years than the Aβ-negative group (Fig. 23; Table 9). Thus, both baseline hippocampal atrophy and Aβ load were significant predictors of future decline. Interestingly, when risk profiles were constructed from the log relative hazard of progressing and degree of hippocampal atrophy or Aβ load, the relationship was linear for hippocampal atrophy, but plateaued at

Table 10
Comparison of methods for increasing power in clinical trials: sample sizes per arm required to detect a 25% reduction in atrophy with 80% power, 5% significance

Strategy	Outcome measure: MCI (AD)						Reference
	ADAS-cog	CDR-SB	Whole brain	Ventricular expansion	Hippocampal volume	Entorhinal complex	
Subject selection by multiple biomarker classifier	<40 (<40)						[86]
No baseline adjustments, no aging			149 (81)	234 (118)	201 (88)		[174]
Best baseline adjustments, no aging			122 (68)	167 (84)	178 (74)		
No baseline adjustments, with aging			739 (235)	944 (254)	648 (179)		
Best baseline adjustments, with aging			605 (197)	675 (181)	573 (150)		
Aβ−42 <192 pg/mL Normal elderly			141	225	467		[160]
APOE ε4 carrier Normal elderly			224	222	703		
All MCI	834	674					[172]
Screening in, best enrichment	260*	191†					
Screening out, best enrichment	517*	351‡					
All MCI	978	437	181	161	186	140	[168]
APOE ε4 enrichment	774	397	135	129	133	100	
Atrophy enrichment	458	191	141	121	107	67	
All MCI	375						[154]
Enrichment with Aβ−42	225						

*FDG-PET.
†Hippocampal volume.
‡11C-PiB-PET.

higher Aβ loads, consistent with a model in which Aβ deposition is an early event in AD progression, whereas neurodegeneration, as evidenced by hippocampal atrophy, occurs later and is thus a better indicator of progression toward dementia.

Using the ADNI database, Schneider et al [170] empirically tested the recommendation that low Aβ-42 and a high t-tau/Aβ-42 ratio can help select those MCI patients most likely to progress to AD throughout the course of a clinical trial. After statistically simulating a number of different clinical trial scenarios with MCI patients with or without biomarker enrichment, they found that selection with either of the biomarker criteria resulted in only minor increases in power for the trial, and concluded that the use of these criteria would likely not result in more efficient clinical trials. In contrast, Beckett et al [154] calculated that restricting a trial population to MCI subjects with CSF Aβ-42 levels of <192 pg/mL would reduce the sample size required from 375 to 226 subjects per arm to detect a 25% change using ADAS-cog as an outcome measure, demonstrating a clear beneficial use of CSF biomarkers in clinical trial population selection (Table 10). Schott et al [160] tested the use of the same cutoff point of CSF Aβ-42 levels in cognitively normal elderly subjects as a selection tool for presymptomatic treatment studies in AD. Those participants with CSF Aβ-42 levels of <192 pg/mL had higher levels of t-tau and p-tau and higher ratios

of tau/CSF Aβ-42 and p-tau/CSF Aβ-42, were more likely to be carriers of the APOE ε4 allele, and had significantly higher whole brain atrophy, ventricular expansion, and hippocampal atrophy over 1 year than participants with higher CSF Aβ-42 levels. Of the six participants who later converted to MCI or AD, five had low or borderline baseline CSF Aβ-42 levels, suggesting that the roughly one-third of healthy elderly subjects with a CSF profile consistent with AD were at greater risk for development of the disease. When sample sizes for clinical trials were calculated for both CSF Aβ-42 levels and APOE ε4 genotype as selection criteria and using whole brain atrophy, ventricular expansion, or hippocampal atrophy as the outcome measure, the smallest size per arm [140] was calculated using selection by CSF Aβ-42 levels and whole brain atrophy as an outcome measure (Table 10).

4.6.1.4. Cognitive

Ito et al [171] evaluated disease progression in clinical studies and drug trials performed between 1990 and 2008 by using a model to assess the effect of cholinesterase inhibitors and placebos on longitudinal ADAS-cog scores in mild-to-moderate AD patients. They found no significant differences in the rate of disease progression between patients taking the placebo versus patients receiving cholinesterase treatment. The only significant covariate in disease

Table 11
Comparison of outcome measure methods in clinical trials: sample size estimates per arm required to detect a 25% reduction in atrophy with 80% power, 5% significance

Outcome measure	Method tested	Sample size AD	Sample size MCI	Reference
Hippocampus	Two scans, 0–6 months	462	949	[121]
	Three scans, 0–6–12 months	255	673	
	Three scans + Markov Chain + *APOE* ε4	86	341	
Clinical	ADAS-cog two tests, 0–6 months	745	4663	
	ADAS-cog three tests, 0–6–12 months	569	8354	
	MMSE two tests, 0–6 months	1280	6300	
	MMSE three tests, 0–6–12 months	780	3353	
Hippocampal atrophy	12-(24)-month	67 (46)	206 (121)	[64]
Hippocampal atrophy	12-month	78	285	[59]
Ventricular expansion	6-month change	342	1180	[175]
Clinical	MMSE	7056	7712	
	ADAS-cog	1607	>20,000	
MRI (Model T/Model D)	Entorhinal	45/65	135/241	[176]
	Inferior temporal	79/117	199/449	
	Fusiform	72/114	185/485	
	Mid temporal	83/122	229/501	
	Hippocampus	67/118	179/510	
	Inferior lateral ventricle	76/157	160/550	
	Whole brain	101/189	158/541	
	Ventricles	86/240	189/1141	
Clinical (Model T/Model D)	CDR-SB	226/236	490/551	
	ADAS-cog	324/283	1232/804	
	MMSE	482/494	1214/1304	
Whole brain atrophy	KN-BSI	81	NA	[51]
	Classic-BSI	120	NA	
TBM	1.5-T MRI/3.0-T MRI	37/48	107/159	[47]
SIENA*	1.5-T MRI/3.0-T MRI	116/92	207/265	
TBM	sKL-MI S6L8[†]	48	88	[177]
Clinical	ADAS-cog	619	6797	
	MMSE	1078	3275	
	CDR-SB	408	796	
TBM	Gray matter atrophy	43	86	[120]
	Temporal lobe atrophy	43	82	
CSF biomarkers	Aβ−42	5,721,531	75,816	
	t-tau	81,292	19,098	
	t-tau/Aβ−42	66,293	533,091	
PET	ROI-avg[‡]		4605	[154]
	logSumZ2PNS[§]		2176	
	logSumZ2PR[§]		1629	
	DD-fROI[¶]		249	
MRI	VBSI**		284	
	Ventricles[††]		277	
	Hippocampus[††]		202	
	BSI[‡‡]		177	
	DD-ROI[†]		73	

*Structural Image Evaluation, using Normalization, of Atrophy (SIENA). See text for more details.

[†]A nonlinear registration algorithm driven by mutual information cost function and with a regularizing term based on the symmetric Kullback–Leibler (sKL) distance.

[‡]Jagust laboratory method.

[§]Foster laboratory method, measures of glucose hypometabolism, log transformed.

[¶]Reiman laboratory method, data-driven summaries applied to independent test set.

**Fox laboratory method, ventricular boundary shift interval as a percentage of baseline brain volume.

[††]Schuff laboratory method (FreeSurfer).

[‡‡]Fox laboratory method, brain shift interval.

progression was baseline ADAS-cog score, suggesting that those patients with a higher (worse) ADAS-cog score at baseline had a significantly worse prognosis and higher rates of cognitive deterioration than those with lower (better) baseline scores (Table 9). Llano et al [96] used a new Ran-dom Forests tree-based multivariate model of ADAS-cog in which the subscores had been weighted according to their contribution to patient discrimination. This model, ADAS.-Tree, predicted conversion of MCI to AD more accurately than baseline MMSE or ADAS-cog and, in addition, was
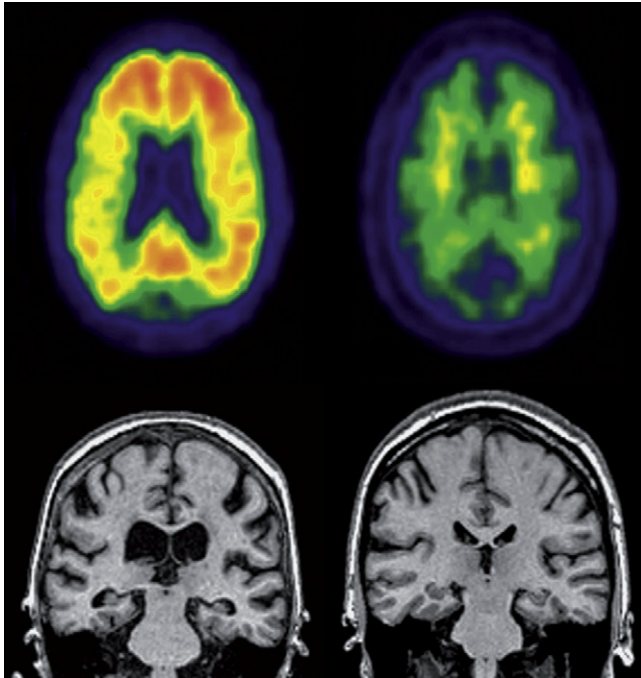
Fig. 23. Pittsburgh compound B-positron emission tomography (PiB-PET) and magnetic resonance imaging (MRI) comparisons of MCI converters versus MCI nonconverters. Left: MCI progressor. Top: positive PiB-PET. Bottom: MRI illustrating atrophic hippocampi and ventricular enlargement. Right: MCI nonprogressor. Top: negative PiB-PET with nonspecific white matter retention but no cortical retention. Bottom: MRI illustrating normal hippocampi and no ventricular enlargement. Reproduced with permission from Ref [152].

a better predictor of conversion than the best single imaging (left inferior temporal cortex), metabolism (left precuneus), or CSF (p-tau$_{181p}$/Aβ-42) biomarkers. The significance of association varied by several orders of magnitude, with the ADAS.Tree four orders of magnitude higher than the next MRI marker, and FDG-PET and CSF biomarkers several orders of magnitude lower than the MRI marker. Moreover, the addition of these markers to the ADAS.Tree model did not result in substantial improvement, providing support for this modified form of ADAS-cog as a useful and effective predictor of future decline (Table 9).

4.6.1.5. Combined modalities

Lorenzi et al [172] tested two strategies for the enrichment of MCI patients in clinical trials using changes in brain structure or metabolism, or changes in CSF biomarkers well known to herald future disease progression. They used hippocampal atrophy (MRI); temporoparietal hypometabolism (FDG-PET); CSF Aβ-42, t-tau, and p-tau; and cortical amyloid deposition (^{11}C-PiB PET) as biomarkers to either screen in MCI-c or screen out MCI-nc. Although both strategies substantially reduced the estimated sample sizes required, the authors found that there was a trade-off between the high proportion of converters screened out in the first strategy and the decreased power and increased estimated sample sizes using the second strategy (Table 10). Kohannim et al

[86] investigated the utility of their machine learning classifier, based on MRI hippocampal and ventricular summaries, *APOE* genotype, and age as features, in subject stratification and found that it reduced the numbers of AD and MCI patients required to detect a 25% slowing of temporal lobe atrophy with 80% power to fewer than 40, a substantial reduction over other methods (Table 10). Walhovd et al [155] examined baseline MRI, FDG-PET, and CSF biomarker data to determine the optimum combination of these biomarkers for the prediction of decline over 2 years. They found that in MCI patients, retrosplenial and cortical thickness predicted decline on the CDR-SB, retrosplenial and entorhinal metabolism predicted decline on the MMSE, and hippocampal volume predicted decline in delayed logical memory. The tau/Aβ-42 ratio also predicted decline in the CDR-SB and MMSE, but less significantly than the MRI and FDG-PET measures (Table 9). Beckett et al [154] found that in MCI and AD patients, baseline glucose metabolism in a range of ROIs predicted cognitive decline, as measured by ADAS-cog in a multivariate model. In univariate models, hippocampal and ventricular volume, Aβ-42, and tau also predicted cognitive decline in MCI patients (Table 9). Both papers support the idea that reduced metabolism and greater brain atrophy at baseline are associated with more rapid cognitive decline, and that CSF biomarkers are less useful indicators of future change. A degree of agreement with these results was found by Landau et al [173], who studied a range of predictors of conversion to AD and cognitive decline, including FDG-PET measures, CSF biomarkers, *APOE* ε4 status, and hippocampal atrophy, that were defined dichotomously according to their ability to separate AD and control subjects. Although all biomarkers were predictive of decline in univariate models, only reduced glucose metabolism and episodic memory (measured by the AVLT) predicted conversion to AD and, in contrast to the studies by Beckett et al [154] and Walhovd et al [155], only p-tau$_{181p}$/Aβ-42 predicted decline in ADAS-cog scores in multivariate models (Table 9). Ewers et al [161] compared the effectiveness of single variables and multiple variables in predicting the conversion of MCI to AD. They found that these best single predictors (right entorhinal cortex and the TMT-B) were comparable in accuracy with the best multiple predictor models, which included right hippocampal volume, CSF p-tau$_{181p}$/Aβ-42, TMT-B, and age (Table 9).

4.6.2. Adjustments for normal aging and baseline characteristics

McEvoy et al [168] also examined the effect of normal aging on the detection of longitudinal change and found that although this did not affect clinical outcome measures such as ADAS-cog and CDR-SB, neuroimaging outcome measures were far more sensitive to atrophy associated with normal aging. They suggested that larger sample sizes are required in clinical trials to account for this effect, and that clinical trials run the risk of being severely

underpowered if normal aging is not taken into account. Schott et al [174] proposed an alternative method for increasing the statistical power of clinical trials without resorting to subject selection procedures that can potentially limit the applicability of studies. They found that by statistically adjusting for a range of baseline characteristics that might account for interindividual differences, and also for normal aging, sample sizes were reduced by 15% to 30% in AD subjects and by 10% to 30% in MCI subjects (Table 10).

4.6.3. Biomarkers as outcome measures

A number of studies have focused on determining the effectiveness of different biomarkers as outcomes in clinical trials by calculating sample size estimates for a hypothetical clinical trial, per arm at either 90% (N90) or 80% (N80) power to detect a 25% improvement in annual rate of decline. Schuff et al [121] used hippocampal volume loss over time, assessed by MRI, as an outcome measure and found that the greatest reductions in sample size were achieved when three serial scans (0, 6, and 12 months) were combined with *APOE* ε4 data using Markov chain analysis to exploit correlations between observations (Table 11). The inclusion of Aβ-42 level data did not further reduce sample size. All MRI hippocampal measures were substantially better than cognitive measures (ADAS-cog and MMSE) as outcome measures. Wolz et al [64] used a 4-D graph cut method to segment the hippocampus and subsequently calculated N80s in the same range as the best combinations of Schuff et al [121] (Table 11). Nestor et al [175] investigated the use of ventricular expansion as an outcome measure and found that ventricular expansion over 6 months was sufficiently sensitive to produce N80s for a hypothetical trial at least an order of magnitude lower than clinical scores (MMSE and ADAS-cog). Moreover, sample sizes were further reduced when the trial population of AD subjects was restricted to carriers of the *APOE* ε4 allele (Table 11). Holland et al [176] examined the utility of longitudinal volumetric change in a variety of ROIs as an outcome measure with which to measure putative disease-modifying medications for AD and MCI. ROIs, including temporal lobe structures and ventricles, and whole brain atrophy were compared with clinical measures in two separate models, one in which the putative drug was presumed to affect both disease and aging-related changes (model T for "total"), and one in which the drug putatively affected only disease-specific changes (model D for "disease-specific"). They found that although imaging measures generally resulted in smaller sample sizes than cognitive measures in both models, model T was the more conservative model for cognitive measures, whereas model D was more conservative for imaging measures. The authors emphasized the importance of comparing both models when comparing across imaging and cognitive outcome measures (Table 11).

Hua et al [177] compared a variety of nonlinear registration methods used in TBM with standard clinical outcome measures and found that a substantial reduction in sample size at 80% power (N80s) was achieved over clinical measures using all TBM methods, with the best TBM measure presenting an eightfold improvement over the best clinical measure (CDR-SB) (Table 11). The same group [120] subsequently compared the use of TBM to measure GM of the entire brain and WM atrophy in the temporal lobe with 1-year changes in CSF biomarkers as outcome measures in a hypothetical clinical trial. The N80s for CSF biomarkers were much larger than those from neuroimaging measures, reflecting their poorer reproducibility, especially in later stages of the disease process (Table 11). Ho et al [47] compared 3.0-T and 1.5-T MRI for tracking disease progression using TBM and an alternative method for measuring the overall percentage brain volume change, Structural Image Evaluation, using Normalization, of Atrophy. The lowest calculated N80 resulted from using TBM on a 1.5-T MRI scanner to detect changes in brain atrophy as an outcome measure (Table 11). Leung et al [51] estimated N80s for both the classic brain BSI MRI technique and their improvement on this, the KN-BSI method, and found that the improved method resulted in lower N80s (Table 11). More recently, using a newly revised TBM method that enforces inverse consistency, Hua et al [178] reported that to demonstrate a 25% slowing of atrophic rates with 80% power, 62 AD and 129 MCI subjects would be required for a 2-year trial and 91 AD and 192 MCI subjects for a 1-year trial.

Beckett et al [154] compared a number of promising MRI and FDG-PET outcome measures. They calculated the sample size that would be required in a two-arm, 1-year clinical trial with 80% power to detect a 25% effect, and found that MRI measures of overall brain change, using either ROIs or BSI techniques, or hippocampal volume required fewest subjects. Brain metabolism measures were generally less effective, requiring substantially larger sample sizes, although the best FDG-PET measure, a data-driven functional ROI, was comparable with many of the MRI measures (Table 11).

4.6.4. Summary and conclusions of papers focused on the improvement of clinical trial efficiency

Strategies for the reduction of sample sizes in clinical trials by the selection of subjects with a significantly worse prognosis and through the use of more effective outcome measures have been developed over the course of ADNI. Studies have found that baseline MRI measures, particularly of hippocampal volume and of whole brain atrophy, outperform measures of glucose hypometabolism or CSF biomarkers in the prediction of future decline. In one instance, a score derived from AD-like patterns of hypometabolism outperformed other single MRI, cognitive, or CSF biomarker measures, but this too was enhanced by the addition of MRI measures. Of the CSF biomarkers, the t-tau/Aβ-42 ratio and the use of a cutoff value of approximately 192 pg/mL Aβ-42 have been shown to best predict future decline. In a manner similar to classification of AD subjects, the use of multiple modalities appears to enhance the prediction of future decline. Interestingly, a weighted version of the ADAS-cog

[96] has been shown to outperform any single MRI measure tested as a predictor of future change and was not improved by the addition of any MRI measure tested. In contrast, MRI and FDG-PET, which have strikingly better signal-to-noise ratios, clearly outperformed cognitive tests as outcome measures of rates of change. Calculated sample sizes for clinical trials required to see a 25% effect at 80% power were lowest for MRI measures of overall morphometric change or of hippocampal volume, followed by those for hypometabolism ROIs and cognitive scores. CSF biomarkers were the least effective outcome measures by several orders of magnitude. Finally, it also will be necessary to study the comparative effectiveness and cost-effectiveness of the AD biomarkers studied in ADNI to determine the optimal way to make use of these biomarkers in the diverse applications needed in AD research. For example, based on the recent studies of Wiegand et al [169], it is possible to impute Aβ measures determined by Aβ imaging using far less expensive measures of CSF Aβ-42 levels. Additional similar studies as well as others focused on the economics of the use of biomarkers in clinical trials and clinical practice are needed.

5. Identification of genetic risk factors for AD

The influence of genetics on the dynamic trajectory of brain development and aging is well established, if not well understood. Studies of twins have estimated the heritability of AD to be between approximately 60% and 80% [179], and until recently the only established genetic risk factor for AD was the *APOE* ε4 allele, which accounts for approximately 50% of AD heritability [180]. The question of accounting for the up to 30% of heritability remaining has only begun to be addressed, and although there have been a number of candidate genes proposed, the majority of them await independent confirmation. ADNI is in the unique position of providing a large cohort with genotype information in addition to imaging and biochemical data that can be leveraged as QTs in uncovering new genetic associations, and as such plays an increasingly important role in the discovery and confirmation of novel genetic risk alleles.

Three main approaches have been taken to investigating the genetic basis of AD. Case–control studies that search for loci with differential frequency between patient groups have identified a number of candidate genes. Typically, markers are used to tag susceptibility loci, usually in 10-kb to 20-kb regions in the genome, that are rarely found to be causal. Using this method, the association of *APOE* ε4 allele with AD has been confirmed, and three new risk loci, *CLU*, *PICALM*, and *CR1*, have been identified and confirmed [181–183]. Further studies have focused on examining relationships between SNPs in a limited number of genes of interest and quantifiable phenotypic characteristics or QTs, such as imaging data or levels of CSF biomarkers. GWAS evaluate a large and dense set of SNP markers distributed throughout the genome, providing an unbiased search for the discovery of new candidate genes. With more than 500,000 markers typically included in a GWAS, a stringent correction for multiple testing is required with typical thresholds of $P < 10^{-8}$ used to reduce false detections. These stringent corrections also greatly reduce power and require extremely large sample sizes to achieve significance in case–control designs. However, the use of quantitative phenotypes such as cognitive, imaging, and fluid biomarker measures can greatly increase the power to detect associations. Where a binary case–control design might require many thousands of samples to detect a gene effect, samples on the scale of ADNI are sufficient for detecting associations with quantitative phenotypes [184]. The emerging field of imaging genetics, which uses imaging data as QTs in GWAS, promises the power to reveal patterns of genetic associations throughout the brain, but is hampered by the computational load required for such high-dimensional studies. Further development of this field, including improvement of existing GWAS methods, is a major goal of the Genetics Core of ADNI [6].

5.1. Case–control studies

Jun et al [185] conducted a meta-analysis case–control study of AD patients and healthy elderly control subjects from 12 different studies, including ADNI, to examine the association of *APOE* ε4, *CLU*, *PICALM*, and *CR1* with AD. They found that *CLU*, *PICALM*, and *CR1* were significantly associated with AD only in Caucasian populations. In contrast, *APOE* ε4 was significantly associated with AD in all ethnic groups and with *PICALM* in white populations, suggesting that *APOE* ε4 and *PICALM* act synergistically and may participate in a common pathological pathway (Table 12). Two of the largest case–control GWAS studies of AD were recently published as companion reports in *Nature Genetics* [186,187]. Both reports included the ADNI-1 data in their analyses (Table 12). These multistage meta-analytic reports included discovery and replication data sets and confirmed each other. These new results bring the total set of confirmed and replicated candidate genes to 10 (*APOE/TOMM40*, *ABCA7*, *BIN1*, *CD2AP*, *CD33*, *CLU*, *CR1*, *EPHA1*, *MS4A4/MS4A6A*, *PICALM*).

Mitochondrial genes are also of great interest in AD, and Lakatos et al [188] studied the incidence of AD in patients belonging to different subgroups (HV, JT, UK, and IWX) of mitochondrial haplogroup N in the ADNI cohort. They found that haplogroup UK had the strongest association with AD, and that this relationship remained significant after adjusting for *APOE* ε4 allele dose. Additionally, they identified five mitochondrial SNPs that were associated with increased risk of AD and suggested that, given the vital role of mitochondria in maintaining cellular energy balance, dysfunctional mitochondria may contribute to AD by causing neuronal oxidative damage. In another case–control design, Kauwe et al. [189] attempted to replicate a study that found that epistatic linkage between two SNPs in the transferrin and hemochromatosis genes was associated with AD risk, suggesting a role

Table 12
AD susceptibility and quantitative trait loci identified by genetic studies of ADNI cohort

SNP	Location of SNP*	Protein	Putative protein function	P value/odds ratio (OR)	Cohort (N)	QT of association	Significant association of APOE?	Study type	Reference
rs11136000	*CLU*	Clusterin	Clearance of Aβ	0.91[†]	ADNI + 11 others (3055 AD, 8169 CN)	N/A		Meta-analysis, case–control	[185]
rs3818361	*CR1*	Complement component [3b/4b] receptor	Clearance of Aβ	1.14[†]					
rs3851179	*PICALM*	Phosphatidylinositol-binding clathrin assembly protein	Synaptic vesicle cycling and/or affects APP processing via endocytic pathways	0.89[†]					
rs104926	*TF*	Transferrin	Increased redox-active iron + oxidative stress	.00016	ADNI + 2 others (1161 AD, 1342 CN)	Association between two genes		Synergy factor analysis	[189]
rs1800562	*HFE*	Hemochromatosis							
rs2986017	*CALHM1*	Calcium homeostasis modulator 1	Increase Aβ through lower intracellular [Ca^{2+}]	.042	ADNI + 1 other (251 AD, 351 CN)	CSF Aβ−42		Limited loci	[192]
rs1868402	*PPP3R1*	Protein phosphatase B	Affects tau phosphorylation	1.17×10^{-5}	ADNI + 2 others (1106 AD, 1216 CN	CSF P-tau$_{181}$		Limited loci	[191]
rs1868402	*PPP3R1*	Protein phosphatase B	Affects tau phosphorylation	6.2×10^{-5}	ADNI + 1 other (776)	CSF T-tau, P-tau$_{181}$		Limited loci	[190]
rs17030379	*PPP3CA*	Protein phosphatase B	Affects tau phosphorylation	2.05×10^{-4}					
rs1408077	*CR1*	Complement component [3b/4b] receptor	Clearance of Aβ	.03	ADNI (171 AD, 364 MCI, 205 CN)	ECT[‡]		Limited loci	[193]
rs3851179	*PICALM*	Phosphatidylinositol-binding clathrin assembly protein	Synaptic vesicle cycling and/or affects APP processing through endocytic pathways	.05, .01		ECT[‡], HV[§]			
rs7561528	*BIN1*	Myc box-dependent-interacting protein 1	Synaptic vesicle endocytosis	.03, .01		TPT[¶], ECT[‡]			
rs10501927	*CNTN5*	Contactin-5	Neurite growth	.002, .05, .02, .02		WML**, PGT[††], TPT[¶], ECT[‡]			
rs2899462	*CYP19A1*	Cytochrome P450, family 19, subunit a, polypeptide 1	Conversion of androgens to estrogens	1.9×10^{-7}	ADNI (176 AD, 115 MCI, 119 CN)	CSF Aβ−42		GWAS	[199]

SNP	Gene	Description	Function	p-value	Cohort	Phenotype		Method	Ref
rs1022422	NCAM2	Neural cell adhesion molecule 2	Neural adhesion, fasciculation of neurons	2.75×10^{-7}					
rs2075650	TOMM40	Translocase of outer mitochondrial membrane	Protein transport across mitochondrial membrane	3.03×10^{-7}					
rs2075650	TOMM40	Translocase of outer mitochondrial membrane	Protein transport across mitochondrial membrane	$<10^{-7}$	ADNI (96 AD, 176 MCI, 102 CN)	$A\beta-42$, $ptau_{181}/A\beta-42$, $t-tau/A\beta-42$	Yes	GWAS	[149]
rs439401	LOC100129500	Unknown function, overlaps with APOE	Unknown	$<10^{-7}$		$A\beta-42$			
rs2121433, rs1374441, rs449362, rs10171238	EPC2	Enhancer of polycomb homolog 2	Formation of heterochromatin	$<10^{-7}$		t-tau			
rs2075650	TOMM40	Translocase of outer mitochondrial membrane	Protein transport across mitochondrial membrane	7.48×10^{-7}	ADNI (172 AD, 208 CN)	HV**		GWAS	[184]
rs1082714	CAND1	Cullin-associated and neddylation-associated 1	Ubiquination, apoptosis	4.93×10^{-6}					
rs11525066	MAGI2	Membrane associated guanylate kinase	Ubiquination, dementia	2.85×10^{-6}					
rs337847	ARSB	Arylsulfatase b	Oxidative necrosis, dementia	6.71×10^{-6}					
rs10781380	PRUNE2	Prune homolog 2	Apoptosis	7.13×10^{-7}					
rs12654281	EFNA5	Ephrin-A5	Hippocampal development	3.72×10^{-7}					
rs11129640	ARPP-21	Cyclic AMP-regulated phosphoprotein, 21 kD	Cellular cAMP signaling pathway	5.57×10^{-8}	ADNI and 1 other (236 AD, 424 MCI, 279 CN)	ECT‡	No	GWAS	[197]
rs1925690	ZNF292	Zinc finger protein 292	Expressed in brain	2.6×10^{-8}		Entorhinal cortical volume			
rs3851179	PICALM	Phosphatidylinositol-binding clathrin assembly protein	Synaptic vesicle cycling and/or affects APP processing via endocytic pathways	1.9×10^{-8}		ECT			

(*Continued*)

Table 12
AD susceptibility and quantitative trait loci identified by genetic studies of ADNI cohort (*Continued*)

SNP	Location of SNP*	Protein	Putative protein function	P value/odds ratio (OR)	Cohort (N)	QT of association	Significant association of APOE?	Study type	Reference
rs2075650	TOMM40	Translocase of outer mitochondrial membrane	Protein transport across mitochondrial membrane	$<10^{-6}$	ADNI (166 AD, 346 MCI, 203 CN)	Multiple brain regions		GWAS	[194]
rs6463843	NXPH1	Neurexophilin 1	Dendrite-axon adhesion	$<10^{-6}$					
rs10932886	EPHA4	EPH receptor A4	Synapse morphology	$<10^{-6}$					
rs7610017	TP63	Tumor protein 63	Unknown	$<10^{-6}$					
rs1085480	GRINB	N-methyl-D-aspartate glutamate receptor	Learning, memory, excitotoxic cell death	1.26×10^{-7}	ADNI (742 AD, MCI, CN)	Temporal lobe volume		GWAS	[196]
rs476463	CSMD2	CUB and sushi domain-containing protein 2	Oligodendroglioma suppressor?	1.27×10^{-6}	ADNI (173 AD, 360 MCI, 206 CN)	Voxels of entire brain		Voxelwise GWAS	[195]
rs2429582	CADPS2	Calcium-dependent secretion activator 2	Synaptic vesicle priming	6.46×10^{-7}					
rs4938933	MS4A4A	Membrane spanning 4 domains subfamily A, member 4	Cell surface protein-receptor?	1.7×10^{-9}	ADNI + 8 others (8309 AD, 7366 CN)	N/A		Meta-analysis, case–control	[186]
rs9349407	CD2AP	CD2-associated protein	Regulation of receptor-mediated endocytosis	8.6×10^{-9}					
rs3865444	CD33	Siglec-3	Clathrin-independent endocytosis	1.6×10^{-9}					
rs11967557	EFHA1	EF-hand domain family member A1	Regulation of cell morphology and motility in epithelial tissues	6.0×10^{-10}					
rs3764650	ABCA7	ATP-binding cassette subfamily A member 7	Membrane transporter highly expressed in brain	4.5×10^{-17}	ADNI + 3 others (6688 AD, 13685 CN)	N/A		Meta-analysis, case–control	[187]
rs610932	MSA4	Membrane spanning 4 domains subfamily A gene cluster	Cell surface protein–receptor?	1.8×10^{-14}					
rs2075650	TOMM40	Translocase of outer mitochondrial membrane	Protein transport across mitochondrial membrane	$<10^{-8}$	ADNI (742 AD, MCI, CN)	Rate of change in hippocampal volume		GWAS	[6]

| rs12449237 | CDH8 | Cadherin 8, type 2 | Calcium-dependent cell adhesion protein implicated in synaptic adhesion; interacts with presenilin | $<10^{-7}$ | ADNI (742 AD, MCI, CN) | Rate of change in hippocampal volume | GWAS | [6] |

*Within or proximal to gene.
†Odds ratio.
‡Entorhinal cortex thickness.
§Hippocampal volume.
¶Temporal pole thickness.
**White matter lesions.
††Parahippocampal gyrus thickness.

for iron in AD pathology. Using synergy factor analysis, they found significant association between bicarriers of the minor alleles of both SNPs and risk for AD in several U.S. and European study populations, including ADNI, providing support for the iron hypothesis (Table 12).

5.2. Studies of limited loci using quantitative phenotypes

Several studies have used knowledge of the model for AD progression by testing the associations between genes potentially involved in AD pathology and CSF biomarkers. Cruchaga et al [190] examined associations between SNPs in 35 genes putatively involved in tau posttranslational modification and CSF levels of p-tau$_{181p}$. They found that SNPs in the gene for protein phosphatase B were associated with higher levels of p-tau$_{181p}$, and that an SNP in the regulatory subunit of protein phosphatase B was more highly expressed in AD patients compared with control subjects (Table 12). These results suggest that genetic variants that alter the activity of protein phosphatase B could contribute to AD pathology by affecting tau phosphorylation. A further study by the same group [191] found that the SNP in the regulatory subunit of protein phosphatase B was associated with the rate of disease progression, and not with the age of onset or risk of AD. In contrast, *APOE* ε4 was associated with lower levels of CSF Aβ-42, increased disease risk, and lower age of onset, providing support for a model in which amyloid deposition is an early event in disease progression and accumulation of hyperphosphorylated tau occurs at a later stage (Table 12). Kauwe et al [192] also used levels of CSF biomarkers as a QT to investigate the predicted biological effects of SNPs in three genes associated with AD. They found that a nonsynonymous coding substitution in the gene for calcium homeostasis modulator 1 (*CAHLM1*), proposed to affect levels of Aβ by modulating intracellular calcium levels, was associated with increased CSF levels of Aβ-42 (Table 12). Associations between levels of CSF biomarkers and SNPs in the two other genes for growth factor receptor-bound protein-associated binding protein 2 (*GAB2*; proposed to influence tau phosphorylation) and sortilin-related receptor (*SORL1*; an apoE receptor proposed to bind Aβ) were not found, perhaps because of power limitations of the study.

Using six imaging measures reflective of AD pathology as QTs, Biffi et al [193] searched for associations between these and SNPs in a range of established and candidate genes for AD risk. They first sought to confirm associations of *APOE*, *PICALM*, *CLU*, and *CR1* with AD, and found that although *APOE* had a strong association with diagnosis, of the remaining identified risk alleles, only *CR1* was associated with AD in the ADNI cohort, possibly reflecting sample size limitations for case–control studies. Two novel loci, *CNTN5* and *BIN1*, were also found to have significant association with AD (Table 12). When the relationship of *APOE* ε4, *CR1*, *CNTN5*, and *BIN1* with imaging measures was examined, it appeared that *APOE* ε4 was associated with

virtually all brain regions, whereas the other loci had a more limited pattern of association, consistent with *APOE* ε4 being the primary AD genetic risk factor and other loci making more modest contributions to the disease.

5.3. GWAS of quantitative phenotypes

In the first ADNI GWAS using the ADNI AD cases and control subjects, Potkin et al [184] confirmed the association of *APOE* with AD and identified a novel AD risk gene, *TOMM40*, encoding a regulatory subunit of a protein translocase in the outer mitochondrial membrane, as being significantly associated with AD. A further GWAS using VBM-derived estimates of hippocampal volume as a QT identified 21 loci with significant association with hippocampal volume including, in addition to *APOE* ε4, genes involved in hippocampal development (*EFNA5*), ubiquination (*MAGI2*, *CAND1*), apoptosis (*PRUNE2*, *CAND1*), necrosis (*ARSB*), and dementia (*MAGI2*, *ARBS*) (Table 12). The involvement of *TOMM40* in numerous brain regions of AD patients was confirmed by Shen et al [194]. This study used a novel whole brain set of ROIs from both VBM and FreeSurfer parcellation as QTs in a GWAS. Of the three SNPs additionally identified as significantly associated with brain volumetric changes, only one, proximal to the *NXPH1* gene encoding neurexophilin (known to promote adhesion between dendrites and axons), had a bilateral pattern of association and was chosen for further study (Table 12). AD patients homozygous for the T allele at this locus displayed reduced GM most significantly in hallmark regions of AD atrophy, such as the hippocampus. This study illustrates the potential power of imaging genetics to identify novel candidate genes that warrant further investigation as AD candidates.

While Shen et al [194] used ROIs covering the brain, Stein et al [195] further extended the dimensionality of imaging genetics studies by carrying out a voxelwise GWAS, which explored associations between hundreds of thousands of SNPs and each of the nearly 32,000 voxels of the entire brain. Although no SNP was found significant at the stringent criteria used in the study, a number of SNPs of interest were identified in or near genes known to have functions relating to brain structure, such as monoamine uptake in neurons (*CAPDS2*), psychiatric illness (*CSMD2* and *CAPDS2*), and neurite growth (*SHB* and *ARP1*) (Table 12). In a second GWAS of a targeted region of TBM-derived structural brain degeneration on MRI, Stein et al [196] identified an SNP located in the gene encoding *N*-methyl-D-aspartate receptor NR2B subunit (*GRIN2B*) that was significantly associated with lower volumes in the temporal lobe bilaterally. Risk alleles at this locus were more prevalent in AD patients of the AD cohort than in healthy elderly control subjects and were additionally associated with decreased MMSE scores (Table 12).

Furney et al [197] also used targeted imaging measures (entorhinal cortex thickness and volume, hippocampal volume, whole brain volume, and ventricular volume) as QTs in a large GWAS involving two cohorts (AddNeuroMed

and ADNI). In addition to confirming a role of *PICALM* as a susceptibility gene for AD and as related to entorhinal thickness, they identified two other loci, *ZNF292* and *ARPP-21*, as potential candidate genes based on associations of flanking SNPs with entorhinal cortex thickness and volume (Table 12).

Most imaging GWAS reports have addressed baseline ADNI data; however, genetic variants predicting rate of progression are of great interest. Saykin et al [6] reported an initial longitudinal analysis of hippocampal volume and GM density using baseline and 12-month scans. In a candidate gene analysis [198], five AD genes from the AlzGene database (alzgene.org) were found to have significant SNPs associated with hippocampal volume or GM density changes, after accounting for *APOE*, baseline diagnosis, and other factors (*NEDD9*, *SORL1*, *DAPK1*, *IL1B*, and *SORCS1*). Next, a longitudinal GWAS was performed on hippocampal volume and GM density, using the MRI measures reported in the paper by Risacher et al [115]. A number of interesting potential candidate genes were identified by this GWAS. In addition to *APOE* and *TOMM40*, an SNP (rs12449237) located at 16q22.1 between *CDH8* (cadherin 8, type II) and *LOC390735* was strongly associated with change in hippocampal volume. *CDH8* codes for a calcium-dependent cell adhesion protein related to synaptic integrity (neuronal adhesion and axonal growth and guidance). Although the cadherin protein has been implicated in AD and is known to interact with presenilin, this was the first indication that genetic variation in *CDH8* may be associated with rate of neurodegenerative changes in the hippocampus. Several other markers did not reach genomewide significance but also showed association signals worthy of follow-up (for volume change: *SLC6A13*; for GM density change: *MAD2L2*, *LOC728574*, *QPCT*, and *GRB2*).

In a QT GWAS of CSF biomarker levels instead of imaging variables, Kim et al [149] examined levels of Aβ-42, t-tau, and p-tau$_{181p}$ and the ratios of p-tau$_{181p}$/Aβ-42 and t-tau/Aβ-42 in the ADNI cohort. They found five SNPs that reached genomewide significance for associations with one or more biomarkers, including the known candidates (*APOE* and *TOMM40*) as well as one hypothetical gene (*LOC10012950*) that partially overlaps *APOE*. Most interestingly, several SNPs in the vicinity of the novel gene *EPC2* (enhancer of polycomb homolog 2) were associated with t-tau levels. *EPC2* is involved in chromatin remodeling and has not been previously associated with AD, yet this gene may be causally associated with mental retardation in a microdeletion syndrome. Along with *EPC2*, SNPs near *CCDC134*, *ABCG2*, *SREBF2*, and *NFATC4* approached significance ($P < 10^5$) in their association with CSF biomarkers and can be considered potential candidate genes for future studies (Table 12). Han et al [199] also used levels of CSF biomarkers as QTs in a GWAS of the ADNI cohort. They found that increasing *APOE* ε4 allele dose was associated with lowered Aβ-42 and elevated t-tau and p-tau$_{181p}$ levels. After adjusting for age and *APOE* genotype, several SNPs

were found to be significantly associated with increased Aβ-42 levels in normal subjects, the most strongly associated being within or proximal to the *TOMM40*, *NCAM2*, and *CYP19A1* genes (Table 12). *NCAM2* encodes neural adhesion molecule 2, a poorly characterized protein implicated in neuronal adhesion and fasciculation of neurons, whereas *CYP19A1* encodes cytochrome P450 aromatase, an enzyme that catalyzes the conversion of androgens to estrogens.

5.4. Summary and conclusions of genetic risk factor studies

Genetic studies of the ADNI cohort have confirmed that the *APOE* ε4 allele is the major genetic risk factor for late-onset AD and that it is associated with atrophy in widespread areas of the brain. Case–control GWAS that have included ADNI data have also confirmed *CLU*, *CRI*, and *PICALM* as AD risk loci and identified a number of other candidate genes. QT GWAS using ADNI phenotypes such as Aβ-42 and tau or imaging measures of brain atrophy have detected genes implicated in the modification or modulation of Aβ or tau proteins, mitochondrial oxidative pathways, iron metabolism, neural adhesion and growth, synaptic plasticity, epigenetic processes, and memory function. A particular contribution of ADNI imaging genetic studies has been to develop methods to expand the dimensionality of GWAS studies to include all regions or voxels of an imaging scan, significantly expanding the potential of the field of imaging genetics to pinpoint specific brain regions influenced by different loci. Although candidate genes await confirmation by independent studies, they promise to unveil biological mechanisms underlying AD pathology.

6. Studies of normal control subjects

With the realization that AD pathology most likely begins to accumulate years in advance of any detectable cognitive effect, a major issue has been determining the proportion of apparently normal control subjects who harbor preclinical AD. As more sensitive biomarkers have been developed, studies have emerged with the goals of ascertaining the utility of these biomarkers in healthy elderly subjects and determining the earliest stage at which incipient AD pathology can be detected. This clearly has implications for development of AD therapies: if AD pathology can be reliably detected at such an early stage, then would existing or novel AD-modifying treatments be more effective when used before clinical symptoms become evident? In tandem with these studies, ADNI's cohort of well-characterized normal control subjects has been used to investigate processes occurring in the brain during healthy aging when there are no clinically detectable underlying pathologies. These two thrusts are often interwoven within the same study, as it becomes more obvious that healthy elderly subjects, although cognitively normal, are in fact a heterogeneous group when examined by other means.

6.1. MRI studies

The question of whether atrophy observed in normal aging is due primarily to normal aging processes or to the development of underlying pathologies is the subject of much debate. Fjell et al [200] presented the first detailed longitudinal study of brain atrophy in healthy elderly subjects aimed at understanding age-related changes in cognitive function. When volume changes in multiple ROIs and across the entire cortex were compared in healthy elderly subjects and AD patients, these authors found that the healthy elderly subjects had an atrophy rate of about 0.5% per year and that volume loss was widely distributed across the brain and included both regions typical of AD-associated atrophy and areas not typically associated with AD, such as the inferior, superior, and middle frontal cortices. The rate of change accelerated with age, especially in those regions associated with AD, possibly because of the existence of preclinical AD pathology superimposed on normal aging processes. The authors believe, however, that the majority of volumetric changes observed in healthy aging are not related to those caused by degenerative diseases. Davatzikos et al [119] used the SPARE-AD index (see section 4.4.2.1. for further description) to examine the degree of AD pathology in healthy elderly subjects and its association with cognitive decline in ADNI and another cohort with longitudinal data available. They found that SPARE-AD scores increased with age, as did the rate of change of the SPARE-AD score. When healthy elderly subjects were divided into groups of high versus low SPARE-AD score, the majority had negative scores. However, a small group with positive scores had significantly lower MMSE scores at baseline, suggesting that a subset of cognitively normal elderly subjects harbored underlying AD preclinical pathology.

In response to a paper by Burgmans et al [201] suggesting that underlying preclinical disorders may lead to the overestimation of GM atrophy in normal aging studies, Fjell et al [202] conducted a meta-analysis of a number of cross-sectional studies. They found that atrophy correlated with age in virtually all ROIs studied, even at younger ages, suggesting a linear trajectory of brain atrophy over time. When 2-year follow-up cognitive data of healthy elderly subjects from the ADNI cohort were used to exclude participants with any indication of cognitive decline, significant atrophy in all ROIs was still found in the remaining "super-stable" cohort. These results support the view that brain atrophy is part of normal aging and not necessarily caused by underlying neuropathological processes. To detect unusually fast atrophy in cognitively normal healthy elderly subjects, Franke et al [92] developed a model of healthy aging by estimating age from MRI scans of normal brain anatomy. Their method (described in more detail in section 3.7) accurately estimated the age of healthy subjects ($r = 0.92$ between real and calculated ages). Using the same method, they also estimated ages of patients with early AD and found that the predicted ages were an average of 10 years higher

than the actual ages, implying that the pattern of AD atrophy does accelerate relative to healthy elderly control subjects.

Murphy et al [203] used an automated method to examine volume changes in 14 cortical and subcortical regions over 6 months in an effort to determine whether atrophy was detectable over the short period in healthy elderly subjects and whether this atrophy was related to 2-year declines in memory-specific neuropsychological tests. They found that volume changes in these regions could be measured and that they were predictive of future clinical decline. The most significant associations were found in the MTL, suggesting that this atrophy could represent the earliest stages of AD and that MRI may be a useful tool in complementing neuropsychological tests in the early detection of those at risk for subsequent cognitive decline.

6.2. Studies of CSF biomarkers and amyloid deposition (^{11}C-PiB PET)

In a manner similar to the examination of MRI markers of AD pathology, there has been interest in assessing the utility of CSF biomarkers in healthy elderly subjects on the basis that an "earlier biomarker horizon" [204] would have great clinical significance. Nettiksimmons et al [204] examined healthy elderly subjects in the ADNI cohort and found three clusters of participants when 11 biomarker and imaging measures were subjected to unsupervised cluster analysis. The first, compact cluster had the most "normal" CSF and MRI measures, whereas the measures of the third, more dispersed group more closely resembled those of MCI patients included in the study for comparison (the second cluster was placed in an intermediate position). The third cluster had a significantly higher proportion of APOE ε4 carriers and scored worse on tests of cognition (ADAS-cog, AVLT), suggesting that this group may harbor the earliest manifestations of AD symptoms. These results provide support for the notion that cognitively normal elderly subjects are in fact a heterogeneous group, a portion of which may progress to MCI in the future. In a study of the relationship between levels of CSF biomarkers and 1-year atrophy in 15 subcortical and 33 cortical ROIs in healthy elderly subjects, Fjell et al [205] reached similar conclusions. They found that levels of CSF biomarkers, especially Aβ-42, correlated with atrophy in many of the regions tested and that atrophy was not restricted to regions most typically associated with AD. When Aβ-42 concentration was plotted against the percentage of annual change in ROIs, there was an inflection point at approximately 175 pg/mL, below which participants had larger brain volume changes over a year, suggesting that Aβ-42 may play a role in changes in brain volume observed in healthy elderly subjects below a certain threshold level. De Meyer et al [159] found that when a biomarker "signature" for AD using levels of Aβ-42, t-tau, and p-tau$_{181p}$ was tested in healthy elderly subjects, there was a bimodal distribution of Aβ-42 levels with a separation point at 188 pg/mL. Although it was unknown whether those participants

with low levels of Aβ-42 in these two studies would develop AD pathology, they once again highlighted the heterogeneity of the cognitively normal healthy elderly group.

In the current model of AD pathogenesis, it is well established that deposition of amyloid plaques is an early event that, in conjunction with tau pathology, causes neuronal damage typically beginning in the hippocampus and resulting in the first clinical manifestations of the disease in the form of episodic memory deficits. Mormino et al [206] investigated the relationship between Aβ deposition, as measured by ^{11}C-PiB PET uptake, hippocampal atrophy, and episodic memory loss in cognitively normal healthy elderly subjects. They found an inverse relationship between ^{11}C-PiB uptake and hippocampal volume and that episodic memory loss was predicted by hippocampal volume, but not by ^{11}C-PiB uptake. The results suggest that low levels of Aβ-42 accumulation in healthy elderly subjects may reflect early stages of AD pathogenesis and may subsequently mediate dementia through an effect on hippocampal volume and the resulting declines in episodic memory.

6.3. Genetic studies of normal control subjects

Although the APOE ε4 allele has been clearly identified as an AD risk allele, the question of whether a second variant in the APOE gene, the ε2 allele, confers a protective effect has been less well studied. Evidence for the protective effect of the APOE ε2 allele came from a study by Hua et al [120], who found reduced CSF volume in the ventricular system of healthy elderly subjects who had the highest frequency of this allele compared with MCI and AD patients. Chiang et al [207] sought to determine the effect of APOE ε2 allele on hippocampal volume and levels of CSF biomarkers in healthy elderly subjects. They found that carriers of the APOE ε2 genotype, constituting approximately 5% of the population, had lower rates of hippocampal atrophy and higher Aβ-42 and lower t-tau and p-tau$_{181p}$ levels compared with the more common (∼70% of population) APOE ε3/ε3 homozygotes, suggesting that lower rates of atrophy could be related to decreased underlying AD pathology and may explain the lower rates of AD among carriers of this allele. A similar finding was reported by Fan et al [208], who examined the relationship between cortical thickness at multiple regions across the brain and APOE genotype in healthy elderly subjects who were grouped as ε2 carriers, ε3 homozygotes, and ε4 carriers. After adjusting for multiple comparisons, they found greater thickness in the superior temporal cortex in ε2 carriers compared with ε3 homozygotes, and in the dorsolateral prefrontal cortex in ε2 compared with ε4 carriers. Moreover, CSF concentrations of Aβ-42, t-tau, and p-tau$_{181p}$ were significantly different in all groups (Fig. 24), although no differences were found in the MMSE between groups. The results of these two studies provided support for the differential effect of APOE alleles on brain structure and on CSF biomarkers.

In addition to risk factors like age and APOE genotype, increased BMI has been associated with frontal, temporal, and
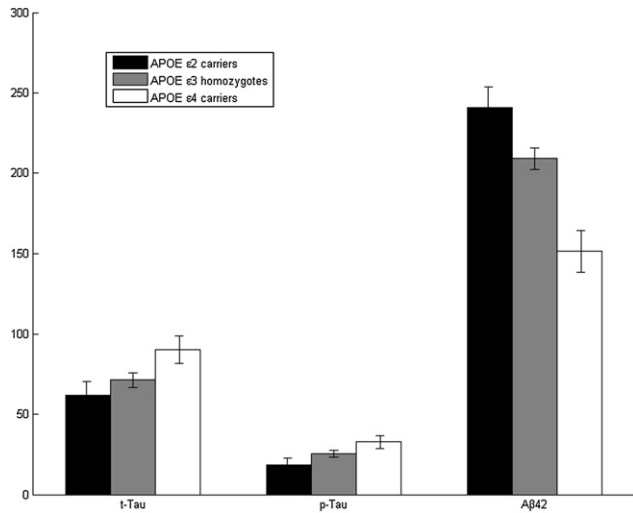
Fig. 24. Mean biomarker levels (t-tau, p-tau, and Aβ-42) for the *APOE* genotype groups. The *APOE* ε2 carriers are represented in black, the ε3 homozygotes in gray, and the ε4 carriers in white. The CSF Aβ-42 levels show a significant stepwise trend downward, from *APOE* ε2 carriers to ε3 homozygotes to ε4 carriers, whereas the t-tau and the p-tau levels show the opposite trend. Reproduced with permission from Ref [208].

subcortical atrophy and may increase susceptibility to AD. Recent studies identified a novel obesity genetic risk factor, a variant of the fat mass and obesity associated (*FTO*) gene, carried by almost one-half of Western Europeans. Ho et al [209] examined the effect of the *FTO* risk allele on brain volumes in healthy elderly subjects and compared its effects on brain structure with that of increased BMI. They found that carriers of the *FTO* risk allele had an 8% to 12% deficit in a subset of areas affected by BMI, predominantly in the frontal and occipital lobes, compared with noncarriers, suggesting that the *FTO* risk allele contributes to, but does not fully account for, the effect of increasing BMI on brain atrophy. Bertam and Heekeren [198] discussed the findings of the study and the need for corroborating the results to determine the influence of genetics on normal brain structure and function.

The idea that common variance in brain structure may be primarily controlled not by polymorphisms resulting in altered protein structure, but by changes in regulatory elements found support in a study by Rimol et al [210]. Using the ADNI cohort, they found that two SNPs located in nonexonic regions of genes for primary microencephaly were correlated with reduced cortical surface in males only, regardless of disease status, and suggested that these polymorphisms may affect gene regulation and result in gross abnormalities in brain structure observed in this disease. More data on the role of common genetic sequence variations in accounting for commonly occurring brain structure variations came from a study by the same group [211] on associations between a common haplotype of the *MECP2* gene and brain structure. Mutations in *MECP2*, encoding methyl-CpG binding protein 2, cause microencephalopathy and are associated with other severe neurodevelopmental disorders, but Joyner et al [211] found that common sequence

variations in this region correlated with reduced cortical surface area in males only of the ADNI cohort. As *MECP2 i*s thought to transcriptionally activate or repress thousands of genes, studies of the influence of such common sequence variations may reveal profound insights into brain structure and development.

6.4. Summary and conclusions of papers focusing on normal control subjects

Heterogeneity of cognitively normal healthy elderly subjects seems to be well supported by these studies, with a number suggesting the existence of a subset of cognitively normal elderly subjects that bears the hallmarks of early AD pathogenesis in terms of changes in brain volume and levels of CSF biomarkers. The extent to which these changes are separate from those of normal aging remains to be fully elucidated. Fjell et al [202] concluded, "We need more knowledge about which factors mediate brain atrophy in healthy elderly and what consequences the changes have for cognitive function." Likewise, several intriguing studies have pointed to the role of genetics in healthy aging, and suggest a protective effect of the *APOE* ε2 allele and increased susceptibility to brain atrophy and perhaps AD conferred by a risk allele at the novel *FTO* locus. Clearly, studies of the healthy elderly control subjects are revealing information not only about the processes of healthy aging but also the initial development of preclinical AD pathology.

7. Worldwide ADNI

Since the inception of ADNI in North America in 2004, there has been worldwide interest in creating programs that are at least partially modeled on the ADNI platform, and that use protocols developed by ADNI for at least part of their studies. Combined, the initiatives represent a concerted effort toward globalization of this concept. Society may well reap the rewards of having not just a well-characterized North American cohort for the development of AD biomarkers but also similarly characterized cohorts globally that may represent diverse ethnic groups, important for determining the applicability of ADNI findings to the world population. Like ADNI, these initiatives from Europe, Japan, and Australia are predicated on the sharing of data, and infrastructure is beginning to be developed to allow full transparency of global results. Future ADNIs are expected to begin in Argentina and China and have recently begun in Korea and Taiwan. All worldwide ADNIs share common goals of increasing understanding of AD onset and progression, both cognitively and physically, establishing globally recognized standards for diagnosis, and ultimately developing methods to allow more efficient clinical trials.

7.1. European ADNI

Frisoni [212] provides an overview of all programs, either completed or underway, in Europe that are in some way

related to ADNI. The ADNI platform was first introduced into Europe in the form of a small cross-sectional pilot study, E-ADNI, which aimed to assess the feasibility of importing ADNI procedures to a European multicenter multicountry setting [213]. E-ADNI was initiated under the auspices of the Alzheimer's Association through the generosity of the HEDCO Foundation and enrolled 49 control, MCI, and AD participants over seven sites in seven countries. The pilot study used all ADNI protocols, with the exception of PET imaging, the feasibility of which had been previously demonstrated, and MRI sequences for the detection of cerebral small vessel damage, a slightly different emphasis of the study. Buerger et al [214] conducted a multicenter feasibility study within E-ADNI and found that the use of fresh, rather than frozen, biological samples increased diagnostic accuracy. Overall, the study demonstrated that apart from age and education, the enrolled cohort was similar to the ADNI cohort in MRI and CSF measures and that implementation of the ADNI platform in Europe was feasible [213].

Other data collection programs in Europe include (1) AddNeuroMed, a public–private initiative with a cohort of 700 control, MCI, and AD subjects across Europe that used ADNI protocols for structural MRI; (2) Pharma-cog, which overlaps to the greatest extent with ADNI and which aims to predict cognitive properties of new drug candidates for neurodegenerative diseases; (3) Swedish ADNI, a small-scale initiative funded by the Alzheimer's Association that used ADNI protocol and which has merged into the larger Swedish BrainPower initiative; and (4) Italian ADNI, a larger project with 480 patients enrolled. These initiatives vary in the size and composition of cohorts enrolled, the length of study, and the frequency and type of data collection. However, they all have the use of standardized ADNI protocols in common for at least some of their data collection [212].

Two additional European programs funded by the Alzheimer's Association focused on harmonization of measurements of both CSF biomarkers [215] and hippocampal volume [216], aiming to create worldwide protocols for standardized hippocampal segmentation and measurement of CSF biomarker concentrations to allow the direct comparison of results generated globally.

Finally, initiatives inspired by ADNI to build infrastructure including a central repository of all data, like that developed at LONI, have been implemented in Europe. NeuGRID is being developed at the European equivalent of LONI, and outGRID aims to synergize neuGRID, LONI, and the Canadian repository CBRAIN and to develop full interoperability. CATI (Centre pour l'Acquisition et le Traitement de l'Image) is the French repository for data sets within that country. ADNI-related programs and initiatives in Europe are summarized in Table 13.

7.2. AIBL study: The Australian ADNI

Often termed the "Australian ADNI," the AIBL has similar goals to ADNI, namely, to better understand disease pathogenesis and to develop tests for an earlier diagnosis of AD, and, to this end, uses ADNI protocols for its imaging studies [217]. Some methodological differences between the two studies include the omission of FDG-PET metabolic investigations and the comparison of amyloid pathology using ^{11}C-PiB PET and Aβ-42 levels in blood plasma instead of from CSF on the basis that obtaining blood plasma is both less expensive and less invasive than lumbar punctures. Perhaps the greatest difference between AIBL and ADNI lies in the approach AIBL is taking to investigating lifestyle factors involved in AD. By collecting extensive neuropsychological and lifestyle data, the study aims to understand which health and lifestyle factors protect or contribute to AD. Like ADNI, however, all data are made available through LONI and are funded by the Alzheimer's Association. Ellis et al [217] reported that one recent finding from the study found that hippocampal atrophy was regionally associated with ^{11}C-PiB retention only in the inferior lobe, leading to a new hypothesis of how Aβ accumulation could disrupt connections between the hippocampus through accumulation in this area (Bourgeat et al., Beta-amyloid burden in the temporal neocortex is related to elderly subjects without dementia. Neurology 2010:74:121–7; see Appendix).

Rowe et al [218] reported on the progress of the neuroimaging arm of the AIBL in characterizing a cohort of 177 healthy elderly subjects, 57 MCI patients, and 53 AD patients. The patient groups had increasing numbers of *APOE* ε4 carriers, increased hippocampal atrophy, and increased cognitive impairment with disease progression. The distribution of ^{11}C-PiB binding in control subjects did not follow a normal distribution, and cluster analysis determined a separation point between low and high ^{11}C-PiB binding groups at a neocortical standardized uptake value threshold of 1.5. This bimodal distribution in normal healthy elderly subjects again echoes the idea of heterogeneity within this group and the existence of a subset of patients with the first manifestations of AD pathogenesis well in advance of any effects on cognition. ^{11}C-PiB binding may therefore play a role in populating and monitoring clinical trials of antiamyloid therapies. Rowe et al [218] also used ^{11}C-PiB PET imaging for diagnosis and found that ^{11}C-PiB scans discriminated between AD and control subjects with an accuracy of 73%, a sensitivity of 98%, and a specificity of 63%, comparable with results obtained using hippocampal volume (accuracy = 73%, specificity = 80%, sensitivity = 78%).

7.3. Japanese ADNI

The need for a Japanese ADNI (J-ADNI) was realized in 2006 when ADNI was beginning in North America and at the end of the Japanese study J-COSMIC (Japan Cooperative SPECT Study on Assessment of Mild Impairment of Cognitive Function) [219]. Iwatsubo [220] reported that J-ADNI was needed not only to meet requirements for global clinical trials of AD drugs about to begin in Japan and to develop the necessary infrastructure for these trials, but was also motivated by the desire of Japanese researchers to improve their clinical science

Table 13
European initiatives related to ADNI

Purpose	Program name	Funding agency	Time frame	Countries
Data collection	Pilot E-ADNI	Alzheimer's Association	2006–2007	IT, FR, GE, NL, SW, DE
	AddNeuroMed	EC	Ongoing, 40 months	FI, PL, UK, IT, GR, FR
	Pharma-Cog WorkPackage 5 (E-ADNI)	EC IMI	Ongoing 5 years	SP, IT, GE, FR
	Swedish ADNI	Alzheimer's Association	2007–2009	SW
	Italian ADNI	NHS	2009–2011	IT
SOP development	International harmonization of CSF Aβ42, t-tau, and p-tau	Alzheimer's Association	2009–2013	40 laboratories (EU, US, Japan, Australia, Brazil)
	EADC-ADNI harmonization of hippocampal volume	Alzheimer's Association Lily-Wyeth	2010–2012	24 centers in EU, US, Canada, Australia
Infrastructure development	NeuGRID	FP7	2008–2011	IT, FR, SP, CH, UK, SW
	OutGRID	FP7	2009–2011	IT, FR, UK, US, CD
	Centre pour l'Acquisition et le Traitement de l'Image (CATI)	French National Foundation on AD and RD	2010–2013	FR

Abbreviations: ADNI, Alzheimer's Disease Neuroimaging Initiative; EC, European Commission; IMI, Innovative Medicines Initiatives; NHS, National Health System; EADC, European Alzheimer's Disease Consortium; FP7, 7th Framework Programme; AD and RD, Alzheimer's disease and related diseases; DE, Denmark; CD, Canada; CH, Switzerland; FI, Finland; FR, France; GE, Germany; GR, Greece; IT, Italy; NL, Netherlands; PL, Poland; SP, Spain; SW, Sweden; UK, United Kingdom; US, United States.

NOTE. Reproduced with permission from Ref [212].
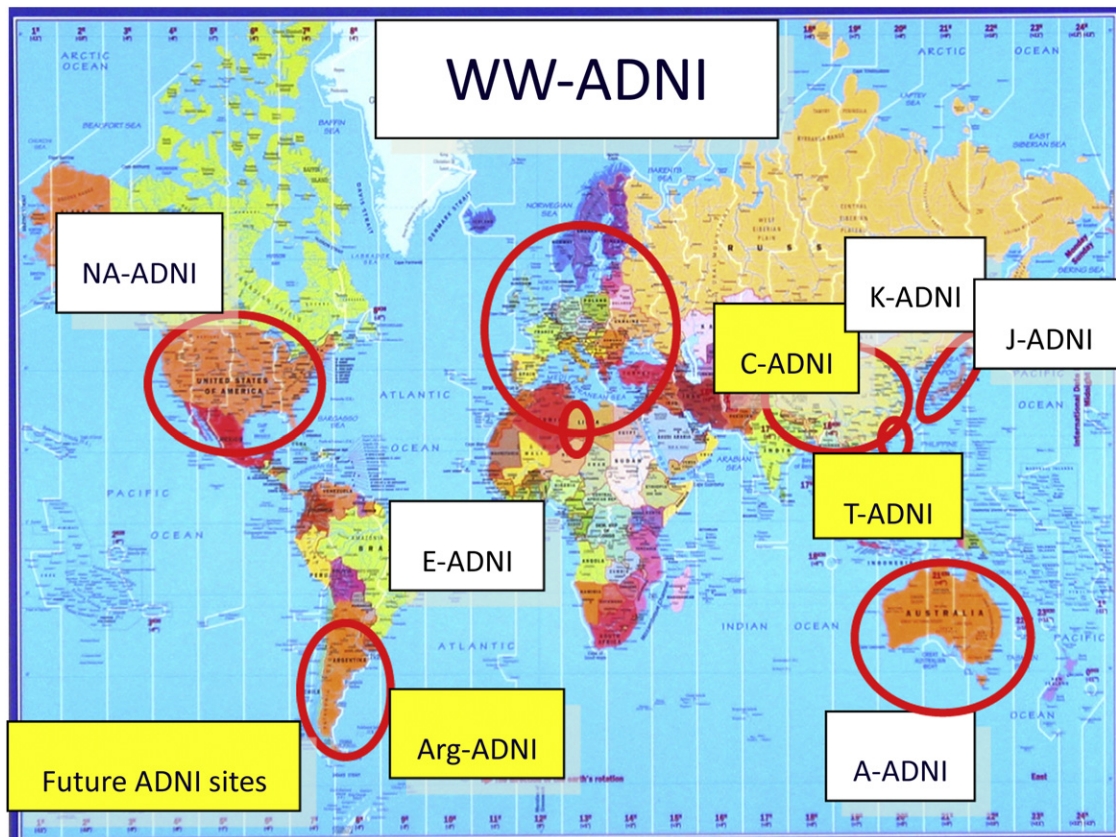
Fig. 25. Worldwide ADNI sites. Abbreviations: NA-ADNI, North American ADNI; Arg-ADNI, Argentinean ADNI; E-ADNI, European ADNI; C-ADNI, Chinese ADNI; K-ADNI, Korean ADNI; J-ADNI, Japanese ADNI; T-ADNI, Taiwanese ADNI; A-ADNI, Australian ADNI.

through international collaboration. A special issue of *Rinsho Shinkeigaku* near the inception of J-ADNI in 2007 reported on ADNI and the need for the establishment of a Japanese version [221], the goals of early detection of AD and biomarker development [222], the methods used by ADNI and adopted by J-ADNI for achieving these goals [219], and the use of ADNI approaches for detecting MCI in neuropathological studies [223]. Funding for J-ADNI was sought and received from both the public and private sector, including Japanese and international companies, to a total of approximately ¥300 million per year [220]. The study began in 2008 and aimed to recruit 300 amnestic MCI patients, 150 patients with early AD, and 150 healthy elderly control subjects from 30 centers across Japan by the end of 2010; participants would then be followed until 2013 using a research protocol designed to maximize compatibility with ADNI [220,224]. Compatibility with ADNI protocols was designed to allow sharing and direct comparison of data and as a way to contribute to global standardization of protocols. Arai et al [224] reported that initial results from ADNI supporting the use of biomarkers in clinical trials contributed to a paradigm shift in Japanese geriatric medicine from defining AD solely by cognitive measures to considering the information available from biomarkers.

7.4. Worldwide ADNI future directions

The establishment of Worldwide ADNI, an umbrella organization of global ADNI efforts, is coordinated by the Alzheimer's Association and is a direct result of ADNI. Information on the countries that have established or plan to establish ADNI sties in their countries can be found at http://www.alz.org/research/funding/partnerships/ WW-ADNI_overview.asp. (Fig. 25). Information on the countries that have established or plan to establish ADNI sties in their countries can be found at http://www.alz.org/ research/funding/partnerships/WW-ADNI_overview.asp. Using standardized protocols developed by ADNI, these programs collectively aim to help define the rate of progression of MCI and AD, and to develop improved methods for identifying the appropriate patient populations to participate in clinical trials. It is anticipated that data generated by these global initiatives will ultimately be shared through a common infrastructure with international researchers. It is clear that ADNI has had and will continue to have a profound and far-reaching impact on the development of methods for the prediction and monitoring of the onset and progression of AD and in gaining a worldwide picture of the physical changes that lead to AD.

8. Disclosures

References

[1] Hardy J. Alzheimer's disease: the amyloid cascade hypothesis: an update and reappraisal. J Alzheimers Dis 2006;9(Suppl 3):151–3.

[2] Mueller SG, Weiner MW, Thal LJ, Petersen RC, Jack C, Jagust W, et al. The Alzheimer's disease neuroimaging initiative. Neuroimaging Clin N Am 2005;15:869–77. xi–xii.

[3] Weiner MW, Aisen PS, Jack CR Jr, Jagust WJ, Trojanowski JQ, Shaw L, et al. The Alzheimer's Disease Neuroimaging Initiative: progress report and future plans. Alzheimers Dement 2010;6. 202.e7–11.e7.

[4] Frisoni GB, Weiner MW. Alzheimer's disease neuroimaging initiative special issue. Neurobiol Aging 2010;31:1259–62.

[5] Petersen RC, Roberts RO, Knopman DS, Boeve BF, Geda YE, Ivnik RJ, et al. Mild cognitive impairment: ten years later. Arch Neurol 2009;66:1447–55.

[6] Saykin AJ, Shen L, Foroud TM, Potkin SG, Swaminathan S, Kim S, et al. Alzheimer's Disease Neuroimaging Initiative biomarkers as quantitative phenotypes: genetics core aims, progress, and plans. Alzheimers Dement 2010;6(3):265–73.

[7] Hampel H, Shen Y, Walsh DM, Aisen P, Shaw LM, Zetterberg H, et al. Biological markers of amyloid beta-related mechanisms in Alzheimer's disease. Exp Neurol 2010;223:334–46.

[8] Clark CM, Davatzikos C, Borthakur A, Newberg A, Leight S, Lee VM, et al. Biomarkers for early detection of Alzheimer pathology. Neurosignals 2008;16:11–8.

[9] Fleisher AS, Donohue M, Chen K, Brewer JB, Aisen PS. Applications of neuroimaging to disease-modification trials in Alzheimer's disease. Behav Neurol 2009;21:129–36.

[10] Shaw LM, Korecka M, Clark CM, Lee VM, Trojanowski JQ. Biomarkers of neurodegeneration for diagnosis and monitoring therapeutics. Nat Rev Drug Discov 2007;6:295–303.

[11] Petersen RC, Jack CR Jr. Imaging and biomarkers in early Alzheimer's disease and mild cognitive impairment. Clin Pharmacol Ther 2009;86:438–41.

[12] Trojanowski JQ, Vandeerstichele H, Korecka M, Clark CM, Aisen PS, Petersen RC, et al. Update on the biomarker core of the Alzheimer's Disease Neuroimaging Initiative subjects. Alzheimers Dement 2010;6:230–8.

[13] Hardy J, Selkoe DJ. The amyloid hypothesis of Alzheimer's disease: progress and problems on the road to therapeutics. Science 2002; 297:353–6.

[14] Jack CR Jr, Knopman DS, Jagust WJ, Shaw LM, Aisen PS, Weiner MW, et al. Hypothetical model of dynamic biomarkers of the Alzheimer's pathological cascade. Lancet Neurol 2010; 9:119–28.

[15] Shaw LM. PENN biomarker core of the Alzheimer's disease Neuroimaging Initiative. Neurosignals 2008;16:19–23.

[16] Jack CR Jr, Lowe VJ, Weigand SD, Wiste HJ, Senjem ML, Knopman DS, et al. Serial PIB and MRI in normal, mild cognitive impairment and Alzheimer's disease: implications for sequence of pathological events in Alzheimer's disease. Brain 2009; 132(Pt 5):1355–65.

[17] Braak H, Del Tredici K. The pathological process underlying Alzheimer's disease in individuals under thirty. Acta Neuropathol 2011;121:171–81.

[18] Dubois B, Feldman HH, Jacova C, Cummings JL, Dekosky ST, Barberger-Gateau P, et al. Revising the definition of Alzheimer's disease: a new lexicon. Lancet Neurol 2010;9:1118–27.

[19] Sperling RA, Aisen PS, Beckett LA, Bennett DA, Craft S, Fagan AM, et al. Toward defining the preclinical stages of Alzheimer's disease: recommendations from the National Institute on Aging-Alzheimer's Association workgroups on diagnostic guidelines for Alzheimer's disease. Alzheimers Dement 2011;7:280–92.

[20] Roberts RO, Geda YE, Knopman DS, Cha RH, Pankratz VS, Boeve BF, et al. The Mayo Clinic Study of Aging: design and sampling, participation, baseline measures and sample characteristics. Neuroepidemiology 2008;30:58–69.

[21] Petersen RC, Roberts RO, Knopman DS, Geda YE, Cha RH, Pankratz VS, et al. Prevalence of mild cognitive impairment is higher in men. The Mayo Clinic Study of Aging. Neurology 2010; 75:889–97.

[22] Games D, Adams D, Alessandrini R, Barbour R, Berthelette P, Blackwell C, et al. Alzheimer-type neuropathology in transgenic mice overexpressing V717F beta-amyloid precursor protein. Nature 1995;373:523–7.

[23] Frank RA, Galasko D, Hampel H, Hardy J, de Leon MJ, Mehta PD, et al. Biological markers for therapeutic trials in Alzheimer's disease. Proceedings of the biological markers working group; NIA initiative on neuroimaging in Alzheimer's disease. Neurobiol Aging 2003; 24:521–36.

[24] Trojanowski J. Searching for the biomarkers of Alzheimer's. Pract Neurol 2004;3:30–4.

[25] Mueller SG, Weiner MW, Thal LJ, Petersen RC, Jack C, Jagust W, et al. Ways toward an early diagnosis in Alzheimer's disease: the Alzheimer's Disease Neuroimaging Initiative. Cogn Dement 2006;5:56–62.

[26] Hampel H, Burger K, Teipel SJ, Bokde AL, Zetterberg H, Blennow K. Core candidate neurochemical and imaging biomarkers of Alzheimer's disease. Alzheimers Dement 2008;4:38–48.

[27] Klunk WE, Engler H, Nordberg A, Wang Y, Blomqvist G, Holt DP, et al. Imaging brain amyloid in Alzheimer's disease with Pittsburgh Compound-B. Ann Neurol 2004;55:306–19.

[28] Klunk WE, Mathis CA. The future of amyloid-beta imaging: a tale of radionuclides and tracer proliferation. Curr Opin Neurol 2008; 21:683–7.

[29] Kung MP, Hou C, Zhuang ZP, Skovronsky D, Kung HF. Binding of two potential imaging agents targeting amyloid plaques in postmortem brain tissues of patients with Alzheimer's disease. Brain Res 2004;1025:98–105.

[30] Schmidt ME, Siemers E, Snyder PJ, Potter WZ, Cole P, Soares H. The Alzheimer's Disease Neuroimaging Initiative: perspectives of the Industry Scientific Advisory Board. Alzheimers Dement 2010; 6:286–90.

[31] Carrillo MC, Sanders CA, Katz RG. Maximizing the Alzheimer's Disease Neuroimaging Initiative II. Alzheimers Dement 2009; 5:271–5.

[32] Toga AW, Crawford KL. The informatics core of the Alzheimer's Disease Neuroimaging Initiative. Alzheimers Dement 2010; 6:247–56.

[33] Jack CR Jr, Bernstein MA, Borowski BJ, Gunter JL, Fox NC, Thompson PM, et al. Update on the magnetic resonance imaging core of the Alzheimer's disease neuroimaging initiative. Alzheimers Dement 2010;6:212–20.

[34] Jagust WJ, Bandy D, Chen K, Foster NL, Landau SM, Mathis CA, et al. The Alzheimer's Disease Neuroimaging Initiative positron emission tomography core. Alzheimers Dement 2010;6:221–9.

[35] Aisen PS, Petersen RC, Donohue MC, Gamst A, Raman R, Thomas RG, et al. Clinical core of the Alzheimer's Disease Neuroimaging Initiative: progress and plans. Alzheimers Dement 2010; 6:239–46.

[36] Cairns NJ, Taylor-Reinwald L, Morris JC. Autopsy consent, brain collection, and standardized neuropathologic assessment of ADNI participants: the essential role of the neuropathology core. Alzheimers Dement 2010;6:274–9.

[37] Cummings JL. Integrating ADNI results into Alzheimer's disease drug development programs. Neurobiol Aging 2010;31:1481–92.

[38] Mueller SG, Weiner MW, Thal LJ, Petersen RC, Jack CR, Jagust W, et al. Ways toward an early diagnosis in Alzheimer's disease: the Alzheimer's Disease Neuroimaging Initiative (ADNI). Alzheimers Dement 2005;1:55–66.

[39] Petersen RC, Trojanowski JQ. Use of Alzheimer disease biomarkers: potentially yes for clinical trials but not yet for clinical practice. JAMA 2009;302:436–7.

[40] Petersen RC. Early diagnosis of Alzheimer's disease: is MCI too late? Curr Alzheimer Res 2009;6:324–30.

[41] Hill D. Neuroimaging to assess safety and efficacy of AD therapies. Expert Opin Investig Drugs 2010;19:23–6.

[42] Becker RE, Greig NH. Alzheimer's disease drug development: old problems require new priorities. CNS Neurol Disord Drug Targets 2008;7:499–511.

[43] Weiner MW. Editorial: imaging and biomarkers will be used for detection and monitoring progression of early Alzheimer's disease. J Nutr Health Aging 2009;13:332.

[44] Ito K, Corrigan B, Zhao Q, French J, Miller R, Soares H, et al. Disease progression model for cognitive deterioration from Alzheimer's Disease Neuroimaging Initiative database. Alzheimers Dement 2011; 7:151–60.

[45] Gunter JL, Bernstein MA, Borowski BJ, Ward CP, Britson PJ, Felmlee JP, et al. Measurement of MRI scanner performance with the ADNI phantom. Med Phys 2009;36:2193–205.

[46] Kruggel F, Turner J, Muftuler LT. Impact of scanner hardware and imaging protocol on image quality and compartment volume precision in the ADNI cohort. Neuroimage 2010;49:2123–33.

[47] Ho AJ, Hua X, Lee S, Leow AD, Yanovsky I, Gutman B, et al. Comparing 3 T and 1.5 T MRI for tracking Alzheimer's disease progression with tensor-based morphometry. Hum Brain Mapp 2010; 31:499–514.

[48] Mortamet B, Bernstein MA, Jack CR Jr, Gunter JL, Ward C, Britson PJ, et al. Automatic quality assessment in structural brain magnetic resonance imaging. Magn Reson Med 2009;62:365–72.

[49] Clarkson MJ, Ourselin S, Nielsen C, Leung KK, Barnes J, Whitwell JL, et al. Comparison of phantom and registration scaling corrections using the ADNI cohort. Neuroimage 2009;47:1506–13.

[50] Bauer CM, Jara H, Killiany R. Whole brain quantitative T2 MRI across multiple scanners with dual echo FSE: applications to AD, MCI, and normal aging. Neuroimage 2010;52:508–14.

[51] Leung KK, Clarkson MJ, Bartlett JW, Clegg S, Jack CR Jr, Weiner MW, et al. Robust atrophy rate measurement in Alzheimer's disease using multi-site serial MRI: tissue-specific intensity normalization and parameter selection. Neuroimage 2010;50:516–23.

[52] Jack CR Jr, Bernstein MA, Fox NC, Thompson P, Alexander G, Harvey D, et al. The Alzheimer's Disease Neuroimaging Initiative (ADNI): MRI methods. J Magn Reson Imaging 2008;27:685–91.

[53] Boyes RG, Gunter JL, Frost C, Janke AL, Yeatman T, Hill DL, et al. Intensity non-uniformity correction using N3 on 3-T scanners with multichannel phased array coils. Neuroimage 2008;39:1752–62.

[54] Leow AD, Klunder AD, Jack CR Jr, Toga AW, Dale AM, Bernstein MA, et al. Longitudinal stability of MRI for mapping brain change using tensor-based morphometry. Neuroimage 2006;31:627–40.

[55] Joshi A, Koeppe RA, Fessler JA. Reducing between scanner differences in multi-center PET studies. Neuroimage 2009;46:154–9.

[56] Shaw LM, Vanderstichele H, Knapik-Czajka M, Figurski M, Coart E, Blennow K, et al. Qualification of the analytical and clinical performance of CSF biomarker analyses in ADNI. Acta Neuropathol 2011; 121:597–609.

[57] Shaw LM, Vanderstichele H, Knapik-Czajka M, Clark CM, Aisen PS, Petersen RC, et al. Cerebrospinal fluid biomarker signature in Alzheimer's disease neuroimaging initiative subjects. Ann Neurol 2009;65:403–13.

[58] Leung KK, Barnes J, Modat M, Ridgway GR, Bartlett JW, Fox NC, et al. Brain MAPS: an automated, accurate and robust brain extraction technique using a template library. Neuroimage 2011; 55:1091–108.

[59] Leung KK, Barnes J, Ridgway GR, Bartlett JW, Clarkson MJ, Macdonald K, et al. Automated cross-sectional and longitudinal hippocampal volume measurement in mild cognitive impairment and Alzheimer's disease. Neuroimage 2010;51:1345–59.

[60] Wolz R, Aljabar P, Hajnal JV, Hammers A, Rueckert D. LEAP: learning embeddings for atlas propagation. Neuroimage 2010; 49:1316–25.

[61] Lotjonen JM, Wolz R, Koikkalainen JR, Thurfjell L, Waldemar G, Soininen H, et al. Fast and robust multi-atlas segmentation of brain magnetic resonance images. Neuroimage 2010;49:2352–65.

[62] Heckemann RA, Keihaninejad S, Aljabar P, Rueckert D, Hajnal JV, Hammers A. Improving intersubject image registration using tissue-class information benefits robustness and accuracy of multi-atlas based anatomical segmentation. Neuroimage 2010; 51:221–7.

[63] Morra JH, Tu Z, Apostolova LG, Green AE, Avedissian C, Madsen SK, et al. Validation of a fully automated 3D hippocampal segmentation method using subjects with Alzheimer's disease mild cognitive impairment, and elderly controls. Neuroimage 2008; 43:59–68.

[64] Wolz R, Heckemann RA, Aljabar P, Hajnal JV, Hammers A, Lotjonen J, et al. Measurement of hippocampal atrophy using 4D graph-cut segmentation: application to ADNI. Neuroimage 2010; 52:109–18.

[65] Huang S, Li J, Sun L, Ye J, Fleisher A, Wu T, et al. Learning brain connectivity of Alzheimer's disease by sparse inverse covariance estimation. Neuroimage 2010;50:935–49.

[66] Calvini P, Chincarini A, Gemme G, Penco MA, Squarcia S, Nobili F, et al. Automatic analysis of medial temporal lobe atrophy from structural MRIs for the early assessment of Alzheimer disease. Med Phys 2009;36:3737–47.

[67] Holland D, Dale AM. Nonlinear registration of longitudinal images and measurement of change in regions of interest. Med Image Anal 2011;15:489–97.

[68] Chupin M, Gerardin E, Cuingnet R, Boutet C, Lemieux L, Lehericy S, et al. Fully automatic hippocampus segmentation and classification in Alzheimer's disease and mild cognitive impairment applied on data from ADNI. Hippocampus 2009;19:579–87.

[69] Morra JH, Tu Z, Apostolova LG, Green AE, Avedissian C, Madsen SK, et al. Automated 3D mapping of hippocampal atrophy and its clinical correlates in 400 subjects with Alzheimer's disease, mild cognitive impairment, and elderly controls. Hum Brain Mapp 2009;30:2766–88.

[70] Wang H, Das S, Pluta J, Craige C, Altinay M, Avants B, et al. Standing on the shoulders of giants: improving medical image segmentation via bias correction. Med Image Comput Comput Assist Interv 2010;13(Pt 3):105–12.

[71] Bossa M, Zacur E, Olmos S. Statistical analysis of relative pose information of subcortical nuclei: application on ADNI data. Neuroimage 2011;55:999–1008.

[72] Bossa M, Zacur E, Olmos S. Tensor-based morphometry with stationary velocity field diffeomorphic registration: application to ADNI. Neuroimage 2010;51:956–69.

[73] Hua X, Leow AD, Lee S, Klunder AD, Toga AW, Lepore N, et al. 3D characterization of brain atrophy in Alzheimer's disease and mild cognitive impairment using tensor-based morphometry. Neuroimage 2008;41:19–34.

[74] Yushkevich PA, Avants BB, Das SR, Pluta J, Altinay M, Craige C. Bias in estimation of hippocampal atrophy using deformation-based morphometry arises from asymmetric global normalization: an illustration in ADNI 3 T MRI data. Neuroimage 2010;50:434–45.

[75] Park H, Seo J. Application of multidimensional scaling to quantify shape in Alzheimer's disease and its correlation with Mini Mental State Examination: a feasibility study. J Neurosci Methods 2011; 194:380–5.

[76] Chen W, Song X, Zhang Y, Darvesh S, Zhang N, D'Arcy RC, et al. An MRI-based semiquantitative index for the evaluation of brain atrophy and lesions in Alzheimer's disease, mild cognitive impairment and normal aging. Dement Geriatr Cogn Disord 2010;30:121–30.

[77] Acosta O, Bourgeat P, Zuluaga MA, Fripp J, Salvado O, Ourselin S. Automated voxel-based 3D cortical thickness measurement in a combined Lagrangian-Eulerian PDE approach using partial volume maps. Med Image Anal 2009;13:730–43.

[78] King RD, George AT, Jeon T, Hynan LS, Youn TS, Kennedy DN, et al. Characterization of atrophic changes in the cerebral cortex using fractal dimensional analysis. Brain Imaging Behav 2009; 3:154–66.

[79] King RD, Brown B, Hwang M, Jeon T, George AT. Fractal dimension analysis of the cortical ribbon in mild Alzheimer's disease. Neuroimage 2010;53:471–9.

[80] Li Y, Wang Y, Xue Z, Shi F, Lin W, Shen D. Consistent 4D cortical thickness measurement for longitudinal neuroimaging study. Med Image Comput Comput Assist Interv 2010;13(Pt 2):133–42.

[81] Risser L, Vialard FX, Wolz R, Holm DD, Rueckert D. Simultaneous fine and coarse diffeomorphic registration: application to atrophy measurement in Alzheimer's disease. Med Image Comput Comput Assist Interv 2010;13(Pt 2):610–7.

[82] Zhang T, Davatzikos C. ODVBA: Optimally-Discriminative Voxel-Based Analysis. IEEE Trans Med Imaging 2011;30:1441–54.

[83] Fan Y, Batmanghelich N, Clark CM, Davatzikos C. Spatial patterns of brain atrophy in MCI patients, identified via high-dimensional pattern classification, predict subsequent cognitive decline. Neuroimage 2008;39:1731–43.

[84] Haense C, Herholz K, Jagust WJ, Heiss WD. Performance of FDG PET for detection of Alzheimer's disease in two independent multi-centre samples (NEST-DD and ADNI). Dement Geriatr Cogn Disord 2009;28:259–66.

[85] Chen K, Ayutyanont N, Langbaum JB, Fleisher AS, Reschke C, Lee W, et al. Characterizing Alzheimer's disease using a hypometabolic convergence index. Neuroimage 2011;56:52–60.

[86] Kohannim O, Hua X, Hibar DP, Lee S, Chou YY, Toga AW, et al. Boosting power for clinical trials using classifiers based on multiple biomarkers. Neurobiol Aging 2010;31:1429–42.

[87] Lemoine B, Rayburn S, Benton R. Data fusion and feature selection for Alzheimer's disease. Lect Notes Comput Sci 2010; 6334:320–7.

[88] Hinrichs C, Singh V, Mukherjee L, Xu G, Chung MK, Johnson SC. Spatially augmented LPboosting for AD classification with evaluations on the ADNI dataset. Neuroimage 2009;48:138–49.

[89] Shen L, Qi Y, Kim S, Nho K, Wan J, Risacher SL, et al. Sparse bayesian learning for identifying imaging biomarkers in AD prediction. Med Image Comput Comput Assist Interv 2010;13(Pt 3):611–8.

[90] Salas-Gonzalez D, Gorriz JM, Ramirez J, Illan IA, Lopez M, Segovia F, et al. Feature selection using factor analysis for

Alzheimer's diagnosis using 18F-FDG PET images. Med Phys 2010; 37:6084–95.

[91] Stonnington CM, Chu C, Kloppel S, Jack CR Jr, Ashburner J, Frackowiak RS. Predicting clinical scores from magnetic resonance scans in Alzheimer's disease. Neuroimage 2010;51:511–7.

[92] Franke K, Ziegler G, Kloppel S, Gaser C. Estimating the age of healthy subjects from T1-weighted MRI scans using kernel methods: exploring the influence of various parameters. Neuroimage 2010; 50:883–92.

[93] Filipovych R, Davatzikos C. Semi-supervised pattern classification of medical images: application to mild cognitive impairment (MCI). Neuroimage 2011;55:1109–19.

[94] Yang W, Hong CX, Xie H, Huang X. ICA-based automatic classification of magnetic resonance images from ADNI data. Lect Notes Comput Sci 2010;6330:340–7.

[95] Pelaez-Coca M, Bossa M, Olmos S. Discrimination of AD and normal subjects from MRI: anatomical versus statistical regions. Neurosci Lett 2011;487:113–7.

[96] Llano DA, Laforet G, Devanarayan V. Derivation of a new ADAS-cog composite using tree-based multivariate analysis: prediction of conversion from mild cognitive impairment to Alzheimer disease. Alzheimer Dis Assoc Disord 2010;25:73–84.

[97] Rousseau F. A non-local approach for image super-resolution using intermodality priors. Med Image Anal 2010;14:594–605.

[98] Gerber S, Tasdizen T, Thomas Fletcher P, Joshi S, Whitaker R. Manifold modeling for brain population analysis. Med Image Anal 2010; 14:643–53.

[99] Habeck C, Stern Y. Multivariate data analysis for neuroimaging data: overview and application to Alzheimer's disease. Cell Biochem Biophys 2010;58:53–67.

[100] Habeck CG. Basics of multivariate analysis in neuroimaging data. J Vis Exp 2010;:41. pii: 1988.

[101] Wu X, Chen K, Yao L, Ayutyanont N, Langbaum JB, Fleisher A, et al. Assessing the reliability to detect cerebral hypometabolism in probable Alzheimer's disease and amnestic mild cognitive impairment. J Neurosci Methods 2010;192:277–85.

[102] Singh N, Fletcher PT, Preston JS, Ha L, King R, Marron JS, et al. Multivariate statistical analysis of deformation momenta relating anatomical shape to neuropsychological measures. Med Image Comput Comput Assist Interv 2010;13(Pt 3):529–37.

[103] Vounou M, Nichols TE, Montana G. Discovering genetic associations with high-dimensional neuroimaging phenotypes: a sparse reduced-rank regression approach. Neuroimage 2010;53:1147–59.

[104] Chen K, Langbaum JB, Fleisher AS, Ayutyanont N, Reschke C, Lee W, et al. Twelve-month metabolic declines in probable Alzheimer's disease and amnestic mild cognitive impairment assessed using an empirically pre-defined statistical region-of-interest: findings from the Alzheimer's Disease Neuroimaging Initiative. Neuroimage 2010;51:654–64.

[105] Silver M, Montana G, Nichols TE. False positives in neuroimaging genetics using voxel-based morphometry data. Neuroimage 2011; 54:992–1000.

[106] Petersen RC, Aisen PS, Beckett LA, Donohue MC, Gamst AC, Harvey DJ, et al. Alzheimer's Disease Neuroimaging Initiative (ADNI): clinical characterization. Neurology 2010;74:201–9.

[107] Epstein NU, Saykin AJ, Risacher SL, Gao S, Farlow MR. Differences in medication use in the Alzheimer's disease neuroimaging initiative: analysis of baseline characteristics. Drugs Aging 2010; 27:677–86.

[108] Schneider LS, Insel PS, Weiner MW. Treatment with cholinesterase inhibitors and memantine of patients in the Alzheimer's Disease Neuroimaging Initiative. Arch Neurol 2011;68:58–66.

[109] Fennema-Notestine C, Hagler DJ Jr, McEvoy LK, Fleisher AS, Wu EH, Karow DS, et al. Structural MRI biomarkers for preclinical and mild Alzheimer's disease. Hum Brain Mapp 2009;30:3238–53.

[110] Karow DS, McEvoy LK, Fennema-Notestine C, Hagler DJ Jr, Jennings RG, Brewer JB, et al. Relative capability of MR imaging and FDG PET to depict changes associated with prodromal and early Alzheimer disease. Radiology 2010;256:932–42.

[111] McDonald CR, McEvoy LK, Gharapetian L, Fennema-Notestine C, Hagler DJ Jr, Holland D, et al. Regional rates of neocortical atrophy from normal aging to early Alzheimer disease. Neurology 2009; 73:457–65.

[112] Hua X, Leow AD, Parikshak N, Lee S, Chiang MC, Toga AW, et al. Tensor-based morphometry as a neuroimaging biomarker for Alzheimer's disease: an MRI study of 676 AD, MCI, and normal subjects. Neuroimage 2008;43:458–69.

[113] Leow AD, Yanovsky I, Parikshak N, Hua X, Lee S, Toga AW, et al. Alzheimer's disease neuroimaging initiative: a one-year follow up study using tensor-based morphometry correlating degenerative rates, biomarkers and cognition. Neuroimage 2009;45:645–55.

[114] Risacher SL, Saykin AJ, West JD, Shen L, Firpi HA, McDonald BC. Baseline MRI predictors of conversion from MCI to probable AD in the ADNI cohort. Curr Alzheimer Res 2009;6:347–61.

[115] Risacher SL, Shen L, West JD, Kim S, McDonald BC, Beckett LA, et al. Longitudinal MRI atrophy biomarkers: relationship to conversion in the ADNI cohort. Neurobiol Aging 2010;31:1401–18.

[116] Schuff N, Tosun D, Insel PS, Chiang GC, Truran D, Aisen PS, et al. Nonlinear time course of brain volume loss in cognitively normal and impaired elders. Neurobiol Aging (in press).

[117] McEvoy LK, Fennema-Notestine C, Roddey JC, Hagler DJ Jr, Holland D, Karow DS, et al. Alzheimer disease: quantitative structural neuroimaging for detection and prediction of clinical and structural changes in mild cognitive impairment. Radiology 2009; 251:195–205.

[118] Misra C, Fan Y, Davatzikos C. Baseline and longitudinal patterns of brain atrophy in MCI patients, and their use in prediction of short-term conversion to AD: results from ADNI. Neuroimage 2009; 44:1415–22.

[119] Davatzikos C, Bhatt P, Shaw LM, Batmanghelich KN, Trojanowski JQ. Prediction of MCI to AD conversion, via MRI, CSF biomarkers, and pattern classification. Neurobiol Aging (in press).

[120] Hua X, Hibar DP, Lee S, Toga AW, Jack CR Jr, Weiner MW, et al. Sex and age differences in atrophic rates: an ADNI study with n=1368 MRI scans. Neurobiol Aging 2010;31:1463–80.

[121] Schuff N, Woerner N, Boreta L, Kornfield T, Shaw LM, Trojanowski JQ, et al. MRI of hippocampal volume loss in early Alzheimer's disease in relation to ApoE genotype and biomarkers. Brain 2009;132(Pt 4):1067–77.

[122] Qiu A, Fennema-Notestine C, Dale AM, Miller MI. Regional shape abnormalities in mild cognitive impairment and Alzheimer's disease. Neuroimage 2009;45:656–61.

[123] Apostolova LG, Morra JH, Green AE, Hwang KS, Avedissian C, Woo E, et al. Automated 3D mapping of baseline and 12-month associations between three verbal memory measures and hippocampal atrophy in 490 ADNI subjects. Neuroimage 2010;51:488–99.

[124] Morra JH, Tu Z, Apostolova LG, Green AE, Avedissian C, Madsen SK, et al. Automated mapping of hippocampal atrophy in 1-year repeat MRI data from 490 subjects with Alzheimer's disease, mild cognitive impairment, and elderly controls. Neuroimage 2009; 45(Suppl 1):S3–15.

[125] Evans MC, Barnes J, Nielsen C, Kim LG, Clegg SL, Blair M, et al. Volume changes in Alzheimer's disease and mild cognitive impairment: cognitive associations. Eur Radiol 2010;20:674–82.

[126] Chou YY, Lepore N, Avedissian C, Madsen SK, Parikshak N, Hua X, et al. Mapping correlations between ventricular expansion and CSF amyloid and tau biomarkers in 240 subjects with Alzheimer's disease, mild cognitive impairment and elderly controls. Neuroimage 2009;46:394–410.

[127] Chou YY, Lepore N, Saharan P, Madsen SK, Hua X, Jack CR, et al. Ventricular maps in 804 ADNI subjects: correlations with CSF biomarkers and clinical decline. Neurobiol Aging 2010;31:1386–400.

[128] Vemuri P, Wiste HJ, Weigand SD, Knopman DS, Shaw LM, Trojanowski JQ, et al. Effect of apolipoprotein E on biomarkers of

amyloid load and neuronal pathology in Alzheimer disease. Ann Neurol 2010;67:308–16.

[129] Andrawis JP, Hwang KS, Green AE, Kotlerman J, Elashoff D, Morra JH, et al. Effects of ApoE4 and maternal history of dementia on hippocampal atrophy. Neurobiol Aging (in press).

[130] Madsen SK, Ho J, Hua X, Saharan PS, Toga AW, Jack CR Jr, et al. 3D maps localize caudate nucleus atrophy in 400 Alzheimer's disease, mild cognitive impairment, and healthy elderly subjects. Neurobiol Aging 2010;31:1312–25.

[131] Greene SJ, Killiany RJ. Subregions of the inferior parietal lobule are affected in the progression to Alzheimer's disease. Neurobiol Aging 2010;31:1304–11.

[132] Vemuri P, Wiste HJ, Weigand SD, Shaw LM, Trojanowski JQ, Weiner MW, et al. MRI and CSF biomarkers in normal, MCI, and AD subjects: diagnostic discrimination and cognitive correlations. Neurology 2009;73:287–93.

[133] Ho AJ, Raji CA, Becker JT, Lopez OL, Kuller LH, Hua X, et al. Obesity is linked with lower brain volume in 700 AD and MCI patients. Neurobiol Aging 2010;31:1326–39.

[134] Langbaum JB, Chen K, Lee W, Reschke C, Bandy D, Fleisher AS, et al. Categorical and correlational analyses of baseline fluorodeoxyglucose positron emission tomography images from the Alzheimer's Disease Neuroimaging Initiative (ADNI). Neuroimage 2009;45:1107–16.

[135] Landau SM, Harvey D, Madison CM, Koeppe RA, Reiman EM, Foster NL, et al. Associations between cognitive, functional, and FDG-PET measures of decline in AD and MCI. Neuro0biol Aging 2011;32:1207–18.

[136] Walhovd KB, Fjell AM, Dale AM, McEvoy LK, Brewer J, Karow DS, et al. Multi-modal imaging predicts memory performance in normal aging and cognitive decline. Neurobiol Aging 2010;31:1107–21.

[137] Wolk DA, Dickerson BC. Fractionating verbal episodic memory in Alzheimer's disease. Neuroimage 2011;54:1530–9.

[138] Chang YL, Bondi MW, Fennema-Notestine C, McEvoy LK, Hagler DJ Jr, Jacobson MW, et al. Brain substrates of learning and retention in mild cognitive impairment diagnosis and progression to Alzheimer's disease. Neuropsychologia 2010;48:1237–47.

[139] Dickerson BC, Wolk DA. Dysexecutive versus amnesic phenotypes of very mild Alzheimer's disease are associated with distinct clinical, genetic and cortical thinning characteristics. J Neurol Neurosurg Psychiatry 2011;82:45–51.

[140] Chang YL, Jacobson MW, Fennema-Notestine C, Hagler DJ Jr, Jennings RG, Dale AM, et al. Level of executive function influences verbal memory in amnestic mild cognitive impairment and predicts prefrontal and posterior cingulate thickness. Cereb Cortex 2010;20:1305–13.

[141] Wolk DA, Dickerson BC, Weiner M, Aiello M, Aisen P, Albert MS, et al. Apolipoprotein E (APOE) genotype has dissociable effects on memory and attentional-executive network function in Alzheimer's disease. Proc Natl Acad Sci USA 2010;107:10256–61.

[142] McDonald CR, Gharapetian L, McEvoy LK, Fennema-Notestine C, Hagler DJ Jr, Holland D, et al. Relationship between regional atrophy rates and cognitive decline in mild cognitive impairment. Neurobiol Aging (in press).

[143] Okonkwo OC, Alosco ML, Jerskey BA, Sweet LH, Ott BR, Tremont G. Cerebral atrophy, apolipoprotein E varepsilon4, and rate of decline in everyday function among patients with amnestic mild cognitive impairment. Alzheimers Dement 2010;6:404–11.

[144] Okonkwo OC, Alosco ML, Griffith HR, Mielke MM, Shaw LM, Trojanowski JQ, et al. Cerebrospinal fluid abnormalities and rate of decline in everyday function across the dementia spectrum: normal aging, mild cognitive impairment, and Alzheimer disease. Arch Neurol 2010;67:688–96.

[145] Cronk BB, Johnson DK, Burns JM. Body mass index and cognitive decline in mild cognitive impairment. Alzheimer Dis Assoc Disord 2010;24:126–30.

[146] Tosun D, Schuff N, Truran-Sacrey D, Shaw LM, Trojanowski JQ, Aisen P, et al. Relations between brain tissue loss, CSF biomarkers, and the ApoE genetic profile: a longitudinal MRI study. Neurobiol Aging 2010;31:1340–54.

[147] Fjell AM, Walhovd KB, Fennema-Notestine C, McEvoy LK, Hagler DJ, Holland D, et al. CSF biomarkers in prediction of cerebral and clinical change in mild cognitive impairment and Alzheimer's disease. J Neurosci 2010;30:2088–101.

[148] Ott BR, Cohen RA, Gongvatana A, Okonkwo OC, Johanson CE, Stopa EG, et al. Brain ventricular volume and cerebrospinal fluid biomarkers of Alzheimer's disease. J Alzheimers Dis 2010;20:647–57.

[149] Kim S, Swaminathan S, Shen L, Risacher SL, Nho K, Foroud T, et al. Genome-wide association study of CSF biomarkers Abeta1-42, t-tau, and p-tau181p in the ADNI cohort. Neurology 2011;76:69–79.

[150] Jagust WJ, Landau SM, Shaw LM, Trojanowski JQ, Koeppe RA, Reiman EM, et al. Relationships between biomarkers in aging and dementia. Neurology 2009;73:1193–9.

[151] Apostolova LG, Hwang KS, Andrawis JP, Green AE, Babakchanian S, Morra JH, et al. 3D PIB and CSF biomarker associations with hippocampal atrophy in ADNI subjects. Neurobiol Aging 2010;31:1284–303.

[152] Jack CR Jr, Wiste HJ, Vemuri P, Weigand SD, Senjem ML, Zeng G, et al. Brain beta-amyloid measures and magnetic resonance imaging atrophy both predict time-to-progression from mild cognitive impairment to Alzheimer's disease. Brain 2010;133:3336–48.

[153] Caroli A, Frisoni GB. The dynamics of Alzheimer's disease biomarkers in the Alzheimer's Disease Neuroimaging Initiative cohort. Neurobiol Aging 2010;31:1263–74.

[154] Beckett LA, Harvey DJ, Gamst A, Donohue M, Kornak J, Zhang H, et al. The Alzheimer's Disease Neuroimaging Initiative: annual change in biomarkers and clinical outcomes. Alzheimers Dement 2010;6:257–64.

[155] Walhovd KB, Fjell AM, Brewer J, McEvoy LK, Fennema-Notestine C, Hagler DJ Jr, et al. Combining MR imaging, positron-emission tomography, and CSF biomarkers in the diagnosis and prognosis of Alzheimer disease. Am J Neuroradiol 2010;31:347–54.

[156] Vemuri P, Wiste HJ, Weigand SD, Knopman DS, Trojanowski JQ, Shaw LM, et al. Serial MRI and CSF biomarkers in normal aging, MCI, and AD. Neurology 2010;75:143–51.

[157] Li Y, Wang Y, Wu G, Shi F, Zhou L, Lin W, et al. Discriminant analysis of longitudinal cortical thickness changes in Alzheimer's disease using dynamic and network features. Neurobiol Aging (in press).

[158] Cuingnet R, Gerardin E, Tessieras J, Auzias G, Lehericy S, Habert MO, et al. Automatic classification of patients with Alzheimer's disease from structural MRI: a comparison of ten methods using the ADNI database. Neuroimage 2010;56:766–81.

[159] De Meyer G, Shapiro F, Vanderstichele H, Vanmechelen E, Engelborghs S, De Deyn PP, et al. Diagnosis-independent alzheimer disease biomarker signature in cognitively normal elderly people. Arch Neurol 2010;67:949–56.

[160] Schott JM, Bartlett JW, Fox NC, Barnes J. Increased brain atrophy rates in cognitively normal older adults with low cerebrospinal fluid Abeta1-42. Ann Neurol 2010;68:825–34.

[161] Ewers M, Walsh C, Trojanowski JQ, Shaw LM, Petersen RC, Jack CR Jr, et al. Prediction of conversion from mild cognitive impairment to Alzheimer's disease dementia based upon biomarkers and neuropsychological test performance. Neurobiol Aging (in press).

[162] van Gils M, Koikkalainen J, Mattila J, Herukka S, Lotjonen J, Soininen H. Discovery and use of efficient biomarkers for objective disease state assessment in Alzheimer's disease. Conf Proc IEEE Eng Med Biol Soc 2010;2010:2886–9.

[163] Desikan RS, Cabral HJ, Settecase F, Hess CP, Dillon WP, Glastonbury CM, et al. Automated MRI measures predict progression to Alzheimer's disease. Neurobiol Aging 2010;31:1364–74.

[164] Kovacevic S, Rafii MS, Brewer JB. High-throughput, fully automated volumetry for prediction of MMSE and CDR decline in mild cognitive impairment. Alzheimer Dis Assoc Disord 2009;23:139–45.

[165] Querbes O, Aubry F, Pariente J, Lotterie JA, Demonet JF, Duret V, et al. Early diagnosis of Alzheimer's disease using cortical thickness: impact of cognitive reserve. Brain 2009;132:2036–47.

[166] Carmichael O, Schwarz C, Drucker D, Fletcher E, Harvey D, Beckett L, et al. Longitudinal changes in white matter disease and cognition in the first year of the Alzheimer disease neuroimaging initiative. Arch Neurol 2010;67:1370–8.

[167] Vemuri P, Wiste HJ, Weigand SD, Shaw LM, Trojanowski JQ, Weiner MW, et al. MRI and CSF biomarkers in normal, MCI, and AD subjects: predicting future clinical change. Neurology 2009;73:294–301.

[168] McEvoy LK, Edland SD, Holland D, Hagler DJ, Roddey JC, Fennema-Notestine C, et al. Neuroimaging enrichment strategy for secondary prevention trials in Alzheimer disease. Alzheimer Dis Assoc Disord 2010;24:269–77.

[169] Weigand SD, Vemuri P, Wiste HJ, Senjem ML, Pankratz VS, Aisen PS, et al. Transforming cerebrospinal fluid Abeta42 measures into calculated Pittsburgh Compound B units of brain Abeta amyloid. Alzheimers Dement 2011;7:133–41.

[170] Schneider LS, Kennedy RE, Cutter GR. Requiring an amyloid-beta1-42 biomarker for prodromal Alzheimer's disease or mild cognitive impairment does not lead to more efficient clinical trials. Alzheimers Dement 2010;6:367–77.

[171] Ito K, Ahadieh S, Corrigan B, French J, Fullerton T, Tensfeldt T. Disease progression meta-analysis model in Alzheimer's disease. Alzheimers Dement 2010;6:39–53.

[172] Lorenzi M, Donohue M, Paternico D, Scarpazza C, Ostrowitzki S, Blin O, et al. Enrichment through biomarkers in clinical trials of Alzheimer's drugs in patients with mild cognitive impairment. Neurobiol Aging 2010;31:1443. e1–51.e1.

[173] Landau SM, Harvey D, Madison CM, Reiman EM, Foster NL, Aisen PS, et al. Comparing predictors of conversion and decline in mild cognitive impairment. Neurology 2010;75:230–8.

[174] Schott JM, Bartlett JW, Barnes J, Leung KK, Ourselin S, Fox NC. Reduced sample sizes for atrophy outcomes in Alzheimer's disease trials: baseline adjustment. Neurobiol Aging 2010;31:1452. e2–62.e2.

[175] Nestor SM, Rupsingh R, Borrie M, Smith M, Accomazzi V, Wells JL, et al. Ventricular enlargement as a possible measure of Alzheimer's disease progression validated using the Alzheimer's disease neuroimaging initiative database. Brain 2008;131(Pt 9):2443–54.

[176] Holland D, Brewer JB, Hagler DJ, Fenema-Notestine C, Dale AM, Weiner M, et al. Subregional neuroanatomical change as a biomarker for Alzheimer's disease. Proc Natl Acad Sci USA 2009; 106:20954–9.

[177] Hua X, Lee S, Yanovsky I, Leow AD, Chou YY, Ho AJ, et al. Optimizing power to track brain degeneration in Alzheimer's disease and mild cognitive impairment with tensor-based morphometry: an ADNI study of 515 subjects. Neuroimage 2009;48:668–81.

[178] Hua X, Gutman B, Boyle CP, Rajagopalan P, Leow AD, Yanovsky I, et al. Accurate measurement of brain changes in longitudinal MRI scans using tensor-based morphometry. Neuroimage 2011;57:5–14.

[179] Gatz M, Reynolds CA, Fratiglioni L, Johansson B, Mortimer JA, Berg S, et al. Role of genes and environments for explaining Alzheimer disease. Arch Gen Psychiatry 2006;63:168–74.

[180] Ashford JW, Mortimer JA. Non-familial Alzheimer's disease is mainly due to genetic factors. J Alzheimers Dis 2002;4:169–77.

[181] Lambert JC, Heath S, Even G, Campion D, Sleegers K, Hiltunen M, et al. Genome-wide association study identifies variants at CLU and CR1 associated with Alzheimer's disease. Nat Genet 2009;41:1094–9.

[182] Harold D, Abraham R, Hollingworth P, Sims R, Gerrish A, Hamshere ML, et al. Genome-wide association study identifies variants at CLU and PICALM associated with Alzheimer's disease. Nat Genet 2009;41:1088–93.

[183] Carrasquillo MM, Belbin O, Hunter TA, Ma L, Bisceglio GD, Zou F, et al. Replication of CLU, CR1, and PICALM associations with alzheimer disease. Arch Neurol 2010;67:961–4.

[184] Potkin SG, Guffanti G, Lakatos A, Turner JA, Kruggel F, Fallon JH, et al. Hippocampal atrophy as a quantitative trait in a genome-wide association study identifying novel susceptibility genes for Alzheimer's disease. PLoS One 2009;4:e6501.

[185] Jun G, Naj AC, Beecham GW, Wang LS, Buros J, Gallins PJ, et al. Meta-analysis confirms CR1, CLU, and PICALM as Alzheimer disease risk loci and reveals interactions with APOE genotypes. Arch Neurol 2010;67:1473–84.

[186] Naj AC, Jun G, Beecham GW, Wang LS, Vardarajan BN, Buros J, et al. Common variants at MS4A4/MS4A6E, CD2AP, CD33 and EPHA1 are associated with late-onset Alzheimer's disease. Nat Genet 2011;43:436–41.

[187] Hollingworth P, Harold D, Sims R, Gerrish A, Lambert JC, Carrasquillo MM, et al. Common variants at ABCA7, MS4A6A/MS4A4E, EPHA1, CD33 and CD2AP are associated with Alzheimer's disease. Nat Genet 2011;43:429–35.

[188] Lakatos A, Derbeneva O, Younes D, Keator D, Bakken T, Lvova M, et al. Association between mitochondrial DNA variations and Alzheimer's disease in the ADNI cohort. Neurobiol Aging 2010; 31:1355–63.

[189] Kauwe JS, Bertelsen S, Mayo K, Cruchaga C, Abraham R, Hollingworth P, et al. Suggestive synergy between genetic variants in TF and HFE as risk factors for Alzheimer's disease. Am J Med Genet B Neuropsychiatr Genet 2010;153B:955–9.

[190] Cruchaga C, Bertelsen S, Kauwe JS, Nowotny P, Shah AR, et al. SNPs in the regulatory subunit of calcineurin are associated with CSF tau protein levels, brain mRNA levels. Alzheimers Dement 2009;5(Suppl 4):P471–2.

[191] Cruchaga C, Kauwe JS, Mayo K, Spiegel N, Bertelsen S, Nowotny P, et al. SNPs associated with cerebrospinal fluid phospho-tau levels influence rate of decline in Alzheimer's disease. PLoS Genet 2010;:6. pii: e1001101.

[192] Kauwe JS, Cruchaga C, Bertelsen S, Mayo K, Latu W, Nowotny P, et al. Validating predicted biological effects of Alzheimer's disease associated SNPs using CSF biomarker levels. J Alzheimers Dis 2010;21:833–42.

[193] Biffi A, Anderson CD, Desikan RS, Sabuncu M, Cortellini L, Schmansky N, et al. Genetic variation and neuroimaging measures in Alzheimer disease. Arch Neurol 2010;67:677–85.

[194] Shen L, Kim S, Risacher SL, Nho K, Swaminathan S, West JD, et al. Whole genome association study of brain-wide imaging phenotypes for identifying quantitative trait loci in MCI and AD: a study of the ADNI cohort. Neuroimage 2010;53:1051–63.

[195] Stein JL, Hua X, Lee S, Ho AJ, Leow AD, Toga AW, et al. Voxelwise genome-wide association study (vGWAS). Neuroimage 2010; 53:1160–74.

[196] Stein JL, Hua X, Morra JH, Lee S, Hibar DP, Ho AJ, et al. Genome-wide analysis reveals novel genes influencing temporal lobe structure with relevance to neurodegeneration in Alzheimer's disease. Neuroimage 2010;51:542–54.

[197] Furney SJ, Simmons A, Breen G, Pedroso I, Lunnon K, Proitsi P, et al. Genome-wide association with MRI atrophy measures as a quantitative trait locus for Alzheimer's disease. Mol Psychiatry (in press).

[198] Bertram L, Heekeren H. Obesity and the brain: a possible genetic link. Alzheimers Res Ther 2010;2:27.

[199] Han MR, Schellenberg GD, Wang LS. Genome-wide association reveals genetic effects on human Abeta42 and tau protein levels in cerebrospinal fluids: a case control study. BMC Neurol 2010;10:90.

[200] Fjell AM, Walhovd KB, Fennema-Notestine C, McEvoy LK, Hagler DJ, Holland D, et al. One-year brain atrophy evident in healthy aging. J Neurosci 2009;29:15223–31.

[201] Burgmans S, van Boxtel MP, Vuurman EF, Smeets F, Gronenschild EH, Uylings HB, et al. The prevalence of cortical gray matter atrophy may be overestimated in the healthy aging brain. Neuropsychology 2009; 23:541–50.

[202] Fjell AM, Westlye LT, Espeseth T, Reinvang I, Dale AM, Holland D, et al. Cortical gray matter atrophy in healthy aging cannot be

explained by undetected incipient cognitive disorders: a comment on Burgmans, et al. (2009). Neuropsychology 2010;24:258–63. discussion 264–6.

[203] Murphy EA, Holland D, Donohue M, McEvoy LK, Hagler DJ Jr, Dale AM, et al. Six-month atrophy in MTL structures is associated with subsequent memory decline in elderly controls. Neuroimage 2010;53:1310–7.

[204] Nettiksimmons J, Harvey D, Brewer J, Carmichael O, Decarli C, Jack CR Jr, et al. Subtypes based on cerebrospinal fluid and magnetic resonance imaging markers in normal elderly predict cognitive decline. Neurobiol Aging 2010;31:1419–28.

[205] Fjell AM, Walhovd KB, Fennema-Notestine C, McEvoy LK, Hagler DJ, Holland D, et al. Brain Atrophy in Healthy Aging Is Related to CSF Levels of A{beta}1-42. Cereb Cortex 2010;20:2069–79.

[206] Mormino EC, Kluth JT, Madison CM, Rabinovici GD, Baker SL, Miller BL, et al. Episodic memory loss is related to hippocampal-mediated beta-amyloid deposition in elderly subjects. Brain 2009; 132(Pt 5):1310–23.

[207] Chiang GC, Insel PS, Tosun D, Schuff N, Truran-Sacrey D, Raptentsetsang ST, et al. Hippocampal atrophy rates and CSF biomarkers in elderly APOE2 normal subjects. Neurology 2010; 75:1976–81.

[208] Fan M, Liu B, Zhou Y, Zhen X, Xu C, Jiang T. Cortical thickness is associated with different apolipoprotein E genotypes in healthy elderly adults. Neurosci Lett 2010;479:332–6.

[209] Ho AJ, Stein JL, Hua X, Lee S, Hibar DP, Leow AD, et al. A commonly carried allele of the obesity-related FTO gene is associated with reduced brain volume in the healthy elderly. Proc Natl Acad Sci USA 2010;107:8404–9.

[210] Rimol LM, Agartz I, Djurovic S, Brown AA, Roddey JC, Kahler AK, et al. Sex-dependent association of common variants of microcephaly genes with brain structure. Proc Natl Acad Sci USA 2010;107:384–8.

[211] Joyner AH, Roddey JC, Bloss CS, Bakken TE, Rimol LM, Melle I, et al. A common MECP2 haplotype associates with reduced cortical surface area in humans in two independent populations. Proc Natl Acad Sci USA 2009;106:15483–8.

[212] Frisoni GB. Alzheimer's disease neuroimaging Initiative in Europe. Alzheimers Dement 2010;6:280–5.

[213] Frisoni GB, Henneman WJ, Weiner MW, Scheltens P, Vellas B, Reynish E, et al. The pilot European Alzheimer's Disease Neuroimaging Initiative of the European Alzheimer's Disease Consortium. Alzheimers Dement 2008;4:255–64.

[214] Buerger K, Frisoni G, Uspenskaya O, Ewers M, Zetterberg H, Geroldi C, et al. Validation of Alzheimer's disease CSF and plasma biological markers: the multicentre reliability study of the pilot European Alzheimer's Disease Neuroimaging Initiative (E-ADNI). Exp Gerontol 2009;44:579–85.

[215] Mattsson N, Andreasson U, Persson S, Arai H, Batish SD, Bernardini S, et al. The Alzheimer's Association external quality control program for cerebrospinal fluid biomarkers. Alzheimers Dement 2011;7:386–95.e6.

[216] Frisoni GB, Jack CR. Harmonization of magnetic resonance-based manual hippocampal segmentation: a mandatory step for wide clinical use. Alzheimers Dement 2011;7:171–4.

[217] Ellis KA, Rowe CC, Villemagne VL, Martins RN, Masters CL, Salvado O, et al. Addressing population aging and Alzheimer's disease through the Australian imaging biomarkers and lifestyle study: collaboration with the Alzheimer's Disease Neuroimaging Initiative. Alzheimers Dement 2010;6:291–6.

[218] Rowe CC, Ellis KA, Rimajova M, Bourgeat P, Pike KE, Jones G, et al. Amyloid imaging results from the Australian Imaging, Biomarkers and Lifestyle (AIBL) study of aging. Neurobiol Aging 2010;31:1275–83.

[219] Fukuyama H. Neuroimaging in mild cognitive impairment [in Japanese]. Rinsho Shinkeigaku 2006;46:791–4.

[220] Iwatsubo T. Japanese ADNI: present status and future. Alzheimers Dement 2010;6:297–9.

[221] Arai H. Alzheimer's disease neuroimaging initiative and mild cognitive impairment [in Japanese]. Rinsho Shinkeigaku 2007;47:905–7.

[222] Ihara Y. Overview on Alzheimer's disease [in Japanese]. Rinsho Shinkeigaku 2007;47:902–4.

[223] Murayam S, Saito Y. Neuropathology of mild cognitive impairment Alzheimer's disease [in Japanese]. Rinsho Shinkeigaku 2007; 47:912–4.

[224] Arai H, Okamura N, Furukawa K, Kudo Y. Geriatric medicine, Japanese Alzheimer's disease neuroimaging initiative and biomarker development. Tohoku J Exp Med 2010;221:87–95.

[225] Li Y, Wang Y, Wu G, Shi F, Zhou L, Lin W, et al. Discriminant analysis of longitudinal cortical thickness changes in Alzheimer's disease using dynamic and network features. Neurobiol Aging (in press).

Appendix

1. Publications arising from AIBL

1.1. AIBL Publication list
2009–present

1.1.1. 2009

[09.03] Bourgeat P, Chetelat G, Villemagne VL, Fripp J, Raniga P, Acosta O, et al. B-amyloid burden in the temporal neocortex is related to hippocampal atrophy in elderly subjects without dementia. Neurology 2010;74:121–7.

[09.04] Ellis KA, Bush AI, Darby D, De Fazio D, Foster J, Hudson P, et al. The Australian Imaging, Biomarkers and Lifestyle (AIBL) study of aging: methodology and baseline characteristics of 1112 individuals recruited for a longitudinal study of Alzheimer's disease. Int Psychogeriatr 2009;21:672–87.

[09.05] Fodero-Tavoletti MT, Cappai R, McLean CA, Pike KE, Adlard PA, Cowie T, et al. Amyloid imaging in Alzheimer's disease and other dementias. Brain Imaging Behav 2009;3:246–61.

[09.06] Fodero-Tavoletti MT, Rowe CC, McLean CA, Leone L, Li QX, Masters CL, Cappai R, Villemagne VL. Characterization of PiB binding to white matter in AD and other dementias. J Nucl Med 2009;50:198–204.

[09.07] Fodero-Tavoletti MT, Mulligan RS, Okamura N, Furumoto S, Rowe CC, Kudo Y, et al. *In vitro* characterisation of BF227 binding to α-synuclein/Lewy Bodies. Eur J Pharmacol 2009;617:54–8.

[09.08] Villemagne VL, McLean CA, Reardon K, Boyd A, Lewis V, Klug G, et al. ^{11}C-PiB PET studies in typical sporadic Creutzfeldt-Jakob disease. J Neurol Neurosurg Psychiatr 2009;80:998–1001.

[09.09] Villemagne VL, Ataka S, Mizuno T, Brooks WS, Wada Y, Kondo M, et al. High striatal amyloid β-peptide deposition across different autosomal Alzheimer's disease mutation types. Arch Neurol 2009;66:1537–44.

[09.10] Okamura N, Fodero-Tavoletti MT, Kudo Y, Rowe CC, Furumoto S, Arai H, Masters CL, Yanai K, Villemagne VL. Advances in molecular imaging for the diagnosis of dementia. Expert Opin Med Diagn 2009;3:705–16.

[09.11] Acosta O, Bourgeat P, Fripp J, Zuluaga MA, Fripp J, Salvado O, Ourselin S. Automated voxel-based 3D cortical thickness measurement in a combined Lagrangian-Eulerian PDE approach using partial volume maps. Med Image Anal 2009;13:730–43.

1.1.2. 2010

[10.01] Bourgeat P, Chételat G, Villemagne VL, Fripp J, Raniga P, Pike K, et al. β-amyloid burden in the temporal neocortex is related to hippocampal atrophy in elderly subjects without dementia. Neurology 2010;74:121–7.

[10.02] Ellis KA, Rowe CC, Villemagne VL, Martins RN, Masters CL, Salvado O, Szoeke C, Ames D; the AIBL Research Group. Addressing population aging and Alzheimer's disease through the Australian imaging biomarkers and lifestyle study: collaboration with the Alzheimer's Disease Neuroimaging Initiative. Alzheimers Dement 2010;6:291–6.

[10.03] Villemagne VL, Perez KA, Pike KE, Kok WM, Rowe CC, White AR, et al. Blood borne amyloid-β dimer correlates with clinical markers of Alzheimer's disease. J Neurosci 2010;30:6315–22.

[10.04] Chételat G, Villemagne VL, Bourgeat P, Pike KE, Jones G, Ames D, et al. Relationship between atrophy and β-amyloid deposition in Alzheimer disease. Ann Neurol 2010;67:317–24. [See also editorial: Rabinovici GD, Roberson ED. Beyond diagnosis: what biomarkers are teaching us about the "bio"logy of Alzheimer disease. Ann Neurol 2010;67:283–5.]

[10.05] Villemagne VL, Pike K, Pejoska S, Boyd A, Power M, Jones G, Masters CL, Rowe CC. ^{11}C-PiB PET A_{Bri} imaging in Worster-Drought syndrome (Familial British Dementia): a case report. J Alzheimers Dis 2010;19:423–8.

[10.06] Lui JK, Laws SM, Li QX, Villemagne VL, Ames D, Brown B, et al. Plasma amyloid-β as a biomarker in Alzheimer's disease: the AIBL Study of Aging. J Alzheimers Dis 2010;20;1233–42.

[10.07] Rowe CC, Ellis KA, Rimajova M, Bourgeat P, Pike KE, Jones G, et al. Amyloid imaging results from the Australian Imaging, Biomarkers and Lifestyle (AIBL) study of aging. Neurobiol Aging 2010:31;1275–83.

[10.08] Chételat G, Villemagne VL, Pike KE, Baron JC, Bourgeat P, Jones G, et al. Larger temporal volume in elderly with high versus low beta-amyloid deposition. Brain 2010;133:3349–58.

[10.09] Rueda A, Acosta O, Couprie M, Bourgeat P, Fripp J, Dowson N, Romero E, Salvado O. Topology-corrected segmentation and local intensity estimates for improved partial volume classification of brain cortex in MRI. J Neurosci Methods 2010;188:305–15.

1.1.3. 2011

1.1.3.1. Published

[11.01] Villemagne VL, Pike KE, Chételat G, Ellis KA, Mulligan R, Bourgeat P, et al. Longitudinal assessment of Aβ burden and cognition in aging and Alzheimer's disease. Ann Neurol 2011;69:181–92.

[11.02] Ellis KA, Rowe CC, Szoeke C, Villemagne VL, Ames D, Chételat G, et al. Advances in structural and molecular neuroimaging in Alzheimer's disease. Med J Aust 2011;194:S20–3.

[11.03] Bahar-Fuchs A, Moss S, Pike KE, Villemagne VL, Masters CL, Rowe C, Savage G. Olfactory deficits and Aβ burden in AD, MCI and healthy ageing: a PiB PET Study. J Alzheimers Dis 2010;22:1081–7.

[11.04] Gupta VB, Laws SM, Villemagne VL, Ames D, Bush AI, Ellis KA, et al. Plasma Apolipoprotein E and Alzheimer's disease risk: the AIBL study of ageing. Neurology 2011;76:1091–8.

[11.05] Sittironnait G, Ames D, Bush AI, Faux N, Flicker L, Foster J, et al. Effects of anticholinergic drugs on cognitive function in older Australians: results from the AIBL Study. Dement Geriatr Cogn Disord (Special ASIA issue). 2011;31:173–8.

[11.06] McBride S, Good N, Szoeke C, Ames D, Martins R, Masters C, et al. A web-based normative data tool for assessing cognitive performance in healthy older Australians. Med J Aust 2011;194:S12–14.

[11.07] Chételat G, Villemagne VL, Pike KE, Ellis KA, Bourgeat P, Jones G, et al. Research Group. Independent contribution of temporal Aβ deposition to memory decline in the predementia phase of Alzheimer's disease. Brain 2011;134(Pt 3):798–807

[11.08] Watt AD, Perez KA, Faux NG, Pike KE, Rowe CC, Bourgeat P, et al. Increasing the predictive accuracy of beta-amyloid blood-borne biomarkers in Alzheimer's disease. J Alzheimers Dis 2011;24:47–59.

[11.09] Villemagne VL, Okamura N, Pejoska S, Drago J, Mulligan RS, Chételat G, et al. In vivo assessment of vesicular monoamine transporter type 2 in dementia with Lewy bodies and Alzheimer's disease. Arch Neurol 2011;68:905–12.